OFFICE OF NAVAL RESEARCH

Contract N00014-85-K-0684

PICOSECOND LASER PULSE INTERACTIONS WITH METALLIC AND SEMICONDUCTING SURFACES

Final Report

September 1, 1985 -- December 31, 1987

Principal Investigators:
E. Mazur and F. Spaepen

Division of Applied Sciences
Harvard University
Cambridge, MA 02138

SECURITY CLASSIFICATION OF THIS PAGE (When Data Entered)

REPORT DOCUMENTATION PAGE		READ INSTRUCTIONS BEFORE COMPLETING FORM
1. REPORT NUMBER Final Report	2. GOVT ACCESSION NO.	3. RECIPIENT'S CATALOG NUMBER
4. TITLE (and Subtitle) Picosecond Laser Pulse Interactions with Metallic and Semiconducting Surfaces		5. TYPE OF REPORT & PERIOD COVERED Final Report 1 Sept. 85- 31 Dec. 87 6. PERFORMING ORG. REPORT NUMBER
7. AUTHOR(s) Eric Mazur and Frans Spaepen		8. CONTRACT OR GRANT NUMBER(s) N00014-85-K-0684
9. PERFORMING ORGANIZATION NAME AND ADDRESS Division of Applied Sciences Harvard University Cambridge, MA 02138		10. PROGRAM ELEMENT, PROJECT, TASK AREA & WORK UNIT NUMBERS
11. CONTROLLING OFFICE NAME AND ADDRESS Office of Naval Research 800 N. Quincy Street Arlington, VA 22217		12. REPORT DATE 31 January 1990 13. NUMBER OF PAGES 78
14. MONITORING AGENCY NAME & ADDRESS(if different from Controlling Office)		15. SECURITY CLASS. (of this report) Unclassified 15a. DECLASSIFICATION/DOWNGRADING SCHEDULE
16. DISTRIBUTION STATEMENT (of this Report)		
17. DISTRIBUTION STATEMENT (of the abstract entered in Block 20, if different from Report) Approved for public release, distribution unlimited.		
18. SUPPLEMENTARY NOTES		
19. KEY WORDS (Continue on reverse side if necessary and identify by block number)		
20. ABSTRACT (Continue on reverse side if necessary and identify by block number) Pump-probe, ellipsometric, and streak camera measurements of the reflectivity following picosecond pulse irradiation of semiconductor, graphite, layered compound, and metal surface are reported. Overheating of crystal and liquid are analyzed. Crystallization of metals is shown to be collision-limited. Kinetic preference for formation of isotropic, small unit cell crystals is established.		

DD FORM 1 JAN 73 1473 EDITION OF 1 NOV 65 IS OBSOLETE
S/N 0102-014-6601

SECURITY CLASSIFICATION OF THIS PAGE (When Data Entered)

PICOSECOND LASER PULSE INTERACTIONS WITH
METALLIC AND SEMICONDUCTING SURFACES

Principal Investigators
Eric Mazur and Frans Spaepen

Preface

This report contains the results of a two-year study of the interaction of picosecond laser pulses with metallic and semiconducting srufaces, and consists for the most part of a collection of published papers.

The study has concentrated on the time-dependence of electronic and structural transitions on a picosecond-to-nanosecond timescale, following irradiation with a picosecond pulse.

The main findings of the work are:

1. Use of streak camera with 1.8 ps resolution allows the reflectivity during the melting of silicon to be studied with improved spatial and temporal resolution following a single pump pulse.

2. Following a 30 ps, 532 nm pump pulse at 470 mJ/cm^2, streak camera measurements show that silicon overheats above its melting temperature by more than 1000K.

3. Pump-probe and ellipsometry measurements on graphite show a substantial decrease of both the imaginary and real parts of the index of refraction when the pump fluence exceeds the melting threshold, indicating that the molten graphite is less metallic.

4. The use of these short probing and excitation times in the graphite studies avoids artifacts arising from evaporation.

5. Pump-probe reflectivity measurements on the layered compounds 1T-TiS_2 and 1T-$TiSe_2$ show a transition to a phase with lower reflectivity, indicating that is not metallic.

6. An analysis of the stability of the liquid created by picosecond laser pulse irradiation shows that on this time scale:
   (i) The loss of mass and energy by surface evaporation is negligible.
   (ii) The steady-state nucleation rate of vapor bubbles is sufficiently small to allow substantial overheating of the liquid above its boiling point.
   (iii) Transient effects can play a role in postponing bubble nucleation.
   (iv) The stability limit of the overheated liquid (spinodal decomposition to the vapor) can be approached to within a few hundered degrees, corresponding to overheats of several thousand degrees.
   (v) The large amounts of mass transport observed after the laser pulse are not the result of evaporation, but are caused by hydrodynamic effects resulting from the recoil pressure induced by surface evaporation.

7. Pump-probe measurements of the time elemental metals (Au, Cu) stay molten give crystallization velocities up to 100 m/s. These can only be obtained by a collision-limited crystallization mechanism.

8. Quenching of Nb-Si following laser irradiation provides a case study of the kinetic preference for crystal formation. It shows, for a sequence of five phases, how higher isotropy and a smaller unit cell size are favored at higher quench rates.

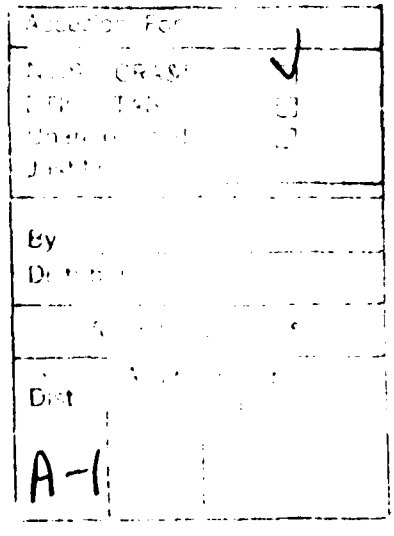

Bibliography

M.Buijis, J.K. Wang, P. Saeta, and E. Mazur, "Laser Melting of Silicon: The First Few Picoseconds," *Nonlinear Opics and Ultrafast Phenomena*, eds. R.R. Alfano and L.J. Rothberg, (Nova Publishers, NY 1990).

J.K. Wang, P. Saeta, M. Buijis, M. Malvezzi, and E. Mazur, "Single-shot Reflectivity Study of the Picosecond Melting of Silicon using a Streak Camera,"*Ultrafast Phenomena*, eds. T. Yajima, K. Yoshihara, C.B. Harris, S. Shionoya (Springer-Verlag) p. 236.

A.M. Malvezzi, G. Reverberi, and N. Bloembergen, "Optical Properties of Picosecond Laser Irradiated Graphite," *Mat. Res. Soc. Symp. Proc.* **100**:483-488 (1988).

C.Y. Huang, A.M. Malvezzi, N. Bloembergen, and F.J. Di Salvo, Jr., "Time-Resolved Picosecond Reflectivity Study of Laser-Excited Layered Compounds," *Mat. Res. Soc. Symp. Proc.* **74**:269-274 (1987) .

F. Spaepen, "Thermodynamics and Kinetics of Melting, Evaporation and Crystallization, induced by Picosecond Pulsed Laser Irradiation," *Ultrafast Phenomena V: Proceedings of the Fifth OSA Meeting*, eds. G.R. Fleming and A.E. Siegman (Springer-Verlag, New York, 1986), pp. 174-178.

F. Spaepen, "Metastable States in Pulsed Laser Quenching," *Hume-Rothery Symposium on Undercooled Alloy Phases, TMS-AIME Symposia Proceedings* (1986), eds. E.W. Collings and C.C. Koch, pp. 187-205.

C.A. MacDonald, A.M. Malvezzi and F. Spaepen, "Picosecond Time-Resolved Measurements of Crystallization in Noble Metals," *Journal of Applied Physics* **65**:129-136 (1989).

F. Spaepen and D. Turnbull, "Crystal Nucleation and Growth in Rapid Solidfication," *Rapid Solidification Processing: Principles and Technologies* **IV**, eds. R. Mehrabian and P.A. Parrish, Conference held Dec. 15-18, 1986 at U. of CA, Santa Barbara (Claitor's Publishing Division: Baton Rouge, LA, 1988) pp.1-12.

W.K.Wang, C.J. Lobb and F. Spaepen, "Formation of Metastable Nb-Si Phases by Picosecond and Nanosecond Pulsed Laser Etching," *Materials Science and Engineering* **97**:325-328 (1988).

Nonlinear Opics & Ultrafast Phenomena
Eds. R.R. Alfano and L.J. Rothberg
Publ. Nova, NY 1990

LASER MELTING OF SILICON: THE FIRST FEW PICOSECONDS

Maarten Buijs, Juen-Kai Wang, Peter Saeta, and Eric Mazur

Division of Applied Sciences and Department of Physics
Harvard University
Cambridge, MA 02138, USA

Abstract

The use of a streak camera makes it possible to improve the study of the melting of silicon during picosecond laser annealing. Its time resolution of 1.8 ps enables us to confirm that the molten silicon is heated above the melting temperature. It also provides spatial information on the melting process.

1. Introduction

Numerous investigations on the phase transition of silicon during ultrafast laser annealing have been performed in recent years. It has been established that the silicon surface melts during a picosecond laser pulse.[1] Because liquid silicon is a metal, the reflectivity increases on melting. This has indeed been observed using optical pump-and-probe techniques.[1-3] Standard picosecond pump-and-probe measurements, however, have some inherent drawbacks. First, they cannot resolve reflectivity changes that occur on a time scale of a few picoseconds, because they integrate over the duration of the probe pulse (typically 20 ps or more). Second, they determine the time profile of the reflectivity for every pump fluence in a step-wise manner by varying the delay between the pump and the probe pulse. This introduces a large amount of scatter in the data points, due to shot-to-shot variations in the pump fluence, and requires a large amount of data to be taken for every time profile of the reflectivity. Also, they provide no spatial information on the melting process.

To obtain both spatial resolution and better time resolution, and to measure the time profile of the reflectivity on a single-shot basis, we use a streak camera with a time resolution of 1.8 ps to detect the probe pulse.

2. Experimental setup

The experimental setup is shown in Fig. 1. The frequency-doubled output (30 ps, 532 nm) of a mode-locked Nd:YAG laser is split into a probe and a pump pulse. The duration of the probe pulse is stretched by splitting it in four, delaying the four resulting pulses with respect to each other, and recombining them spatially to form a longer probe pulse of 120 ps duration. The probe pulse then images an area around the 100-μm wide melting area onto the entrance slit of a streak camera (Hamamatsu Photonics C1587).

The entrance slit of the camera is split into two parts. The larger part is used to image the probe pulse, the smaller part to image a fraction of the pump pulse. The latter serves as the timing reference.

To enhance the sensitivity of our measurements, the probe pulse is *p*-polarized and the probe angle of incidence is 65°, close to Brewster's angle. At this angle the reflectivity of solid silicon is small (about 10%), leading to an increase in reflectivity on melting by a factor of 8.

3. Results and Discussion

The streak images of two measurements are shown in Figs. 2a and 2b. The time axis is displayed vertically, with time increasing from top to bottom. The full height of the image corresponds to 190 ps. The horizontal axis reflects the spatial profile. The pump pulse is shown on the left side and has a duration of about 30 ps. The stretched probe pulse covers most of the image. The bright part is where the silicon surface is melting. Spatially it reflects the Gaussian intensity profile of the pump pulse. The time profile allows one to study the melting dynamics.

Both measurements were performed at the same laser fluence. In the case shown in Fig. 2b, some surface irregularity leads to the formation of a surface plasma in the region where the absorbed energy is highest. The plasma absorbs the incoming probe light, leading to the dark area in the center of the melting region. This clearly emphasizes the need for spatial resolution. An integrating detector would give rise to erroneous conclusions about the reflectivity.[4]

Fig. 3 shows the reflectivity profile at the center of the melting region, between the two white lines, in Fig. 2a. The reflectivity reaches the value for liquid silicon within the 30-ps duration of the pump pulse. The high time resolution of the streak camera enables us to confirm that the reflectivity follows the trend predicted by numerical simulations of heating above the melting temperature in silicon.[2] According to a Drude model one expects a decrease in reflectivity of molten silicon when it is heated above the

melting temperature. The laser fluence in Figs. 2a and 2b is 470 mJ/cm^2 which is more than twice as large as the melting threshold for silicon (200 mJ/cm^2). A numerical solution of the one-dimensional heat equation shows that at this fluence the temperature of the liquid silicon exceeds the melting temperature by more than 1000 K.

Measurements with longer and more uniform probe pulses are currently in progress.

Acknowledgments

We thank Professor Malvezzi for his help with the experiment. MB acknowledges a Fellowship from the Netherlands Organization for Scientific Research (NWO). PS acknowledges a Ph.D.-Fellowship from AT&T Bell Laboratories. This work was supported by Hamamatsu Photonics K.K., and by the Joint Services Electronics Program under contract with Harvard University.[5]

References

1. J.M. Liu, H. Kurz and N. Bloembergen, *Appl. Phys. Lett.*, 41, 643 (1982)
2. P.M. Fauchet and K.D. Li, *Mat. Res. Soc. Symp. Proc.*, 100, 477 (1988)
3. D. von der Linde and N. Fabricius, *Appl. Phys. Lett.*, 41, 991 (1982)
4. I.A. Boyd, S.C. Moss, T.F. Bogess and A.L. Smirl, *Appl. Phys. Lett.*, 46, 366 (1985)
5. Contract number: N00014-84-K-046

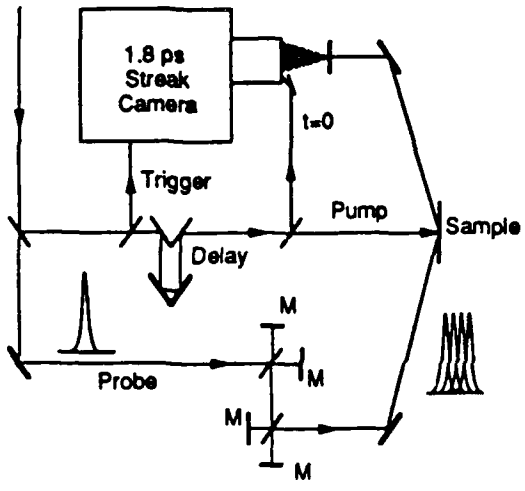

Fig. 1. Experimental setup

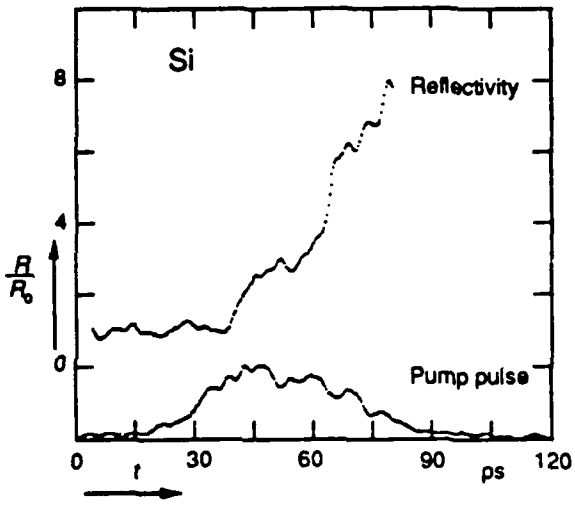

Fig. 3. Reflectivity of silicon during melting with a picosecond laser pulse. R_0 is the reflectivity of solid silicon. The lower trace shows the intensity of the pump pulse.

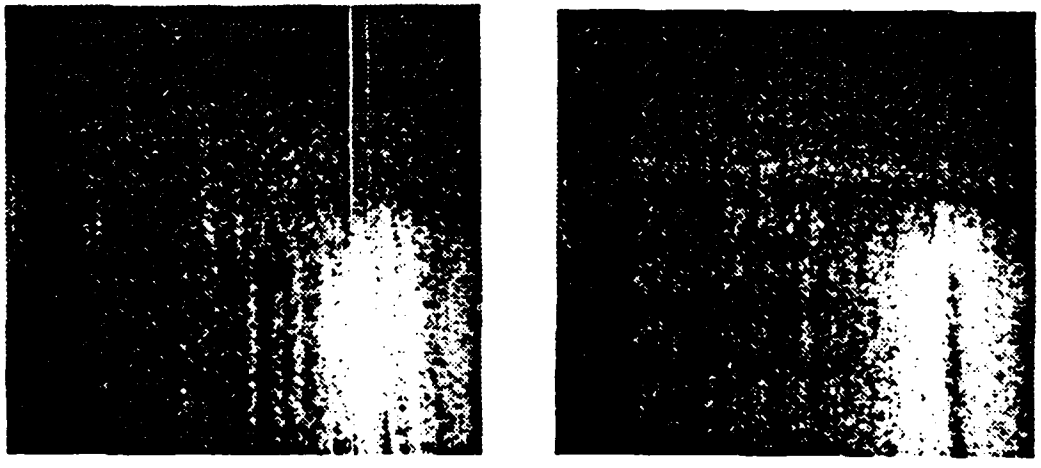

(a) (b)

Fig. 2. Streak camera images of laser melting of silicon. Laser fluence is 470 mJ/cm^2. The white lines in (a) indicate the region used for analysis of the reflectivity.

Ulrafast Phenomena VI
Ed. T. Yajima, K. Yoshihara, C.B. Harris, S. Shionoya
Springer Verlag, page 236

Single-shot reflectivity study of the picosecond melting of silicon using a streak camera

Juen-Kai Wang, Peter Saeta, Maarten Buijs, Marco Malvezzi,[1] *and Eric Mazur*

Division of Applied Sciences and Department of Physics, Harvard University, Cambridge, MA 02138, USA

1. Introduction

Numerous investigations on the phase transition of silicon during picosecond laser annealing have been performed in recent years. It has been well established that the silicon surface melts during a picosecond laser pulse.[2] Because liquid silicon is a metal, the reflectivity increases on melting. This has indeed been observed using optical pump-and-probe techniques.[2-4] Standard picosecond pump-and-probe measurements, however, have some serious inherent drawbacks. First, they cannot resolve reflectivity changes that occur on a time scale of a few picoseconds, because they integrate over the duration of the probe pulse (typically 20 ps or more). Second, they determine the time profile of the reflectivity for every pump fluence in a step-wise manner by varying the delay between the pump and the probe pulse. This introduces a large amount of scatter in the data points, due to shot-to-shot variations in the pump fluence, and requires a large amount of data to be taken for every time profile of the reflectivity. Also, they provide no spatial information on the melting process.

To obtain spatial resolution, a better time resolution, and to measure the time profile of the reflectivity on a single-shot basis, we use a streak camera with a time resolution of 1.8 ps for the detection of the probe pulse.

2. Experimental setup

The frequency-doubled output (30 ps, 532 nm) of a mode-locked Nd:YAG laser is split into a probe and a pump pulse. The duration of the probe pulse is stretched by splitting it in four, delaying the four resulting pulses with respect to each other, and recombining them spatially to form a longer probe pulse of 120 ps duration. The probe pulse then images an area around the 100-μm wide melting area onto the entrance slit of a streak camera (Hamamatsu Photonics C1587).

The entrance slit of the camera is split into two parts. The larger part is used to image the probe pulse, the smaller part to image a fraction of the pump pulse. The latter acts as the timing reference.

To enhance the sensitivity of our measurements, the probe pulse is *p*-polarized and the probe angle of incidence is chosen to be 65°, close to Brewster's angle. At this angle the

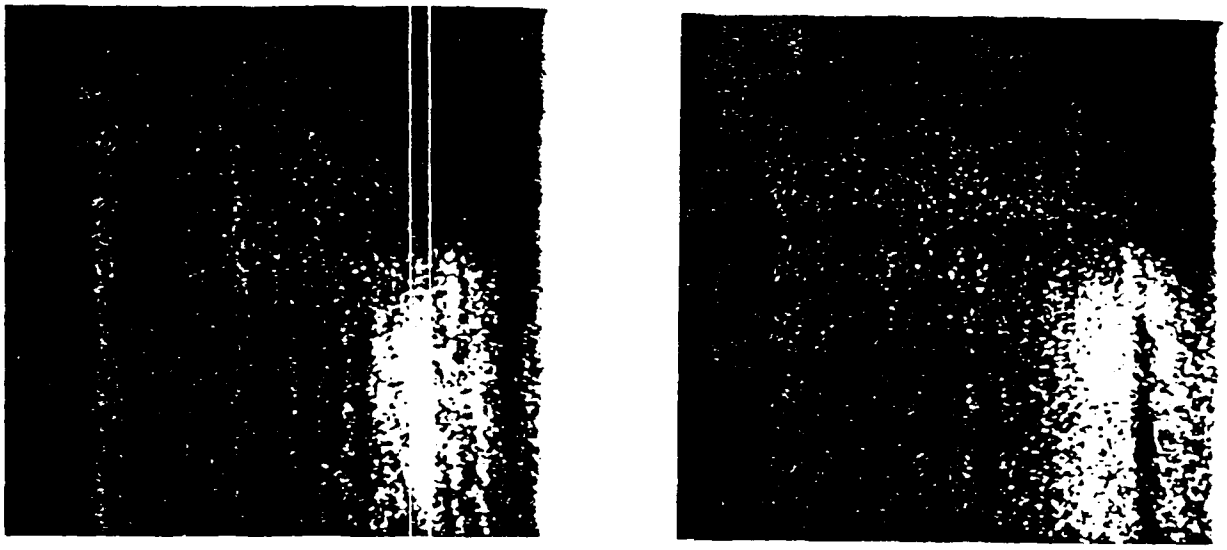

(a) (b)

Fig. 1. Streak camera images of laser melting of silicon. Laser fluence is 470 mJ/cm^2. The white lines in (a) indicate the region used for analysis of the reflectivity.

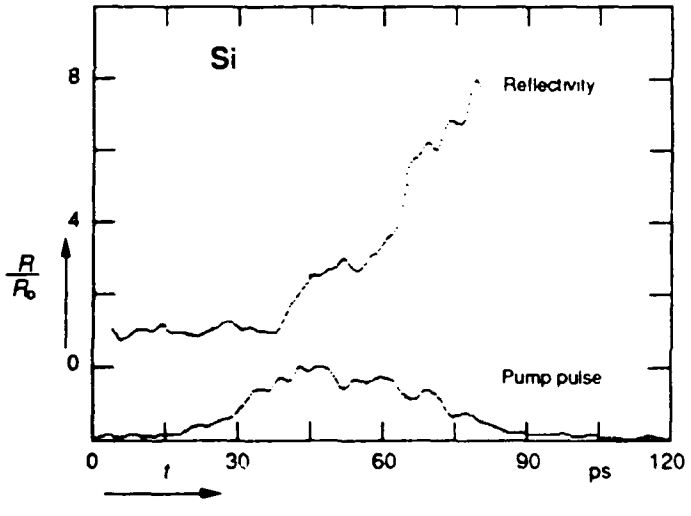

Fig. 2. Reflectivity of silicon during melting with a picosecond laser pulse. R_0 is the reflectivity of solid silicon. The lower trace shows the intensity of the pump pulse.

reflectivity of solid silicon is small (about 10%), leading to an increase in reflectivity on melting of a factor of 8.

3. Results and Discussion

The streak images of two measurements are shown in Figs. 1a and 1b. The time axis is displayed vertically, with time increasing from top to bottom. The full height of the image corresponds to 190 ps. The horizontal axis reflects the spatial profile. The pulse shown on the left side, with a width of about 30 ps, is the pump pulse. The stretched probe pulse covers most of the image. The bright part is where the silicon surface is melting. Spatially it reflects the Gaussian intensity profile of the pump pulse. The time profile allows one to study the melting dynamics.

Both measurements were performed at the same laser fluence. In the case shown in Fig. 1b, some surface irregularity leads to the formation of a plasma on the surface in the region where the absorbed energy is highest. The plasma scatters the incoming probe light, leading to the dark area in the center of the melting region. This clearly emphasizes the need for spatial resolution. An integrating detector would give rise to erroneous conclusions about the reflectivity.[5]

Fig. 2 shows the reflectivity profile at the center of the melting region, between the two white lines, in Fig. 1a. The reflectivity reaches the value for liquid silicon within the 30-ps duration of the pump pulse. The high time resolution of the streak camera enables us to confirm, that the reflectivity follows the trend predicted by numerical simulations of heating above the melting temperature in silicon.[3] According to a Drude model one expects a decrease in reflectivity of molten silicon when it is heated above the melting temperature. The laser fluence in Figs. 1a and 1b is 470 mJ/cm^2 which is more than twice as large as the melting threshold for silicon (200 mJ/cm^2). A numerical solution of the one-dimensional heat equation shows that at this fluence the temperature of the liquid silicon exceeds the melting temperature by more than 1000 K.

Measurements with longer and more uniform probe pulses are currently in progress.

Acknowledgments

MB acknowledges a Fellowship from the Netherlands Organization for Scientific Research (NWO). PS acknowledges a Ph.D.-Fellowship from AT&T Bell Laboratories. This work was supported by Hamamatsu Photonics K.K., and by the Joint Services Electronics Program under contract with Harvard University.[6]

References

1. Permanent address: Istituto di Fisica Applicata, Pavia, Italy
2. J.M. Liu, H. Kurz and N. Bloembergen, *Appl. Phys. Lett.*, 41, 643 (1982)
3. P.M. Fauchet and K.D. Li, *Mat. Res. Soc. Symp. Proc.*, 100, 477 (1988)
4. D. von der Linde and N. Fabricius, *Appl. Phys. Lett.*, 41, 991 (1982)
5. I.A. Boyd, S.C. Moss, T.F. Bogess and A.L. Smirl, *Appl. Phys. Lett.*, 46, 366 (1985)
6. Contract number: N00014-84-K-0465

OPTICAL PROPERTIES OF PICOSECOND LASER IRRADIATED GRAPHITE

A.M.MALVEZZI,G.REVERBERI AND N. BLOEMBERGEN
Division of Applied Sciences, Harvard University, Cambridge, MA 02138, USA

ABSTRACT

We have employed pump-and-probe techniques coupled to ellipsometry to measure the transient complex index of refraction at 1.064 μm of higly oriented pyrolitic graphite (HOPG) interacting with 20 ps, .532 μm laser pulses. When the laser pump fluence exceeds the threshold value for melting, measurements indicate a substantial decrease of both real and imaginary parts of the index of refraction, thus confirming that molten graphite becomes less metallic. Measurements provide also direct evidence of the insensitivity of our picosecond results to evaporation from the irradiated surface.

INTRODUCTION

High temperature phases of laser heated materials have recently been studied with several techniques. In particular, post irradiation diagnostics of nanosecond irradiated samples with optical and electron microscopy, Raman scattering, Rutherford backscattering etc. have determined the existence of a liquid state at high temperature in layered compounds such as graphite [1,2]. In our laboratory, instead, picosecond time resolved optical techniques have been used to investigate directly Highly Oriented Pyrolitic Graphite (HOPG) samples during the irradiation with 0.53 μm, 20 ps laser pulses. The advantage of this ultrashort excitation is that high surface temperatures are obtained with minimum irradiation energy, while optical probing at short times avoids effects connected with the evaporation from the sample surface [3].

Using time resolved pump and probe techniques, we have previously reported a net decrease of normal incidence reflectivity for some selected wavelengths in a range extending from the IR to the UV, when the laser excitation exceeded a given threshold fluence level [4,5]. The observations were consistent with a decrease, at high temperature, of the complex index of refraction and thus of the dielectric function of HOPG, indicating a less metallic behavior of the material.

In order to evaluate quantitatively the transient complex index of refraction $n_t = n + i\,k$, two simultaneous measurements must be performed on the sample under identical conditions. Since HOPG is highly absorbing, the easiest way is to measure the reflectivity of the sample at two different (orthogonal) polarizations at various angles of incidence [6]. This paper reports on the application of this ellipsometric technique to the case of graphite. The complex index of refraction of HOPG above the melting point has been deduced experimentally for a wavelength of 1.06 μm. The qualitative results previously obtained [4] are confirmed.

Mat. Res. Soc. Symp. Proc. Vol. 100. ©1988 Materials Research Society

EXPERIMENTAL METHOD

Our experimental setup consisted of a modified version of the usual pump and probe scheme. HOPG samples, with the c-axis perpendicular to the surface, were irradiated with 0.53 μm, 20 ps laser pulses. A second pulse at 1.06 μm, was passed through a variable delay line and a polarizer plus a $\lambda/2$ plate, in order to control the polarization. The reflected beam was analysed by a polarizing beam splitter in the two directions s- and p- , perpendicular and parallel to the plane of incidence, respectively. Signal to noise ratios greater than 10^3 for each polarization channel were obtained. The sample could be rotated so as to achieve angles of incidence of the probe beam between 13^o and 80^o. The angle between pump and probe beams was kept fixed at 7^o, a procedure which neither changed synchronization nor the ratio between pump and probe spot areas.

Absolute calibration was performed using glass, fused silica and crystalline silicon surfaces as calibration standards. Most of the errors associated with measurements illustrated in figures 3 - 5 are related to spot-to spot differences in reflectivity of our HOPG sample surface.

RESULTS AND DISCUSSION

Several sets of experimental runs as a function of incident laser fluence (J/cm^2) were performed with varying time delays between pump and probe pulses and at different angles of incidence. The general features of the s-reflectivity curves versus laser fluence are illustrated in figure 1 where the probe pulse impinging on the target at 75^o to the normal is delayed by

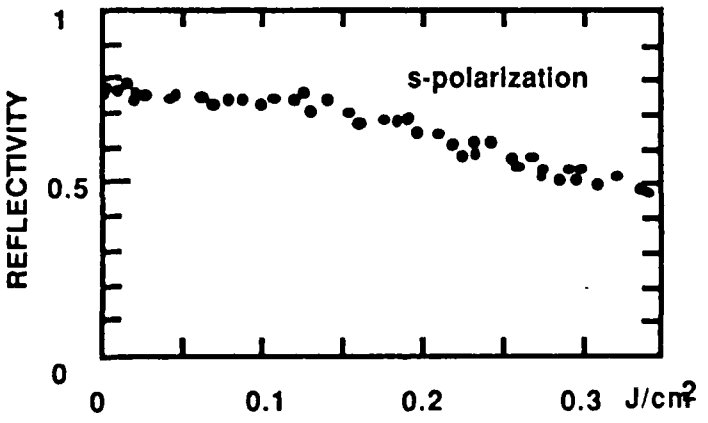

Figure 1: Graphite reflectivity at 1.06 μm for s-polarized radiation impinging at 75^o, as a function of the fluence of a 20 ps, 0.53 μm laser heating pulse, taken 200 ps after irradiation.

200 ps from the pump pulse. The reflectivity stays in general almost constant at lower pump fluence levels and exhibits a slow decrease above the critical fluence for melting, F_{th}. This decrease is more pronounced at low angles of incidence ϑ and tends to level off at high ϑ values. This behavior is similar to what is observed at normal incidence. Absolute p-reflectivity values are always less than the corresponding ones for the s-case. Their dependance versus laser fluence exhibits a more

complex behavior. The low fluence regime is characterized at delay times just after irradiation by a small reflectivity decrease with a recovery at fluences close to the critical value F_{th}. This behavior seems consistent with the formation and rapid decay of an excess of plasma density near the surface, as in the case of semiconducting surfaces. For $\vartheta < 60^{o}$, the onset of the phase transformation is indicated by a decrease of the reflectivity. For high angles of incidence, $\vartheta > 60^{o}$, on the contrary, the transition is marked by a sudden increase of the reflectivity, up to a factor of ≈ 2, which strikingly resembles what is observed in the case of semiconductors like silicon. Figure 2 illustrates one such case for $\vartheta = 75^{o}$ and a delay of 200 ps. As for silicon a reduction of the reflectivity is observed at high fluence. This may be interpreted as due to overheating of the absorbing liquid surface and to the effects of surface evaporation and ionization in a similar manner as occurred in liquid silicon.

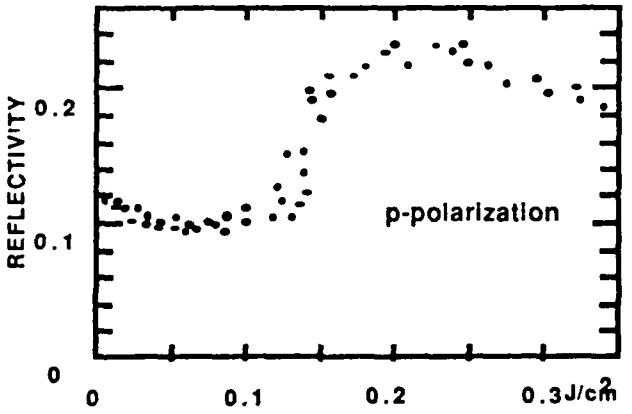

Figure 2: Graphite reflectivity at 1.06 μm for p-polarized radiation impinging at 75°, as a function of the fluence of a 20 ps, 0.53 μm laser heating pulse, taken 200 ps after irradiation.

Other information on these processes may be obtained by plotting our reflectivity data as a function of time for different excitation levels. In particular, figure 3 shows the time evolution of s-reflectivity at 75° incidence for fluences at and above the critical value F_{th} for surface melting. For all three fluence levels illustrated, the reflectivity appears to decrease initially during the laser pulse. At $F = F_{th}$, the decrease is followed by a recovery of the reflectivity in ≈ 200 ps to a constant final value R_{∞}. At higher fluences the intermediate reflectivity variations disappear. Instead, a sharper drop, continuing up to times ≈ 500 ps after irradiation, is apparent. It is followed by a slow recovery to R_{∞}, presumably connected with the cooling of the surface.

The corresponding variations of p-reflectivity with time are shown in figure 4. Here, the increase in reflectivity occurring at near-threshold fluence values only at later times indicates that for the first 200 ps after irradiation the cloud of evaporating material is not responsible for the complex reflectivity variations observed, which we attribute to the hot HOPG surface. The characteristic times for reflectivity increase are clearly dependent upon laser input fluence. They are consistent with an ultrafast phase transformation occurring at earlier times with higher irradiation levels. The fact that

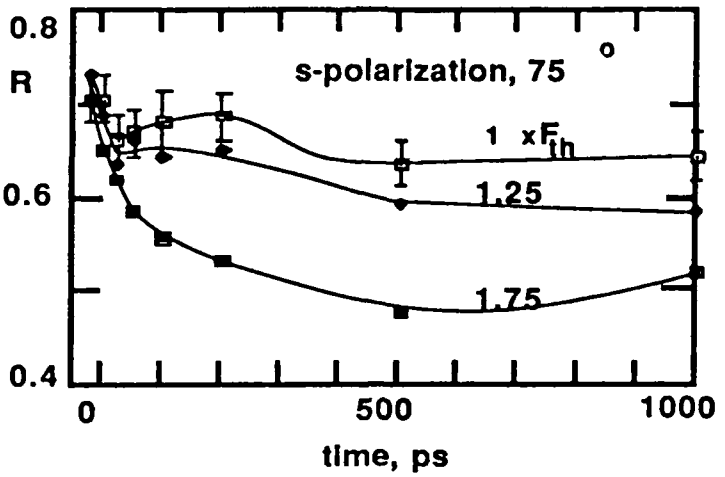

Figure 3: Time evolution of s-reflectivity in graphite for 1.06 μm radiation at 75° incidence angle, for the 20 ps, 0.53 μm pump fluence levels indicated. The critical fluence for surface melting, F_{th}, corresponds to 0.14 J/cm^2.

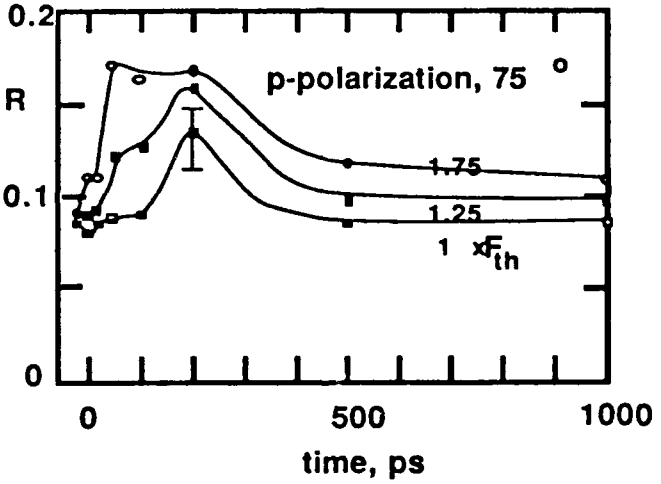

Figure 4: Time evolution of p-reflectivity in graphite for 1.06 μm radiation at 75° incidence angle, for the 20 ps, 0.53 μm pump fluence levels indicated. Note the different scale on the reflectivity axis.

the maximum of reflectivity is reached long after the exciting laser pulse may be due to the presence of interference effects connected with the formation and evolution of a molten layer on the surface of the sample. The observed changes in p-reflectivity reveal the extremely fast dynamics of the heating and cooling of HOPG. The decay of the high reflectivity phase can be interpreted as the onset of surface cooling due to both thermal conduction into the bulk and evaporation of material from the surface.

The variation of the experimental data taken at different angles of incidence are summarized in figure 5, where experimental p- and s-reflectivity obtained with F = 1.75 F_{th}, ≈200 ps after HOPG irradiation are plotted versus angle of incidence. The continuous, thin lines in figure 5 denote reflectivity of unirradiated HOPG as derived from our calibration measurements. These results correspond to an initial ordinary

complex index of refraction n_o = 2.9 + i 2.06, in agreement with published cw data [7]. Since graphite is a negative uniaxial crystal, its extraordinary index has some influence on the p-reflectivity of the HOPG sample. The low temperature p-reflectivity can be fitted best by assuming n_e = 2. +i 0.25

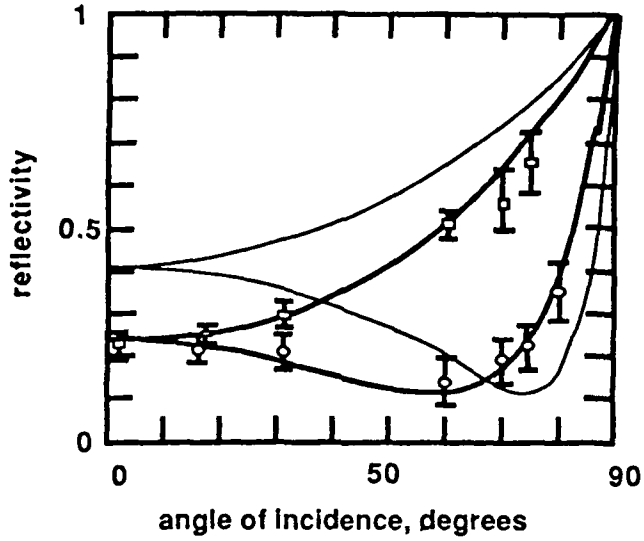

Figure 5: 1.06 μm s (upper curves) and p (lower curves) reflectivities of graphite versus angle of incidence. Continuous thin line: best fitted values at room temperature, evaluated with n_o = 2.9 + i 2.06, . Data points: measured reflectivities ≈200 ps after a 20 ps, 0.53 μm, 1.75 F_{th} excitation laser pulse. The thick continuous curve is calculated from the best fitting index of refraction n_{ht} = 1.3+i 1.2.

The two curves for p-reflectivity versus angle of incidence for room and high temperature, respectively, cross each other at an angle between 60 and 70°. This implies that the pseudo Brewster angle ϑ_{HT} for the high temperature case is smaller than the corresponding angle ϑ_{LT} at room temperature. This is per se an indication that graphite has a lower, transient index of refraction when excited above the critical fluence level F_{th}. The reflectivity measurements performed in this time range obviously are <u>not</u> affected by optical opacity generated by an evaporating cloud of material, since reflectivity changes at high fluence have an opposite sign with polarization.

Assuming isotropic conditions for the high temperature medium, the data illustated in figure 5 are consistent with a complex index of refraction n_{ht} ≈ 1.3+i 1.2, evaluated by best fitting to the experimental points. This value for n is smaller than the initial one, in agreement with our earlier measurements and interpretation [4]. In particular the pseudo Brewster angle in the high temperature phase is smaller than for room temperature HOPG, as the increase of p-reflectivity for high angles of incidence indicates. The data indicate that the high temperature phase is less metallic in character than graphite, and may even exhibit a band gap. The layered structure characteristic of graphite disappears due to cross linking. Perhaps the high temperature phase could be better modeled as a distorted diamond structure. Theoretical band calculations, based on an isotropic (cubic) structure, predict the existence of a bandgap [8]. Systematic investigations over a wavelength interval

extending from the ultraviolet to the infrared may eventually reveal the electronic structure of the high temperature phase. Such experiments are feasible by the techniques described in this note.

CONCLUSIONS

By coupling ultrashort laser techniques with ellipsometry, the index of refraction of materials in transient, out of equilibrium conditions may be directly evaluated. In particular, time resolved optical properties of materials heated above melting may be studied before substantial evaporation occurs. By extending this technique to a wide wavelengths interval,crucial information on the electronic structure of molten graphite might be obtained.

ACKNOWLEDGEMENTS

We wish to thank Dr. Chao Yen Huang for many important comments and suggestions throughout this work, which has been supported by the Office of Naval Research under contract N.00014-84-K-04654

REFERENCES

1. T.Venkatesan, D.C.Jacobson, J.M.Gibson, E.S.Elman, G.Braunstein M.S.Dresselhaus and G. Dresselhaus, Phys.Rev.Letters 53, 360 (1984)

2. J.S.Speck,J.Steinbeck, G.Brunstein, M.S.Dresselhaus, and T.Venkatesan, Mat. Res. Soc. Symp.Proc. 51, 263 (1986)

3. N.Bloembergen, Mat. Res. Soc. Symp.Proc. 51, 3 (1986)

4. A.M.Malvezzi, N.Bloembergen and C.Y.Huang, Phys.Rev.Letters 57, 146 (1986)

5. C.Y.Huang, A.M.Malvezzi, N.Bloembergen and J.M.Liu, Mat. Res. Soc. Proc. 51, 245 (1986)

6. P.M.Fauchet, W.L.Nigham Jr, Appl. Phys. Letters 48, 785 (1986)

7. E.A.Taft and H.R.Philipp, Phys.Rev.138, A197 (1965)

8. M.Cohen, private communication

TIME-RESOLVED PICOSECOND REFLECTIVITY STUDY OF LASER-EXCITED LAYERED COMPOUNDS

C.Y.HUANG*, A.M.MALVEZZI**, N. BLOEMBERGEN** AND F.J.DI SALVO, JR.***

* Los Alamos National Laboratory, Los Alamos, New Mexico USA
** Division of Applied Sciences, Harvard University, Cambridge, MA 02138, USA
*** AT&T Bell Laboratories, Murray Hill, N.J. 07974, USA

ABSTRACT

We have employed the pump-and-probe technique to perform picosecond time resolved measurements of the reflectivity changes in two archetypal layered compounds, 1T-TiS_2 and 1T-$TiSe_2$ probed at 1.064 μm after pumping by 20 ps, .532 μm laser pulses. At the threshold fluence, ~ 40 mJ/cm^2, the reflectivity drops sharply, marking the occurrence of a phase transformation on the surface of the sample. Above threshold, the reflectivity reaches a value as low as ~0.1 at high fluences, strongly suggesting that, like in graphite, the high temperature phase is not metallic.

INTRODUCTION

Very recently, the transient optical properties of crystalline graphite surfaces excited by visible picosecond laser pulses have been investigated with 20 - 30 ps time resolution [1,2]. Reflectivity measurements at low excitation levels have revealed the presence of a fast decaying elecron-hole plasma evolving from the initial semimetallic configuration. More interestingly, at a well defined pump threshold value of ~140 mJ/cm^2 a phase transition occurs, which is characterized by lower reflectivity values. We have concluded that the high temperature phase is not metallic, having a lower value of the index of refraction, but, rather, intermediate between the one of graphite and that of diamond. This unexpected new phase is presumably caused by a strong perturbation of the spatial arrangement of carbon atoms in the graphite lattice, which consists of hexagonally arranged, loosely stacked atomic layers. The question thus arises whether the electronic properties of the high temperature phase originate from a particular initial structure. For this reason, it is of interest to investigate other archetypal layered compounds.

In this paper, we have chosen two crystalline layered compounds, 1T-TiS_2 and 1T-$TiSe_2$. The titanium atoms are octahedrally coordinated with chalcogen atoms forming a chalcogen-metal-chalcogen sandwich layer configuration.[3] In a plane, atoms are hexagonally packed. However, the coordination around the non-metal is quite lopsided, leading to the marked cleavage properties perpendicular to the hexagonal symmetry axis. The basic atomic structure of loosely coupled X - Ti - X (X = S, Se) atom sheet sandwiches makes the mechanical, thermal and electrical properties extremely anisotropic, like those of graphite. The lattice constants for TiS_2 [4] are slightly smaller

Mat. Res. Soc. Symp. Pr. - Vol. 74. - 1987 Materials Research Society

than those of $TiSe_2$.[5] It is now well established that the former is an extrinsic semiconductor with an indirect band gap of 0.2 - 0.3 eV, [6-9] but it is normally non-stoichiometric and thus exhibits metallic conductivity arising from an excess of Ti atoms. $TiSe_2$ is an intrinsic semimetal.[10-12] All these physical properties are similar to those of graphite. Hence, it is of importance to perform experiments on the high temperature regime for these compounds and then compare the results with those of highly oriented pyrolitic graphite (HOPG).[1,2]

EXPERIMENTAL RESULTS

We have performed a series of time-resolved picosecond pump-and-probe measurements similar to those made on HOPG.[1,2] The pumping was provided by 20 ps pulses at 0.532 μm by frequency doubling the output of an active-passive mode-locked Nd-YAG laser system. The variable time delayed 1.064 μm pulses

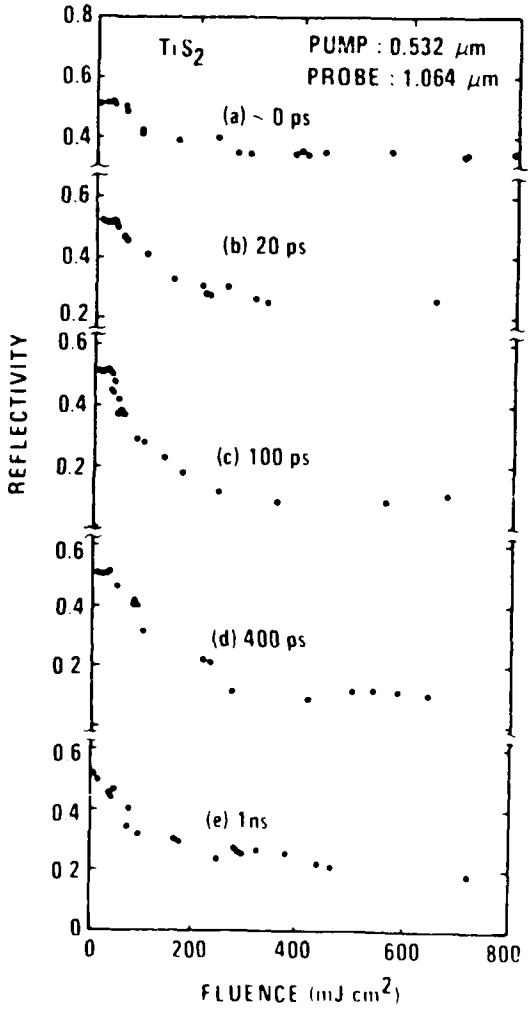

Figure 1. Reflectivity of 1T-TiS_2 at 1.064 μm as a function of 0.532 μm pump fluence at the delay times shown.

were used to monitor the reflectivity at the center of the excited surface. Near normal incidence angles are employed for both pump and probe laser beams. All the samples used in this work were single crystals.

We have found that a damage spot appears on the sample above a fixed green pump fluence value. Our optical micrographs show the appearance of a black ring marking the damage area. Its formation suggests the occurrence of a phase transformation. The size of the ring strictly follows the spatial variations of the gaussian fluence distribution of the laser beam, indicating the thermal origin of the effect. The extrapolated value of the threshold fluence is $F_{th} = 43$ mJ/cm^2

Figure 1 shows our reflectivity results obtained on 1T-TiS_2 single crystal probed at 1.064 μm as a function of the 0.532 μm pumping fluence at the different delay times t_d. As Figure 1 (a - d) shows, the reflectivity drops sharply around 40 mJ/cm^2 for all positive delay times t_d, in agreement with the value of F_{th} obtained from the post-experimental examination of the damaged area discussed above. Consequently, like in HOPG, we may identify F_{th} as the threshold fluence for an ultrafast phase transition. The drop is particularly pronounced at ≈100 ps, where the reflectivity reaches a value as low as ≈ 0.1 from the initial value of 0.52. This variation exceeds the similar variation in the reflectivity observed in HOPG at the same wavelength. It has been shown that for a delay time of ≈ 10 ps, only one atomic layer can escape the surface of the sample,[13] giving a negligible contribution to the reflectivity. As shown in Fig. 1-(a), even when the probe pulse overlaps the pump pulse (t_d ~ 0 ps) the reflectivity drops above the threshold fluence value, thus clearly demonstrating that the decrease of the reflectivity is not due to evaporation.

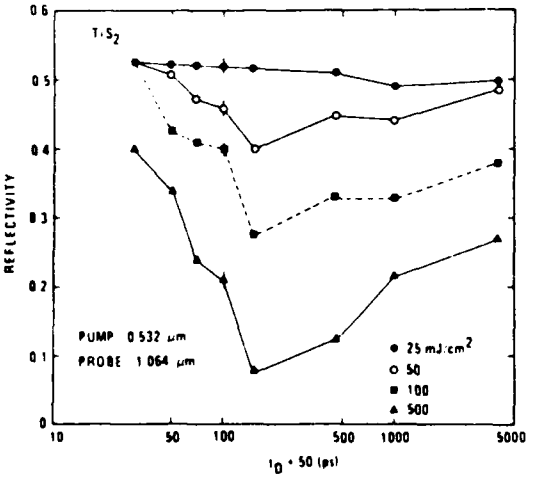

Figure 2. Reflectivity of 1T-TiS_2 at 1.064 μm as a function of probe delay time t_d, for various pump fluences. The origin of t_d is shifted by 50 ps.

In Figure 2 we plot the measured reflectivity as a function of the delay time, t_d. Note that the time origin in the abscissa has been shifted by 50 ps in order to accommodate the data taken

before the arrival of the pump pulse. At 25 mJ/cm^2, the reflectivity is practically time independent. At fluences greater than F_{th}, the reflectivity values are decreasing at first, reaching a minimum at ≈ 200 ps, and then recover to higher levels. This behavior of the reflectivity clearly indicates the occurrence of a transient new phase induced by the pump laser pulse and presumably terminated by heat dissipation in the bulk of the crystal. The lack of data on the thermal properties of these compounds prevents quantitative estimates. The final value $R_\infty \approx .35$ of the reflectivity taken at very long delay times is lower than the initial one, indicating the presence of a permanent damage on the surface as soon as the threshold fluence value F_{th} is exceeded.

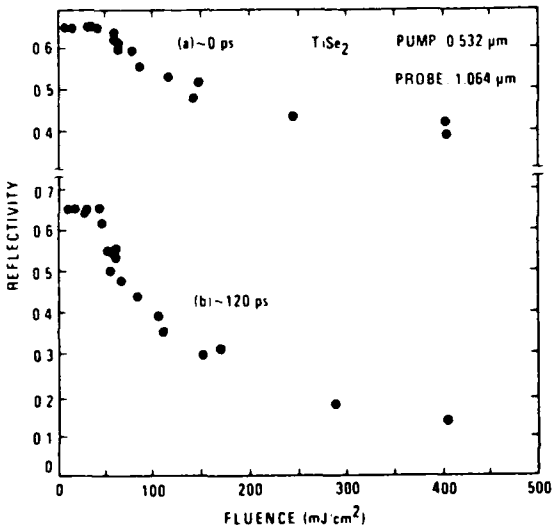

Figure 3. Reflectivity of 1T-$TiSe_2$ at 1.064 μm as a function of 0.532 μm pump fluence at the delay (a) - 0 ps and (b) - 120 ps.

The reflectivity data for the semimetal 1T-$TiSe_2$, illustrated in Figure 3, are qualitatively similar to those for the semiconductor 1T-TiS_2. Also, the temporal behavior at the different fluences appears similar to the one presented in Fig 2. Our results indicate that the high temperature optical behavior of these two materials is independent of the initial electronic properties of these two layered compounds.

CONCLUSIONS

The transient optical properties of TiS_2 and $TiSe_2$ crystals under picosecond visible excitation have been investigated at 1.064 μm with picosecond time resolution. Below the threshold fluence of ≈40 mJ/cm^2 for 20 ps, 0.532 μm pump laser pulses, no significant changes in the reflectivity at 1.064 μm for both materials have been observed. Due to the small value of the band gap in TiS_2 as compared to the probing photon energy, the plasma contribution to the dielectric constant appears to be negligible. Presumably, longer wavelengths and/or larger incidence angles have to be used to detect plasma effects from the optical response of these materials.

At fluences exceeding the threshold value F_{th} the reflectivity decreases to values as low as ≈ 0.1. These reflectivity changes occur during the exciting laser pulse. This suggests that the high temperature phase of these compounds is not metallic. The laser pump pulse gives rise to a transition from a semimetallic or small-band-gap semiconducting electronic structure into a rather transparent phase, where a smaller number of carriers interacts with the incoming laser pulse. Light can therefore travel into the material for distances exceeding the original extinction depth. Comparison [14] of the morphology of picosecond with nanosecond laser irradiated graphite indicate that ultrafast melting occurs at fluences exceeding F_{th}. Similar considerations apply here for $TiSe_2$ and TiS_2 , the critical value for melting being lower due to the different optical and thermal properties of these compounds.

This comparative study suggests that a similar, non-metallic high temperature phase exists for archetypal layered structures other than graphite. The electronic properties at high temperatures could originate from the initial presence of a layered structure which undergoes heavy disruption under laser excitation. A deeper insight, however, is necessary to unravel the true nature of the structure. The transient optical properties, as derived i.e. by pump-and-probe experiments or time-resolved ellipsometry at different wavelengths, can provide useful information if coupled with other firm optical and thermal data on the materials under study.

ACKNOWLEDGMENTS

This work is supported by the U.S. Department of Energy and by the Office of Naval Research under contract N00014-85-K-0684.

REFERENCES

1. C.Y.Huang, A.M.Malvezzi, N.Bloembergen and J.M.Liu, *Mat. Res. Soc. Proc.* 51,245 (1986)
2. A.M.Malvezzi, N.Bloembergen, and C.Y.Huang, *Phys. Rev. Lett.* 57, 146 (1986)
3. See, for example, J.A.Wilson and A.D.Yoffe, *Adv. Phys.* 18, 193 (1969)
4. J.Bernard and Y.Jeannin, in *Advances in Chemistry, Non - Stoichiometric Compounds*, p.191 (1961), American Chemical Society, Washington, D.C.
5. D.L.Greenway and R.Nitsche, *J. Phys. Chem. Solids* 26, 1445 (1965)
6. C.H.Chen, W.Fabian, F.C.Brown, K.C.Woo, B.Davis, and B.Delong,*Phys. Rev.* B 21, 615 (1980)
7. J.J.Barry, H.P.Hughes, P.C.Klipstein and R.H.Friend, *J. Phys.* C 16, 393 (1983)
8. P.C.Klipstein and R.H.Friend, *J. Phys.* C 17, 2713 (1984)
9. H.P.Vaterlaus and F.Levy, *J. Phys.* C 18, 2351 (1985)
10. R.H.Friend, D.Jerome, W.Y.Liang, J.C.Mikkelsen, and A.D.Yoffe,*J. Phys.* C 10, L705 (1977)
11. R.Z.Bachrock, M.Skibowski, and F.C.Brown, *Phys. Rev. Lett.* 37, 40 (1976)
12. F.J.DiSalvo, D.E.Moncton and J.V.Waszezak, *Phys. Rev.* B

14, 4321 (1976)
13. N.Bloembergen, *Mat. Res. Soc. Proc.* 51, 3 (1986)
14. J.Steinbeck, G.Braunstein, J. Speck, M.S.Dresselhaus, C.Y.Huang, A.M.Malvezzi and N.Bloembergen, *Mat. Res. Soc. Proc.*, this volume.

Ultrafast Phenomena V: Proceedings of the Fifth USA Meeting, eds. G.R. Fleming ...
A.E. Siegman (Springer-Verlag, New York, 1986), pp. 174-178

Thermodynamics and Kinetics of Melting, Evaporation and Crystallization, Induced by Picosecond Pulsed Laser Irradiation

F. Spaepen

Division of Applied Sciences, Harvard University,
Cambridge, MA 02138, USA

1. Introduction

The irradiation of a strongly absorbing solid surface with a short laser pulse is a means of concentrating thermal energy in a very thin layer. The timescale considered in this paper is greater than 1 ps, which is longer than the time constants for most electronic relaxation processes, so that only thermal effects need be considered [1]. In a strongly absorbing solid (metal, UV on semiconductors) the absorption depth, α^{-1} (α: absorption coefficient), is less than the thermal diffusion length during irradiation, $l_T = (D_{th} t_p)^{1/2}$ (D_{th}: thermal diffusivity; t_p: pulse length). For a 30 ps pulse on iron, the example used in all further discussion, these lengths are 200 Å and 500 Å, respectively. A general discussion of the two regimes corresponding to the relative values of α^{-1} and l_T can be found in a review paper by Bloembergen [2]. It is worth noting that for $t_p < 1$ps, $l_T < \alpha^{-1}$, so that shortening the pulse further no longer leads to a steeper temperature gradient and a higher quench rate.

If the fluence is low enough so that no visible permanent surface damage occurs (typically around 100 mJ/cm^2), a liquid layer of thickness l_T with a temperature of several thousand degrees is created during the irradiation. Further melt-in, to a maximum thickness d of a few thousand Å, occurs until the crystal-melt interface temperature drops to the equilibrium melting temperature, T_m; this stage lasts on the order of 100 ps. Upon further cooling, the interface temperature drops below T_m, and the crystal regrows. The thermal parameters of this cooling process can be estimated simply by a dimensional analysis based on the thickness of the molten layer, d, and the temperature of the melt, T_m, as shown in Table 1 [3].

Table 1. Thermal Parameters in Melt Quenching of Metals with a 30 ps Laser Pulse. From [3]

Melt temperature	T_m	$= 10^3$ K
Melt thickness	d	$= 10^{-7}$ m
Temperature gradient	$\nabla T = T_m/d$	$= 10^{10}$ K/m
Cooling rate	$\dot{T} = D_{th} \nabla T/d$	$= 10^{12}$ K/s
Melt lifetime	$\tau = T_m/\dot{T}$	$= 10^{-9}$ s
Isotherm velocity	$u_T = \dot{T}/\nabla T$	$= 100$ m/s
Heat-flow limited crystal growth velocity	$u_h = \kappa \nabla T/ \Delta H_{c,v}$	$= 230$ m/s

The metastable phases formed in this process are: the crystal overheated above T_m, the liquid overheated above the boiling point, T_b, the liquid undercooled below T_m, and, possibly, new metastable crystalline phases or glasses. This paper gives a concise review of the thermodynamic stability of these phases, and the kinetics of the transitions between them.

2 Kinetics of Crystallization

The theory of the motion of interphase boundaries has been reviewed in detail in a number of papers [4]. The results for crystallization, which are easily generalized for other transitions, can be summarized as follows. The crystal growth velocity can be written as

$$u = f k \lambda [1 - \exp(- \frac{\Delta G_c}{RT_i})] \quad , \tag{1}$$

where k is the atom jump frequency across the crystal-melt interface, f is the fraction of interface sites that can incorporate a new atom, λ is the interatomic distance, ΔG_c is the difference in molar free energy between crystal and melt, and T_i is the interface temperature. If the undercooling of the interface, $\Delta T_i = T_m - T_i$, is small, (1) can be linearized to

$$u = k \lambda \ (\Delta T_i / T_i) \quad . \tag{2}$$

The crystal growth rate also depends on the rate at which the heat of crystallization, $\Delta H_{c,v}$ per unit volume, can be removed. Since this must occur by heat flow down the temperature gradient at the interface, $\nabla_i T$, the heat flux, J, must obey the relations

$$J = u \Delta H_{c,v} = \kappa \nabla_i T \quad , \tag{3}$$

where κ is the thermal conductivity. Equation (3) can be turned around to define a heat flow-limited velocity:

$$u_h = \kappa \ \nabla_i T / \Delta H_{c,v} \quad , \tag{4}$$

which, for the example used here, is also listed in Table 1. Combining (2) and (4) then gives for metals

$$u_h / k \lambda = (T_m - T_i) / T_i \quad . \tag{5}$$

The maximum growth velocity of a crystal, $u_{max} = k\lambda$, is determined by the nature of the atomic rearrangements that control the growth process. In pure metals, dilute alloys or compounds with simple crystal structures, k can be taken as the frequency of thermal vibration (~ Debye frequency), so that $u_{max} \sim u_s$, the speed of sound in the liquid, which is around 3000 m/s for Fe. This is called the *collision-controlled* regime, because the growth occurs by simple impingement of the liquid atoms onto the crystal. This is confirmed by direct measurements of the growth velocity of pure metals and disordered alloys (Au, Cu, Cu-Au) by transient reflectivity [5] which yield large values (>100 m/s) that can only be accounted for by a collision-controlled mechanism. From (5) and the values from Table I, the interface in Fe is found to be undercooled by only 128 K. An undercooling of at least 295 K is required for homogeneous crystal nucleation to be appreciable [6].

In more concentrated alloys or in compounds with a more complicated crystal structure, where a change of the nearest neighbor configuration, i.e. diffusion, is necessary, the jump frequency can be taken as D/λ^2, and

$u_{max,D} = D_l/\lambda$, which is on the order of 10 m/s. This is the *diffusion-controlled* regime. Table I shows that for picosecond laser quenching $u_{max,D} << u_T, u_h$, so that this type of growth can easily be suppressed. The interface temperature drops far below T_m, and glasses can be formed. This is confirmed by numerous experiments on binary metallic systems (e.g., Ni-Nb [7]), in which glasses have been formed by ps irradiation at compositions where the intermetallic crystalline compounds have a large unit cell, or in which long-range chemical order must be established.

3. The Overheated Crystal

Melting of a crystal is a first-order transition, which usually occurs heterogeneously, i.e., by nucleation of the liquid and motion of a liquid-crystal interface. Since for most materials $\sigma_{cv} > \sigma_{lv} + \sigma_{cl}$ (σ_{ij}: surface tension of the interface between phases i and j; c: crystal; v: vapor; l: liquid), there is no barrier to nucleation of the liquid at the surface of the pure crystal [8]. It should be kept in mind, however, that, if the crystal is covered with a high melting layer (e.g., an oxide) and the surface tension of the resulting interface is low, nucleation of the melt may require some overheating of the crystal.

The motion of the crystal-melt interface is governed by the kinetics described in Section 2. During the initial stages of the melt-in phase the temperature gradients are an order of magnitude greater than during regrowth. This means that the heat-flow limited crystal growth velocity, given by (4) is also an order of magnitude greater than the value listed in Table I, or about 2000 m/s. For pure metals, where $u_{max} = u_s \sim 3000$ m/s, (5) gives for the overheating: $\Delta T_i = 0.66\ T_i$, which for Fe corresponds to an overheating of several thousand degrees. For materials where melting is diffusion-limited, the overheating is even higher.

The overheating required to make homogeneous nucleation of the melt (i.e., in the interior of the crystal) the dominant mechanism can be estimated from classical nucleation theory [8], which gives the following expression for the *steady state* nucleation frequency (number of nuclei per unit volume and time):

$$I = N\,k \exp\left(-\frac{16\pi}{3}\frac{\sigma^3}{\Delta G_v^2\, k_B T}\right), \qquad (6)$$

where N is the number of atoms per unit volume, k is the interfacial jump frequency, ΔG_v is the free energy difference per unit volume, σ is the crystal-melt interfacial tension, and k_B is Boltzmann's constant.

The minimum nucleation frequency required can be estimated as: $I_{min} = \alpha / a^2 t_p$, where a is the minimum lateral distance between nuclei for inducing melting throughout the layer. Using $a = 1\mu m$ gives a value for I_{min} of 10^{30} $m^{-3}s^{-1}$. (It should be kept in mind that the analysis is very insensitive to the choice of I_{min}). Using a conservatively high estimate for σ, 0.3 N/m [6], an overheating of 600 K is found to be sufficient to exceed I_{min} in Fe. The transient time for establishing the steady-state nucleation rate [9] can be estimated as the time required to assemble a critical nucleus of radius $r^* = -2\sigma/\Delta G_v$, which is $r^*/k\lambda$; for the example of Fe overheated by 600 K, this is only a few ps, so that homogeneous nucleation of the melt can be considered possible here.

For systems where the melting kinetics are relatively slow (i.e. the jump frequency, k, scaling both nucleation and growth is small) it is possible to overheat far enough to reach the stability limit of the crystal. This is the temperature at which the shear modulus, μ, vanishes, and at

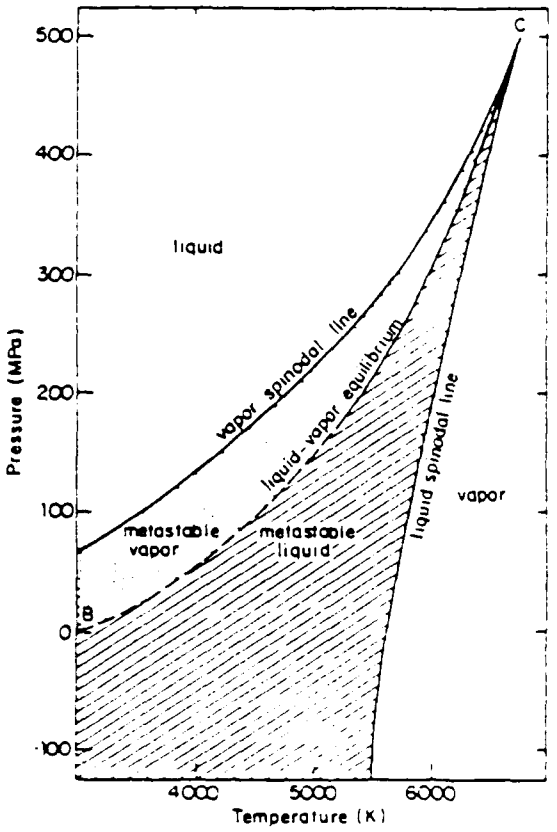

Fig. 1. P-T diagram for Fe, calculated from the van der Waals model and the critical parameters [14].

which melting can occur homogeneously by unlimited thermal shear displacements throughout the crystal. An extrapolation based on typical values of $d\mu/dT$ [10] sets this stability limit at about $2T_m$.

4 The Overheated Liquid

That liquids can be overheated considerably above their melting temperature is a well-known experimental fact [11], which has been qualitatively understood since van der Waals (Figure 1). The liquid can be overheated into the metastable region, where nucleation of a vapor bubble is necessary to induce the transformation, up to the spinodal line, where the liquid-vapor surface tension, σ_{lv}, and hence the nucleation barrier, vanish. Figure 1 shows that at atmospheric pressure (0.1 MPa), this instability occurs at 5700 K.

A calculation of the rate of homogeneous bubble nucleation, based on the classical expression similar to (6), taking into account the roughly linear decrease of σ_{lv} with temperature to the spinodal [12], shows that the temperature of the overheated liquid must be within a few hundred degrees from the spinodal for the nucleation rate to exceed $I_{min} = 10^{30}$ $m^{-3}s^{-1}$, estimated above. An estimate of the transient time for this transformation is $r^*/\Gamma\lambda^3$ ($\Gamma = p/\sqrt{2\pi mkT}$, the impingement rate of the vapor atoms), which is 7 ps for the present example. Given that this is a lower limit (perfect sticking is assumed in calculating Γ), and that the extreme overheat required for nucleation is only present during a fraction of t_p, the transient effects probably enhance the stability of the overheated liquid.

In a typical ps melt quenching experiment the fluence is not high enough to reach the extreme temperatures required for bulk vaporization.

Only surface evaporation needs to be considered, which can be estimated conveniently from the impingement rate, Γ, of the equilibrium vapor phase. It has been shown that the loss of mass and energy by this mode is negligible in ps experiments [13].

The permanent surface damage (holes) sometimes observed in ps experiments is therefore not due to direct evaporation, but to *mechanical* displacement of the liquid by the recoil pressure of the evaporating atoms. This is confirmed by the morphology of the displaced material. Direct evidence of the recoil pressure can be obtained by observing the vibration of a metallic reed pulse irradiated at one end and clamped at the other [14].

The author's work in this area is supported by the Office of Naval Research under contract number N00014-85-K-0684.

References

1. For a review of these relaxation processes, see W.L. Brown: Mat. Res. Soc. Symp. Proc. 23, 9 (1984).
2. N. Bloembergen: In *Laser-Solid Interactions and Laser Processing*, ed. by S. D. Ferris, H.J. Leamy and J.M. Poate (AIP, New York 1979) p. 1.
3. F. Spaepen and C.J. Lin: In *Amorphous Metals and Non-Equilibrium Processing*, ed. by M. von Allmen (Les Editions de Physique, Les Ulis, France 1984), p. 65.
4. F. Spaepen and D. Turnbull: In *Laser Processing of Semiconductors*, ed. by J.M. Poate and J.W. Mayer (Academic, NY 1982), p. 15.
5. C.A. MacDonald, A.M. Malvezzi and F. Spaepen: Mat. Res. Soc. Symp. Proc. 51, (1985) in press.
6. D. Turnbull: J.Appl. Phys. 21, 1022 (1950).
7. C.J. Lin and F. Spaepen: Acta Metallurgica 34, in press.
8. D. Turnbull: Sol. St. Phys. 3, 225 (1956)
9. K.F. Kelton, A.L. Greer and C.V. Thompson: J. Chem. Phys. 79, 6261 (1983). This paper also contains an extensive review of earlier work.
10. H.J. Frost and M.F. Ashby: *Deformation-Mechanism Maps* (Pergamon, NY 1982).
11. R.E. Apfel: J. Acoust. Soc. Am. 49, 145 (1971).
12. J.W. Cann and J.E. Hilliard: J. Chem. Phys. 28 , 258 (1958).
13. C.J. Lin: Ph.D. thesis, Harvard University (1983).
14. Landolt-Börnstein Tables, Vol. II, Part 1, Mechanisch-Thermische Zustandgrössen, ed. by H. Borchers et al. (Springer, Berlin 1971) p. 332.

Hume-Rothery Symposium on Undercooled Alloy Phases, TMS-AIME Symposia Proceedings (1986), eds. E.W. Collings and C.C. Koch, pp. 187-205

METASTABLE STATES IN PULSED LASER QUENCHING

Frans Spaepen

Division of Applied Sciences
Harvard University
Cambridge, MA 02138

It is reviewed how irradiation of a metallic surface with a short laser pulse leads to the successive formation of these metastable states: overheated crystal, overheated liquid, undercooled liquid, and metastable crystal or glass. The stability of a liquid overheated above its melting temperature is analyzed. The thermodynamics and kinetics of melting and crystallization of pure metals and alloys are reviewed. The results of quenching experiments on the Nb-Si system are used to illustrate how phases with high isotropy and small unit cell size are kinetically favored.

Introduction

Irradiating the surface of a strongly absorbing solid (metal, semiconductor) with a short laser pulse is a method for depositing thermal energy in a very thin surface layer, which, as a result, is first melted and subsequently quenched at a very high rate. Picosecond laser pulsing can produce quench rates exceeding 10^{12} K/s, making it the fastest liquid quenching method available.

In the first part of this paper the three stages of the process (energy deposition, melt-in, and cooling) are analyzed in some detail, and three metastable states are identified: the overheated crystalline solid (above its melting point), the overheated liquid (above the boiling point), and the undercooled liquid (below the melting point).

The second part of the paper is a detailed analysis of the overheated liquid state. It is shown that the liquid can remain in this metastable state over a considerable temperature range above its boiling point, and that, as a result, the loss of mass or energy by evaporation is negligible in picosecond laser quenching.

In the third part of the paper the thermodynamic restrictions on the type of transformations that can occur on the very short timescale of the laser quenching process are discussed. The selection of the actual transformation from the remaining allowed ones depends on the kinetics of the competing crystallization processes. Depending on the degree of structural rearrangement required to form a crystal from the melt, the process can be collision- or diffusion-controlled. It will be shown that only for the simplest crystal structures or dilute solutions is growth collision-controlled and fast enough to be insuppressible, even by picosecond laser quenching.

In the last part of the paper, two applications are presented. First, it is demonstrated that fast pulsed laser irradiation is one of the few methods available for overheating metals far above their melting temperature. As an example of the solidification products obtained by pulsed laser quenching, a set of recent experiments on the Nb-Si system is reviewed. It is an illustration of the kinetic hierarchy, discussed by Turnbull in the first paper of these proceedings, in which the formation of isotropic systems and systems with small unit cells is kinetically favored.

Laser Processing Mechanism

A number of detailed analyses have been made of the processes of energy deposition, heating and cooling in pulsed laser irradiation of solid surfaces

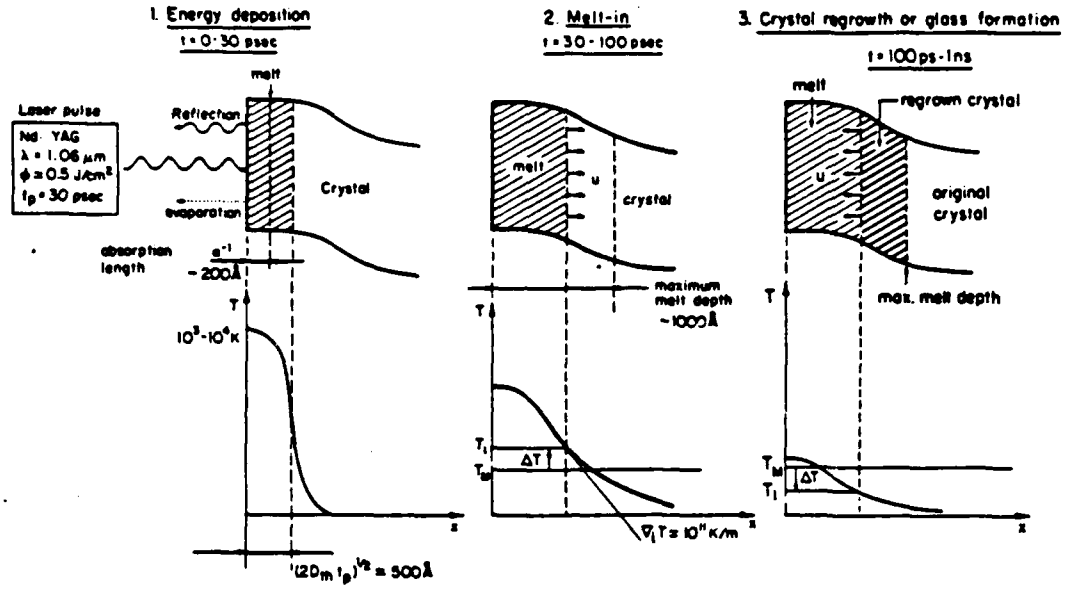

Fig. 1 - Schematic illustration of the mechanism of pulsed laser quenching.

(1-3). These three stages are illustrated in Figure 1, with parameters corresponding to the experiments to be described later.

During the first stage, the laser energy is deposited in a layer of thickness α^{-1}, where α is the absorption coefficient. For optical light on metals, or for UV light on semiconductors, this layer is a few hundred Å thick. Since the transfer of the energy from the electrons, which interact with the light, to the lattice occurs within less than 1 ps (4), the energy deposition process, which lasts for the duration of the pulse, t_p, can be considered a purely thermal one (5). The thermal diffusion length during that time is $\ell_T = (2D_{th}t_p)^{1/2}$, which, for metals is between 250 and 700 Å, depending on the thermal diffusivity ($D_{th} = 10^{-4}$ to 10^{-5} m^2/s). For fluences, ϕ, in the range indicated in Figure 1, a layer of thickness ℓ_T is melted and heated to several thousand degrees.

Note that for a pulse duration of less than 1 ps, ℓ_T is less than α^{-1}. The thickness of the initial molten layer, and hence also the thermal gradients, are then independent of the pulse duration. Femtosecond pulses, therefore, although very useful for time-resolved spectroscopy of the various phenomena associated with the irradiation process, do not produce a higher quench rate. A general discussion of the regimes associated with the relative values of ℓ_T and α^{-1} can be found in Bloembergen's paper (1).

Following the termination of the irradiation pulse, the heat from the very hot liquid continues to diffuse into the substrate, which results in further melting, until the temperature of the crystal-liquid interface drops

to the equilibrium melting temperature. For the conditions of Figure 1, the maximum melt depth, d, is about 1000 Å. As will be shown below, the overheating of the crystal during the melt-in process is considerable. The thermal gradients are very high (10^{11} K/m), as is the melt-in velocity ($u \sim 10^3$ m/s). The duration of the melt-in stage of the process is therefore on the order of $d/u \sim 100$ ps.

The third stage is that of resolidification, either by regrowth of the underlying crystal, by growth of a new crystal, or by glass formation if the melt cools to its configurational freezing point before the crystallization front passes. A number of sophisticated numerical analyses have been made of the thermal quantities of this process, but their order of magnitude can easily be estimated from dimensional arguments. The temperature scale is set by the melting temperature, T_m, which is on the order of 10^3 K. The length scale is set by the melt depth $d \sim 10^{-7}$ m. The corresponding temperature gradient is then $\nabla T = T_m/d \sim 10^{10}$ K/m, and the cooling rate $\dot{T} = D_{th} \nabla T/d \sim 10^{12}$ K/s. The lifetime of the melt can be estimated as $\tau = T_m/\dot{T} = 10^{-9}$ s, which is in agreement with the experimental values obtained from transient reflectivity measurements (6-9). The velocity with which the isotherms move toward the surface during cooling is an important quantity to be compared to the crystal growth velocity, and can be estimated as $u_T = \dot{T}/\nabla T \sim 100$ m/s. These parameters, together with those for a "conventional" melt quenching process such as melt spinning, are summarized in Table I, using the thermal data for iron.

Table I. Thermal Parameters in Melt Quenching

		Laser Quenching	Melt Spinning
Melt temperature	T_m(K)	10^3	10^3
Melt thickness	d(m)	10^{-7}	5×10^{-5}
Temperature gradient	∇T(K/m)	10^{10}	2×10^{7}
Cooling rate	$\dot{T}$(K/s)	10^{12}	4×10^{6}
Melt lifetime	t(s)	10^{-9}	not applicable
Isotherm velocity	u_T(m/s)	100	0.2
Heat-flow limited crystal growth velocity	u_h(m/s)	230	0.5

The Overheated Liquid State

As discussed in the previous section, a molten layer with a thickness ℓ_T and a temperature of several thousand degrees is formed in during the energy deposition stage of the pulsed laser processing. Since the boiling

point, T_b, of, for example, liquid iron is 3160 K (at 1 atm), it is important to consider whether the liquid can be overheated and hence be preserved for later quenching, or is lost by fast evaporation above T_b.

1. Thermodynamic Stability Limit

That liquids can be overheated considerably above their boiling temperature is a well-known experimental fact (10,11) that can be explained simply by the van der Waals equation of state:

$$\left(p + \frac{a}{V^2}\right)(V-b) = RT \qquad (1)$$

where a and b are constants.

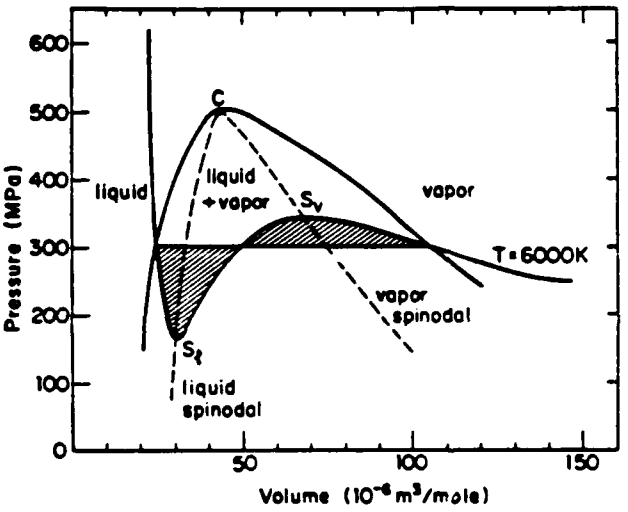

Fig. 2 - P-V diagram for iron, showing one isotherm, the liquid-vapor coexistence domain, and the spinodal lines. The diagram is based on a van der Waals model using the critical point parameters of ref. (12).

Figure 2 shows an isotherm, calculated from the critical point in Fe (12):

$$T_c = 8a/27Rb = 6753 \text{ K} \qquad (2)$$

$$p_c = a/27b^2 = 501 \text{ MPa} \qquad (3)$$

$$V_c = 3b = 43 \text{ cm}^3/\text{mole} . \qquad (4)$$

It should be kept in mind that these values for p_c and T_c are probably lower limiting ones. For example, a critical temperature as high as 10000 K has been quoted for Fe (12).

The equilibrium pressure and volumes for the liquid-vapor transition at a given temperature are found by the Maxwell equal area construction, as

shown by the cross-hatched areas on the p-V diagram of Figure 2. The locus of the equilibrium points forms the coexistence curve (solid line), inside which the equilibrium state consists of a mixture of vapor and liquid.

As long as the compressibility of the liquid is positive, however, (i.e., the slope of the isotherm is negative) the liquid can be overexpanded into the coexistence region up to S_ℓ, a point first labeled by van der Waals as the *spinodal point.* Similarly, the vapor can be overcompressed down to the spinodal point S_v. The locus of the spinodal points is easily obtained from the equation of state (1), by requiring $dp/dV = 0$, which gives:

$$p = \frac{a}{V^2}\left(1 - \frac{2b}{V}\right) \tag{5}$$

and is indicated by the dashed line on Figure 2.

In the region between the coexistence line and the spinodal line, the liquid or vapor are *metastable.* This means that in order to form the vapor phase from the liquid it is necessary to nucleate a bubble, which occurs at a finite frequency. Similarly, in order to form a liquid from the metastable vapor requires nucleation of a droplet. Inside the spinodal line the nucleation barrier vanishes: a fluctuation of any size is stable, and vaporization or condensation occurs rapidly by *spinal decomposition* of the liquid or vapor into two phases.

Figure 3 shows the metastable regions for the liquid and vapor of Fe on a p-T diagram. The spinodal lines and the upper part of the equilibrium line (solid line) have been calculated from the van der Waals model and the critical parameters listed above. The dashed part of the equilibrium line has been adjusted to go through the boiling point at 1 atm (0.1 MPa).

In laser heating of a molten surface at atmospheric pressure, rapid vaporization by spinodal decomposition throughout the liquid can only occur if the temperature exceeds that of the liquid spinodal line at 1 atm, $T_{s,\ell}$. This can be calculated precisely by putting $p = 0$ in equation (5), and using the critical point relations (2)-(4):

$$T_{s,\ell} = \frac{27}{32} T_c \,. \tag{6}$$

For iron, using the lower limiting critical parameters (2)-(4), this temperature is estimated to be at least 5700 K, as can be checked on Figure 3. It could actually be as high as 8400 K, if T_c is 10000 K.

If the temperature of the liquid exceeds $T_{s,\ell}$, the decomposition proceeds very rapidly, but an analysis of its time dependence requires a quantitative kinetic theory. The theory of spinodal decomposition is well

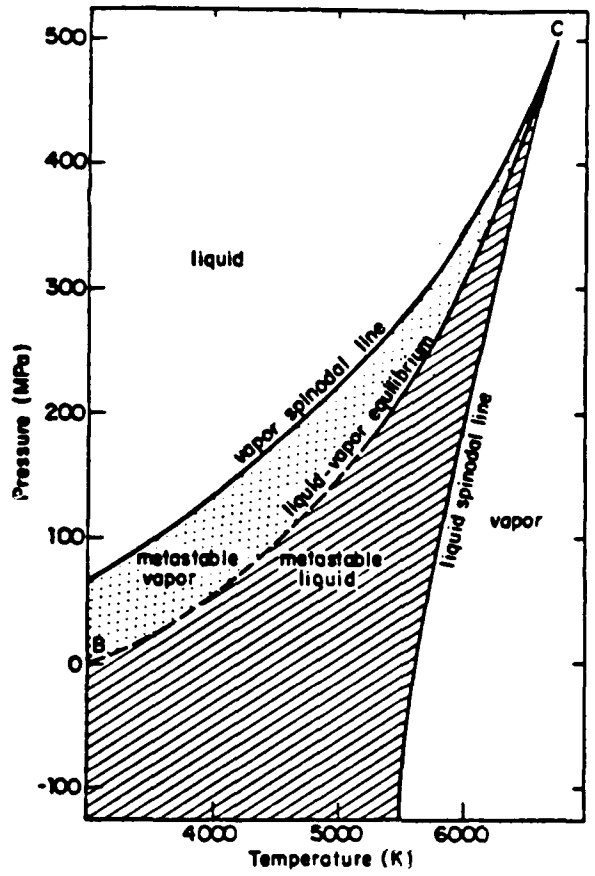

Fig. 3 - P-T diagram showing the liquid-vapor equilibrium line, the spinodal lines and the metastable regions for liquid and vapor. The diagram is based on a van der Waals model using the critical point parameters of ref. (12).

developed (13-15), and explains the minimum length scale for decomposition by taking into account the contribution of very steep gradients (in density or concentration) to the free energy of an inhomogeneous system. Although an estimate of the gradient energy coefficient for liquid metals can in principle be obtained from the same mean field interactions that lead to the van der Waals model, we can simply use the average interatomic distance in the equilibrium vapor phase at $T_{s,\ell}$ (~6 Å) as a lower limit for the length scale of the density fluctuations. An approximate argument similar to the one used below to estimate the time required for assembling a critical vapor nucleus (section 3) can then be invoked here for the formation of a fluctuation. It is therefore possible that, because of the very short time scale of picosecond pulsed laser irradiation, the liquid can even sustain some overheating above $T_{s,\ell}$.

2. Steady State Nucleation

If the temperature of the molten layer does not reach $T_{s,\ell}$, formation of the vapor inside the liquid requires nucleation of a bubble. Classical nucleation theory (16-18) give the following expression for the *steady state* nucleation frequency (number of nuclei per unit volume and time):

$$I = \frac{NkT}{h} \exp\left(-\frac{16\pi\sigma^3}{3p^2kT}\right) \tag{7}$$

where N is the number of atoms per unit volume, k is Boltzmann's constant, h is Planck's constant, p is the equilibrium pressure at the temperature T (p is much larger than the ambient pressure here), and σ is the liquid-vapor surface tension.

The *minimum* nucleation frequency required to cause vaporization throughout the liquid layer in laser quenching can be estimated as:

$$I_{min} = \frac{\alpha}{a^2 t_p} \tag{8}$$

where a is the maximum distance traveled in a time t_p by the vapor-liquid interface of a nucleated bubble; $a = 1$ μm is taken as an absolute upper limit. This gives a value for I_{min} of 2×10^{30} m^{-3}s^{-1}. The maximum temperature to be considered here is $T_{s,\ell}$, so that an estimated $T = 5500$ K is used in the analysis below; it should be kept in mind that the results are very insensitive to the choice of the values for T and I_{min}. The equilibrium vapor pressure at this temperature can be read from Figure 3: $p = 200$ MPa.

Equation (1) can now be used to calculate a maximum value for the liquid-vapor surface tension, σ, for the nucleation frequency to exceed I_{min}. This gives a value $\sigma_{max} = 0.17$ N m^{-1}. The surface tension of liquid iron at the melting point (1812 K) is 1.788 N m^{-1} (19). Since the surface tension decreases roughly linearly with increasing temperature and vanishes at the spinodal $T_{s,\ell}$ (14), the surface tension drops below σ_{max} only if the temperature comes within a few hundred degrees from $T_{s,\ell}$.

3. Transient Nucleation

Equation (7) describes the isothermal *steady state* nucleation frequency, i.e., the rate, per unit volume, at which bubbles form if a steady state population of vapor embryos has been established. Establishing such a population after a sudden change in temperature, however, requires a certain amount of time, during which the nucleation rate increases to its steady state

value (20). Usually, this transient effect is only important in transformations in condensed systems, where the atomic mobility is relatively low. In vapor-liquid transitions, the transient time is much shorter and can usually be ignored. On the very short time scale of pulsed laser irradiation, however, transient effects may be important, and may be a stabilizing factor against copious nucleation in the overheated liquid.

Although an exact analysis of the transient problem is very time-consuming, a lower limit of the transient time, τ, can be estimated by considering the time it takes to form a critical vapor nucleus by evaporation of the liquid.

For large equilibrium vapor pressures p, the critical nucleus radius is given in the classical theory by:

$$r^* = \frac{2\sigma}{p} \tag{9}$$

which, for the nucleation example above is 17 Å.

The rate of evaporation can be estimated from the kinetic theory of gases. The maximum number of atoms evaporating from a unit surface per second is, in equilibrium, equal to the number impinging on that surface from the vapor, which is:

$$\Gamma = \frac{p}{\sqrt{2\pi m k T}} \tag{10}$$

where m is the atomic mass. For the above conditions, this is about $10^{30}\ m^{-2}s^{-1}$. If the sticking coefficient, q, of the vapor atoms is less than unity, Γ is reduced to (17):

$$\Gamma' = \Gamma \frac{q}{2-q} \quad . \tag{11}$$

The time to form a spherical nucleus of radius r^* can then be estimated by considering that at any time during the growth of the vapor bubble the total volume of the atoms evaporating from the surface of the bubble (of instantaneous area A) is equal to the instantaneous increase in the bubble volume, or:

$$A\Omega\Gamma\, dt = A\, dr \tag{12}$$

where Ω is the atomic volume of the atoms in the vapor phase. Figure 2 shows that for the conditions considered here the molar volume of the vapor is around 150 cm^3, which corresponds to $\Omega = 250$ $Å^3$. Equation (12) then integrates simply to give the minimum time to form the critical nucleus:

$$\tau = \frac{r^*}{\Omega\Gamma} \quad . \tag{13}$$

The holes, therefore, are not a result of evaporation *per se*, but of *mechanical* displacement of the liquid layer by the large recoil pressure of the evaporation ("splashing"). The morphology of the displaced material around the hole is often direct evidence of this splashing phenomenon, as is the finding of substrate atoms near the hole on the top side of supported thin films (21).

Direct evidence of the recoil pressure can be obtained from the following experiment (22). A thin ribbon, clamped at one end, is irradiated by a laser pulse at the free end, which results in visible vibration. The impulse (force × time) of the recoil pressure calculated from the vibration amplitude is in general agreement with the order of magnitude of the temperatures and times discussed above.

Thermodynamics and Kinetics

The short time scale of the picosecond melt quenching process puts restrictions on the transformations that can occur. For the entire liquid layer, of thickness, $d = 1000$ Å, to crystallize during the cooling time, τ, of 1 ns, the velocity must be at least, $u = d/\tau \sim 100$ m/s. The time, t_1, to crystallize a monolayer at this speed is about 3 ps, and the distance an atom can diffuse in that time, $(D_\ell t_1)^{1/2}$, is less than an interatomic distance. (D_ℓ is the diffusivity in the liquid phase). This means that under these short pulsed laser quenching conditions no long-range diffusion can occur, and that the only possible transformations are *partitionless* ones, either growth of a crystal of the same composition of the liquid, or glass formation.

The thermodynamic restrictions imposed by the partitionless conditions are illustrated by the phase diagram of Figure 4, which contains two primary solid solutions (α,δ) and two intermetallic compounds (β,γ). The free energy diagram in Figure 4 shows how the T_0-lines for the transformations of these four phases from the liquid are constructed. At a sufficiently low temperature, T_g, the atomic transport rate in the liquid state becomes negligibly small, so that no more transformations can occur on a reasonable time scale. The liquid is then configurationally frozen and becomes a glass. For a composition in the range $x' - x''$ in Figure 4, no crystallization is possible under picosecond laser quenching conditions, and therefore only glass formation is thermodynamically possible. This criterion for glass formation is only a *sufficient* one, and not a necessary one, as has been claimed (23,24). In fact, more often than not, picosecond quenching experiments yield glasses over a wide range of compositions below the T_0-lines for both intermetallic compounds and primary solutions. To explain this, it is necessary to consider the kinetics of partitionless crystallization in some detail.

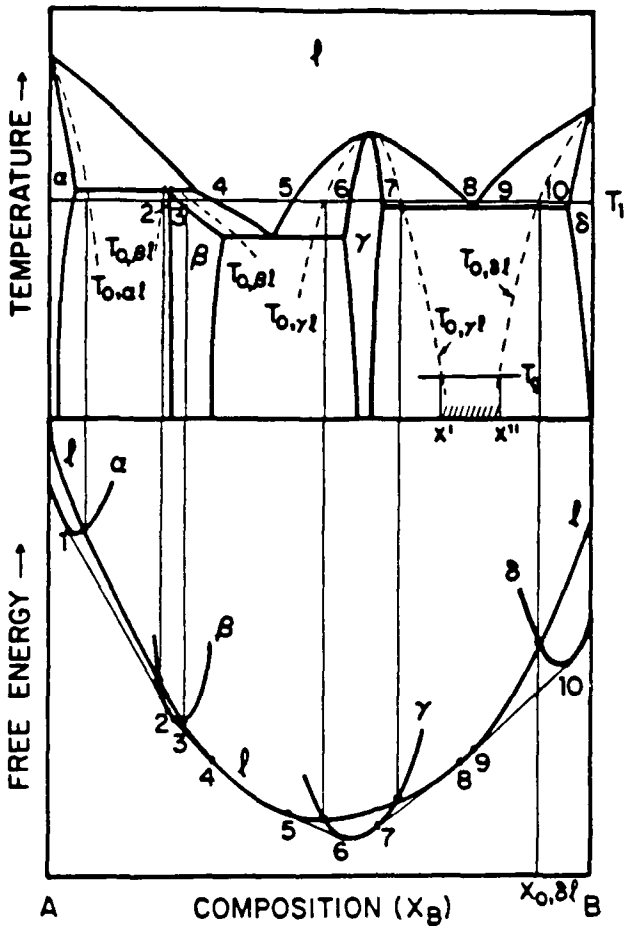

Fig. 4 - Schematic phase diagram (top), and corresponding free energy diagram at temperature T_1 (bottom), illustrating the construction of the T_0-lines for the primary solid solutions and the intermetallic compounds. In the composition range x' - x" (dashed), only glass formation is possible under conditions of partitionless solidification. The numbers correspond to the same compositions in the top and bottom diagrams.

The basic theory for crystal growth far from equilibrium has been formulated by Turnbull, and can be found in a number of publications (25,26), including the first paper in the present volume. The crystal growth velocity can be written as:

$$u = fk\lambda\left[1 - \exp\left(-\frac{\Delta G_c}{RT_i}\right)\right] \qquad (15)$$

where k is the atom jump frequency across the crystal-melt interface, f is the fraction of interface sites that can incorporate a new atom, λ is the interatomic distance, ΔG_c is the difference in molar free energy between crystal and melt, and T_i is the interface temperature.

If the undercooling of the interface, $\Delta T_i = T_m - T_i$, is small, the driving free energy can be approximated by:

$$\Delta G_c = \Delta S_c \Delta T_i \tag{16}$$

where ΔS_c is the molar entropy of crystallization. The exponential in equation (15) can be linearized to:

$$u = fk\lambda \frac{\Delta S_c}{R} \frac{\Delta T_i}{T_i} \tag{17}$$

where, for metals, $f \sim 1$ and $\Delta S_c \sim R$.

The crystal growth rate also depends on the rate at which the heat of crystallization, $\Delta h_{c,v}$ per unit volume, can be removed. Since this must occur by heat flow down the temperature gradient at the interface, $\nabla_i T$, the heat flux, J, must obey the relations:

$$J = u\Delta h_{c,v} = \kappa \nabla_i T \tag{18}$$

where κ is the thermal conductivity. Conversely, equation (18) can be turned around to define a heat flow-limited velocity:

$$u_h = \frac{\kappa \nabla_i T}{\Delta h_{c,v}} \quad . \tag{19}$$

Table I gives values for u_h for the laser quenching conditions as well as for melt spinning.

Combining equations (17) and (19) then gives for metals:

$$\frac{u_h}{k\lambda} = \frac{T_m - T_i}{T_i} \quad . \tag{20}$$

In conventional solidification, the interface kinetics are much faster than the rate of heat removal, so that $u_h << k\lambda$, and ΔT_i is small. This type of growth is called *heat flow-limited*. In laser quenching, depending on the nature of the interface rearrangements (see below), the rate of heat removal can be much faster than the interface kinetics, so that $u_h >> k\lambda$, and the undercooling, ΔT_i, is large, so that metastable phases can be formed. This corresponds to *interface-limited* growth.

The maximum growth velocity of a crystal, $u_{max} = k\lambda$, is determined by the nature of the atomic rearrangements that control the growth process. In pure metals, dilute alloys or compounds with simple crystal structures, k can be taken as the frequency of thermal vibration. (~ Debye frequency), so that $u_{max} \sim u_s$, the speed of sound in the liquid, which is on the order of several thousand m/s. This is called the *collision-controlled* regime, because the growth occurs by simple impingement of the liquid atoms onto the crystal.

In more concentrated alloys or in compounds with a more complicated crystal structure, where a change of the nearest neighbor configuration, i.e. diffusion, is necessary, the jump frequency can be taken as D_ℓ/λ^2, and $u_{max,D} = D_\ell/\lambda$, which is on the order of 10 m/s. This is the *diffusion-controlled* regime. Table I shows that for picosecond laser quenching $u_{max,D} << u_T, u_h$, so that this type of growth can easily be suppressed. Equation (20) shows that under these conditions T_i falls far below T_m, and glass formation becomes possible.

Although in partitionless growth of crystals there is no *long-range* diffusional transport, the growth can still be diffusion-controlled if a drastic change of the nearest neighbor environment is necessary to transform the liquid structure into the crystalline one. This is the case, for example, in metal-metalloid alloys such as Fe-B, where the chemical interaction leads to a very pronounced short-range order in the liquid (9 Fe atoms around each B in a capped trigonal prism arrangement (27)), which is very different from that in the crystal (B interstitial in bcc Fe (28)). As a result, it is possible to produce Fe-B glasses containing as little as 5 at.% B (28), which is far below the T_o-line. Similarly, if the unit cell of an intermetallic compound is large, or if long-range chemical order must be established, crystal growth is diffusion-limited, and the growth of these compounds is easily suppressed in picosecond pulsed laser quenching. Numerous experiments on a variety of binary metallic systems (Ni-Nb, Ni-Mo, Co-Mo, Nb-Co (8, 30-34)) have demonstrated that glasses can be formed at the intermetallic compositions. On the other hand, in pure metals with simple crystal structures, and by extension, disordered alloys with the same simple structures (e.g., disordered fcc in Cu-Co or Ag-Cu), growth is collision-limited and cannot be suppressed even by picosecond pulsed laser quenching. This is confirmed by direct measurements of the growth velocity of pure metals and disordered alloys (Au, Cu, Cu-Au) by transient reflectivity (8,9) which yield large values (> 100 m/s) that can only be accounted for by a collision-controlled mechanism.

Applications

1. Overheating of Crystals

It is well known that the interior of large crystals can be heated well above the melting temperature if the kinetics of melting are much slower than the rate of thermal diffusion, as is the case for oxides (35). In metals the kinetics of melting are much faster, so that overheating is much more difficult to achieve. One method, in which conventional heating is used, consists of surrounding a small single crystal with a higher melting coherent layer to

prevent surface nucleation of the interior melt. Overheating of silver crystals, coated by a gold layer, by 7.5 K has been reported (36). "Conventional" rapid heating methods, for example by sending a high current pulse through a thin metallic wire, also give overheating of no more than a few degrees (37).

Rapid heating with pulsed lasers provides a unique method for overheating crystals considerably above their melting temperature, as can be seen from the following argument. During the initial stages of the melt-in phase the temperature gradients are an order of magnitude greater than during regrowth. This means that the heat-flow limited crystal growth velocity, given by equation (19), is also an order of magnitude greater than the value listed in Table I, or about 2000 m/s. For pure metals, where $u_{max} = u_s \sim 3000$ m/s, equation (20) gives for the overheating: $\Delta T_i = 0.66\ T_i$, which, for a melting point of 1000 K, corresponds to an overheating of 2000 K.

The obvious drawback of the method is the short duration of the overheating (< 100 ps), which requires fast diagnostic techniques for studying the crystal or possible homogeneous nucleation of the melt in this state.

2. Quenching of Nb-Si Alloys

The Nb-Si system is of interest because of the prediction that the Nb_3Si compound with the A-15 structure should have a very high superconducting transition temperature. Since at 25 at.% Si there are no stable compounds in this system (see the phase diagram of Figure 5), a variety of methods have been used to produce metastable phases. As illustrated in Figure 5, conventional melt quenching methods produce an amorphous phase in the vicinity of the eutectics (38). Non-stoichiometric A-15 phases have also been found (39,40). At the 25 at.% Si composition, however, conventional melt quenching yields a compound with the tetragonal Ti_3P structure (41).

We have recently completed a study of this system using pulsed laser quenching of thin alloy films (~ 1000 Å) supported on various substrates (42-44). Although we did not succeed in obtaining an A-15 phase (the quench rates were too high in all attempts for this), it is still useful to review the various phases that were obtained at different cooling rates. Figure 5 illustrates the results.

At the highest quench rates (> 10^{12} K/s), obtained in the thinnest sections of the spots irradiated with a 30 ps pulse on a copper substrate the amorphous phase was formed over a wide composition range. Such broadening of the range of amorphous phase formation is consistent with our earlier observations on other metal-metalloid and metal-metal systems.

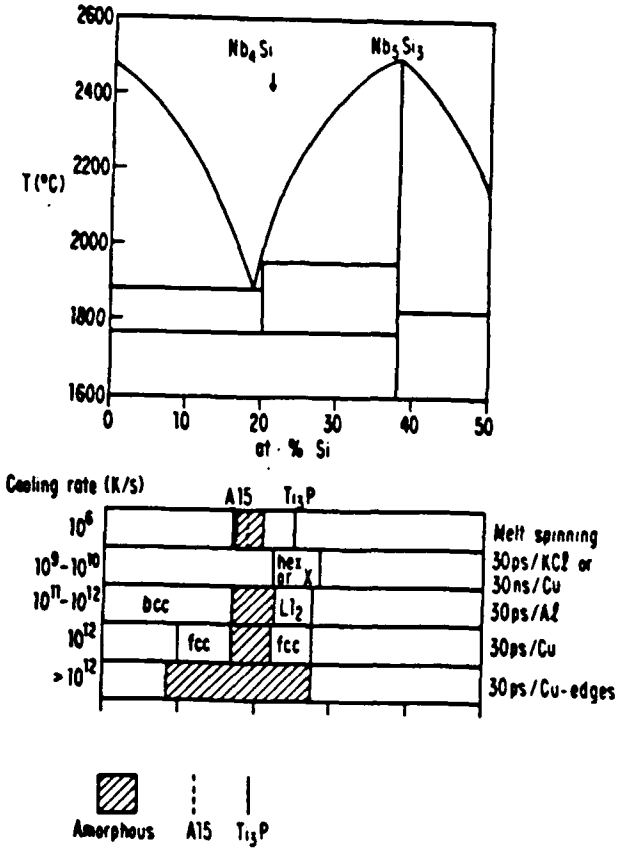

Fig. 5 - Phase diagram of the Nb-Si system (top), and schematic illustration of the phases obtained by different methods of liquid quenching. The melt spinning results are from refs. (38-41); the laser quenching results are from refs. (42-44). The pulse length and the substrate for the laser experiments are indicated.

At slightly lower quench rates (10^{12} K/s), obtained in the remaining area of those spots, a new phase was found: a disordered f.c.c. solid solution (43). Although the formation of disordered f.c.c. solid solutions in metal-metal alloys cannot be suppressed by picosecond laser quenching, the growth rate of the f.c.c. phase in this system, although still the highest one observed, is probably slightly lower due to the short-range order around the Si.

By lowering the quench rate to 10^{11} - 10^{12} K/s by supporting the films on an aluminum substrate, a supersaturated b.c.c. solid solution was found at low Si contents, and an ordered f.c.c. phase (Ll_2, Cu_3Au-type) around 25 at.% Si.

A cooling rate of 10^9 - 10^{10} K/s was obtained, either by supporting the ps-irradiated films on a salt substrate, or by irradiating the films on a copper substrate with a 30 ns pulse. Under these conditions two entirely new phases were found around 25 at.% Si: a hexagonal phase with a 250 $Å^3$ unit

cell and an as yet unidentified phase (44).

It is interesting to note the degree of isotropy and the unit cell size of the phases formed at 25 at.% Si in order of decreasing quench rate: amorphous (isotropic, no unit cell), disordered f.c.c. (1 atom unit cell, cubic point group), ordered f.c.c. (4 atom unit cell, cubic point group), hexagonal (~ 16 atom unit cell, uniaxial point group), Ti_3P-type (32 atom unit cell, uniaxial point group). This is a good illustration of the principle, stated in Turnbull's paper in this volume, that phases are increasingly kinetically favored (i.e., are more difficult to suppress by quenching) with increasing isotropy and decreasing unit cell size.

Acknowledgements

The author's work in this area is supported by the Office of Naval Research under contract number N00014-85-K-0684.

References

1. N. Bloembergen, in *Laser-Solid Interactions and Laser Processing*, ed. by S.D. Ferris, H.J. Leamy and J.M. Poate, AIP, New York (1979), p. 1.

2. F. Spaepen and C.J. Lin, in *Amorphous Metals and Non-Equilibrium Processing*, ed. by M. von Allmen, Les Editions de Physique, Les Ulis, Frace (1984), p. 65.

3. F. Spaepen, in *Laser Surface Treatments of Metals*, ed. by C.W. Draper and P. Mazzoldi, NATO ASI Series, Martinus Nijhoff, Dordrecht, The Netherlands (1986), in press.

4. For a review of these relaxation processes, see W.L. Brown, Mat. Res. Soc. Symp. Proc., 23, 9 (1984).

5. If the laser power is high enough to ignite a plasma in front of the surface (see e.g., J.A. McKay and J.T. Schriempf, in *Laser-Solid Interactions and Laser Processing*, ed. by S.D. Ferris, H.J. Leamy, and J.M. Poate, AIP, New York (1979, p. 55), the energy deposition time can be longer than the pulse duration, depending on the relaxation time of the plasma. In the quenching experiments described here, however, the fluence is carefully selected to be large enough to melt the surface, and yet small enough to avoid visible surface damage, which would be caused also by the shock wave emitted by the plasma expansion. In practice this was done by producing a small damage hole at the center of the indicated spot; the remaining area has thus simply undergone melting and resolidification.

6. J.M. Liu, R. Yen, H. Kurz, and N. Bloembergen, Appl. Phys. Lett., 39, 755 (1981).

7. C.A. MacDonald, Ph.D. Thesis, Harvard University (1986).

8. C.A. MacDonald and F. Spaepen, in *Laser Surface Treatments of Metals*, ed. by C.W. Draper and P. Mazzoldi, NATO ASI Series, Martinus Nijhoff, Dordrecht, The Netherlands (1986), in press.

9. C.A. MacDonald, A.M. Malvezzi and F. Spaepen, Mat. Res. Soc. Symp. Proc., 51 (1986), in press.

10. H. Wakeshima and K. Takata, J. Phys. Soc. Japan, 13, 1398 (1958).

11. R.E. Apfel, J. Acoust. Soc. Am., 49, 145 (1971).

12. Landolt-Börnstein Tables, Volume II, Part 1, Mechanisch-Thermische Zustandgrössen, ed. by H. Borchers et al., Springer, Berlin, (1971), p. 332.

13. J.W. Cahn, Acta Metall., 9, 795 (1961).

14. J.W. Cahn and J.E. Hilliard, J. Chem. Phys., 28, 258 (1958). It should be noted that close to the spinodal temperature g deviates from the rough linearity, and approaches zero as $(T-T_{s,\ell})^{3/2}$. (D.R. Nelson, private communication).

15. J.E. Hilliard, in *Phase Transformations*, American Society for Metals, Metals Park, Ohio, (1970), 497.

16. M. Volmer, *Kinetik der Phasenbildung*, Steinkopff, Dresden and Leipzig, (1939), p. 156.

17. R.E. Apfel, Ph.D. Thesis, Harvard University (1970).

18. J.C. Fisher, J. Appl. Phys., 19, 1062 (1948).

19. A.V. Grosse, J. Inorg. Nucl. Chem., 26, 1349 (1964).

20. K.F. Kelton, A.L. Greer and C.V. Thompson, J. Chem. Phys., 79, 6261 (1983). This paper also contains an extensive review of earlier work.

21. C.J. Lin and F. Spaepen, Scripta Metall., 17, 1259 (1983).

22. C.J. Lin, Ph.D. Thesis, Harvard University (1983).

23. T.B. Massalski, Proc. 4th Int. Conf. on *Rapidly Quenched Metals*, ed. by T. Masumoto and K. Suzuki, Jap. Inst. Metals, Sendai (1982), p. 203.

24. W.J. Boettinger, Proc. 4th Int. Conf. on *Rapidly Quenched Metals*, ed. by T. Masumoto and K. Suzuki, Jap. Inst. Metals, Sendai (1982), p. 99.

25. D. Turnbull, in *Physical Processes in Laser-Materials Interactions*, NATO-ASI Proc., ed. by M. Bertollotti, Plenum, NY (1983), p. 117.

26. F. Spaepen and D. Turnbull, in *Laser Processing of Semiconductors*, ed. by J.M. Poate and J.W. Mayer, Academic, NY (1982), p. 15.

27. For a review of the short-range order in metal-metalloid glasses, see J.M. Dubois and G. Le Caer, Acta Metall., 32, 2101 (1984).

28. R. Ray and R. Hasegawa, Sol. St. Comm., 27, 471 (1978).

29. C.J. Lin and F. Spaepen, Appl. Phys. Lett., 41, 721 (1982).

30. C.J. Lin, F. Spaepen and D. Turnbull, J. Non-Cryst. Solids, 61/62, 767 (1984).

31. C.J. Lin and F. Spaepen, Mat. Res. Soc. Symp. Proc., 28, 75 (1984).

32. C.J. Lin and F. Spaepen, in *Chemistry and Physics of Rapidly Solidified Materials*, ed. by B.J. Berkowitz and R.O. Scattergood, TMS-AIME, NY (1983), p. 273.

33. C.J. Lin and F. Spaepen, "Nickel-Niobium Alloys Obtained by Picosecond Pulsed Laser Quenching," Acta Metallurgica, 34, 1367 (1986).

34. F. Spaepen, Proc. Int. Conf. on *Cryogenic Materials*, ed. by T. Orlando and S. Foner, Plenum, NY (1986), in press.

35. N.G. Ainslie, J.D. MacKenzie and D. Turnbull, J. Phys. Chem., 65, 1718 (1961).

36. J. Däges, H. Gleiter and J.H. Perepezko, Mat. Res. Symp. Proc., 57, (1986), in press.

37. S.E. Khaikin and H.P. Benet, Compt. rend. acad. sci. U.R.S.S., 23, 31 (1939).

38. A. Inoue and T. Masumoto, Sci. Rep. Res. Inst. Tohoku University, A28, 165 (1980).

39. R.M. Waterstrat, F. Haenssler and J. Müller, J. Appl. Phys., 50, 4763 (1979).

40. K. Togano, H. Kamakura and K. Tachikawa, Phys. Lett. 76A, 83 (1980).

41. W. Rossteutscher and K. Schubert, Z. Metallk., 56, 813 (1965).

42. W.K. Wang, C.J. Lobb and F. Spaepen, in preparation.

43. W.K. Wang and F. Spaepen, J. Appl. Phys., 58, 4477 (1985).

44. W.K. Wang and F. Spaepen, J. Appl. Phys. (1986), in press.

Picosecond time-resolved measurements of crystallization in noble metals

C. A. MacDonald,[a] A. M. Malvezzi,[b] and F. Spaepen
Division of Applied Sciences, Harvard University, Cambridge, Massachusetts 02138

(Received 16 June 1988; accepted for publication 29 August 1988)

Crystallization rates in pure metals have been measured by monitoring changes in reflectivity on a picosecond time scale during pulsed laser quenching. Multilayered films were used to establish that the transient decreases in reflectivity correspond to melting. Depth profiling with Auger electron spectroscopy on laser-irradiated areas showed complete mixing of the layers, which could only have occurred by melting. Crystallization velocities as high as 100 m/s were measured. These growth speeds are too large to be the result of a crystallization process governed by liquid state diffusion. The results of computer simulations based on a collision-limited growth model for crystallization were consistent with the measurements.

I. INTRODUCTION

Short pulse lasers (tens of picoseconds) deposit heat in a very thin region near the surface of a sample.[1,2] If sufficient energy is deposited, a melt nucleates at the surface and propagates inward. During this period the underlying crystalline material can be superheated substantially above the melting temperature. After the end of the laser pulse the molten layer begins to cool as heat flows into the interior of the sample. When the temperature of the melt/crystal interface drops below the melting temperature, the interface reverses direction and returns to the surface. The large thermal gradients present in short pulsed laser quenching experiments can result in substantial undercooling of the interface below the melting temperature. A complete theory for the kinetics of crystallization that adequately predicts the velocity of this interface as a function of its temperature is still being developed.[3-5] There has been extensive work devoted to measurements of interface velocities in silicon by monitoring transient optical and electrical properties during and after the laser pulse.[6] These experiments were facilitated by the dissimilarity of the crystal and its melt. Upon melting, silicon changes from a covalently bonded semiconducting solid with four nearest neighbors to a metallic liquid with high coordination number. The normal incidence reflectivity differs by a factor of 2 and the dc conductivity by a factor of 30. On the other hand, the theoretical analysis of crystallization in silicon is hampered by this same dissimilarity. Further, since the structural change upon crystallization is simpler in metals than in silicon, it might be expected to be faster. In order to achieve high velocities, it is necessary to produce large thermal gradients such as those that occur following picosecond pulsed laser quenching. This work, and previous measurements by this group,[7,8] constitute the first measurements of the kinetics of crystallization in metals during pulsed laser quenching, and the only ones to date in the picosecond regime.

[a] Currently at Physics Dept., The University at Albany, State University of New York, Albany, NY 12222.
[b] Currently at Dipartimento di Elettronica, Universitá di Pavia, Via Abbiategrasso 209, Pavia, Italy.

II. EXPERIMENTAL TECHNIQUE

A. Optical

The experiment was conducted with a standard pump/probe optical setup, shown in Fig. 1. The 30-ps Nd:YAG pulse at 1.06 μm was doubled to produce a 20-ps green (0.53 μm) pump pulse, used to melt the sample. The spot sizes were a few hundred microns in diameter. The reflectivity of the sample was probed in the center of the irradiated area with a small fraction of the remainder of the 1.06-μm pulse at a variable delay relative to the pump pulse. Data from this system were collected with an IBM PC XT.[9] By closing a shutter to block the pump beam, the probe beam could be fired alone to determine the initial and final reflectivity of each spot. A fresh portion of the sample was irradiated at each measurement. To reduce the effect of spot-to-spot variations in reflectivity, the measurements were normalized to the initial value for each spot. Figure 2 displays a typical plot of the change in reflectivity with a delay of 2 ns (crosses) and of several seconds (circles) between the pump beam and probe pulses. For low fluences (region I), there was no change in reflectivity. For moderate fluences (region II), a small change in reflectivity was observed at 2 ns, with nearly

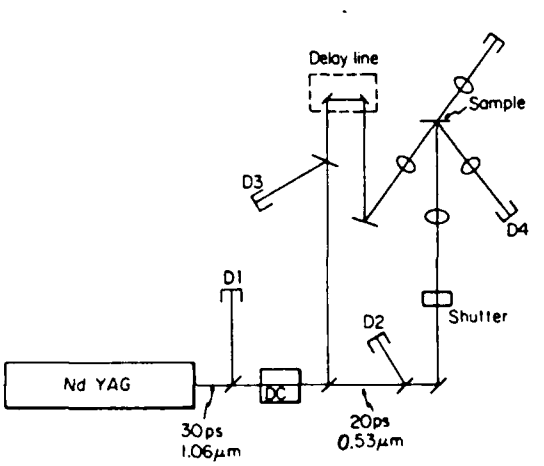

FIG. 1. Schematic diagram of the time-resolved reflectivity apparatus. D1–D5 detectors; DC: doubling crystal.

 0021-8979/89/010129-08$02.40

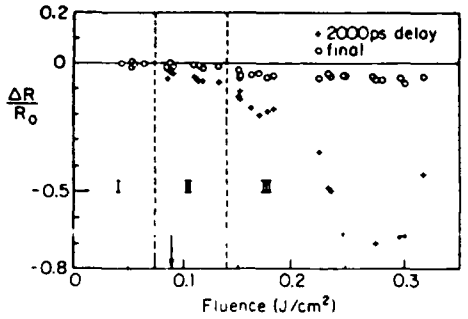

FIG. 2. Relative change in reflectivity of a copper/gold artificial multilayer with 10-nm repeat length, irradiated with a 20-ps pulse. Crosses: 2-ns delay; Circles: several seconds delay.

complete recovery. Finally, for large fluences (region III), large and permanent drops in reflectivity were observed.

To analyze this data it was necessary to determine whether melting leads to a decrease or increase in sample reflectivity. Simple free-electron Drude calculations predict that the reflectivity is unity below the plasma frequency, and zero above. In a real (finite temperature) system, electron-phonon collisions reduce the reflectivity for frequencies below the plasma frequency. Since the plasma frequency for metals is in the near UV (or in the blue-green region for the yellow metals like copper and gold), the probe frequency (1.06 μm) is well below the plasma frequency for these experiments. Increases in temperature further reduce the reflectivity. On the other hand, melting, with its associated disorder, increases the electron-phonon interaction, and hence is also expected to lower the reflectivity. Thus, the changes in reflectivity seen in the middle region in Fig. 2 might *a priori* be associated with either heating or melting. Since small changes in film preparation can result in large differences in reflectivity, the literature contains widely varying values for reflectivity changes upon melting, which are therfore not useful for direct comparison with the present experimental data.[10]

B. Sample preparation and characterization

The experiment was performed on bulk specimens of copper, aluminum, and silver, and on thin films of copper, gold, silver, and aluminum on a variety of substrates (in order of increasing conductivity: glass slides, polished silicon wafers, and sapphire crystals). All samples exhibited similar behavior. The bulk samples, while providing faster cooling rates because of their higher thermal conductivities, exhibited larger spot-to-spot variations in reflectivity and localized melting on polishing scratches or etch pits left from electropolishing. Films produced by vapor deposition in a chamber with no facility for *in situ* cleaning tended to adhere poorly to the substrate. Better results were obtained by rf sputtering in a SEM coater after *in situ* plasma etching. Figure 3 displays a typical 100-nm-thick gold film, deposited by the latter method on a silicon substrate, after laser irradiation. The ring pattern resulted from the circularly symmetric Gaussian intensity profile of the beam.

The best samples (with high reflectivity, good adhesion, and low spot-to-spot variation) were obtained by ion beam

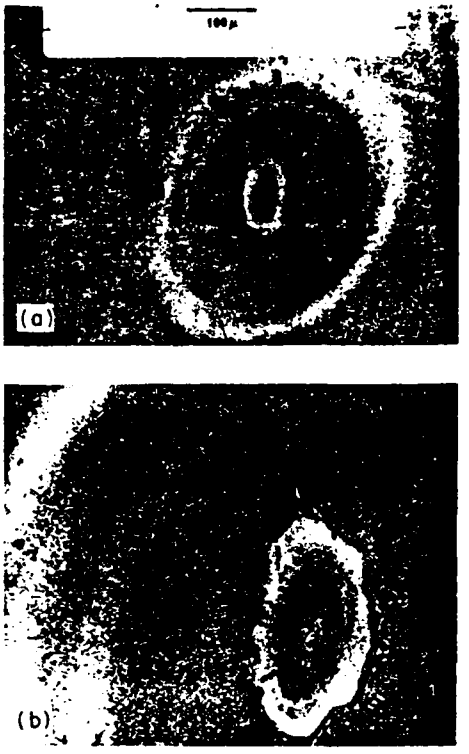

FIG. 3. Optical micrograph of a 0.1-μm-thick gold film on a silicon substrate irradiated with a 20-ps pulse. (a) Ring pattern resulting from the Gaussian intensity distribution of the beam; (b) detail of the laser damage at the center of the spot.

sputtering in a previously described system.[11] This system not only allowed deposition of the largest variety of materials, but also the production of artificial multilayered films. These films were used to determine if the characteristic reflectivity decreases could be associated with melting. Alternate layers of materials that are completely miscible in the liquid and solid states (copper/gold and copper/nickel) were produced with repeat lengths of 2.5 to 20 nm, which were measured by x-ray diffraction.[12] Solid-state diffusion rates are too slow to allow substantial mixing during the short time in which the films were hot after a laser pulse. The diffusivity in these metals just below their melting temperature does not exceed $\sim 10^{-8}$ cm^2/s. If the sample remains at this temperature for 1 ns, the diffusion distance $(Dt)^{1/2}$ is only 0.03 nm. Thus, if substantial mixing of the film is observed after laser irradiation, melting must have occurred. A comparison of the Auger electron spectroscopy (AES) sputter profiles of a copper/nickel multilayer of 10 nm repeat length near and inside a laser spot (Fig. 4) clearly shows the mixing. In order to make valid comparisons between the results from multilayered and pure films, it must be established that they have similar optical properties. This was done by calculating the reflectance of the multiple layer structure shown in Fig. 5, first for a pure gold film, and then for a metal film consisting of alternate layers of gold and copper. The coefficients of reflectance and the forward and back transmission were computed[13] from the values $n = 0.194$, $k = 5.57$ for solid gold[14] and $n = 1.38$, $k = 7.2$ for liquid gold,[15] and were used recursively to calculate the overall reflectance of the system as a function of the depth of

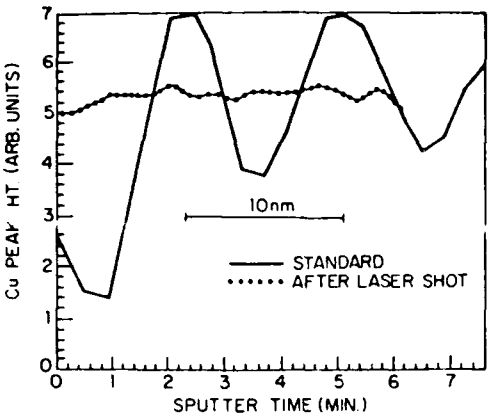

FIG. 4. Auger electron spectroscopy depth profile of the copper/gold multilayer of Fig. 2. The solid line is for an area adjacent to a laser spot. The dotted line is for an area irradiated with the fluence marked in Fig. 2.

the molten layer. The results for pure gold are shown in Fig. 6(a). The reflectivity falls off by a few percent, and levels off at a liquid depth equal to the optical absorption length. Figure 6(b) displays the results for a gold/copper multilayer of 20-nm repeat length, using $n = 0.92$, $k = 7.7$ for solid copper and $n = 0.43$, $k = 5.6$ for liquid copper (from the same references as the respective gold data).

Figure 2 shows the reflectivity change of a copper/gold multilayer after a laser pulse as a function of fluence. This reflectivity behavior was also typical of pure films and bulk specimens. An AES profile of a spot irradiated with the fluence marked in Fig. 2 (in the center of region II) is shown in Fig. 4. The AES profile clearly shows that region II can be associated with melting. Bright- and dark-field optical micrographs of the spot profiled in Fig. 4 are shown in Figs. 7(a) and 7(b). Only a very faint contrast is seen marking the circular irradiated area at this fluence. A spot irradiated at higher fluence is seen in Figs. 7(c) and 7(d). The faint region here surrounds a dark-ringed mottled region. The circular shapes of the features are the result of the circularly symmetric Gaussian spatial profile of the laser beam. If a particular damage feature of radius r can be associated with a fluence threshold f_{th}, this radius can be related to the average pulse fluence f and the Gaussian radius σ. The average pulse fluence is defined as the pulse energy E divided by the Gaussian area $f = E/\sigma^2$. The radius r is thus given by

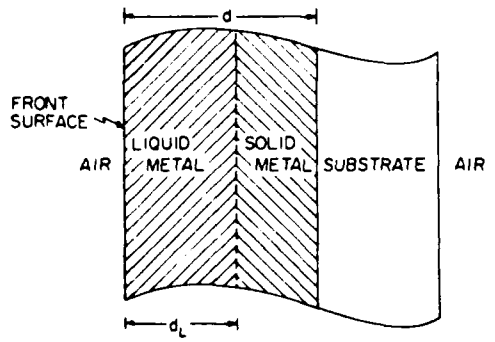

FIG. 5. Schematic diagram of the layer configuration used in the reflectivity calculations of partially molten films.

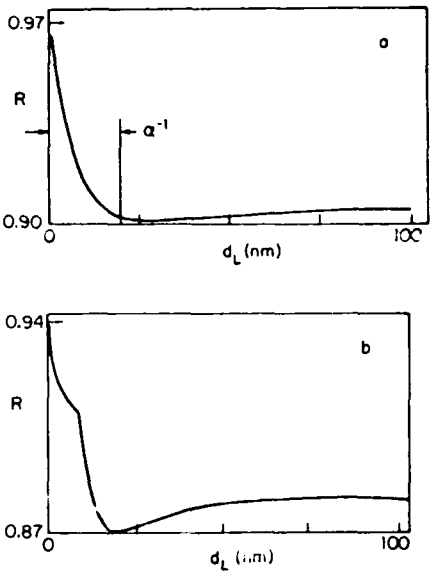

FIG. 6. Reflectivity of partially molten 100-nm-thick films, calculated as a function of the thickness of the liquid layer (d_l) for the geometry of Fig. 5. The angle of incidence is 10°. (a) Pure gold film; (b) multilayer consisting of alternating 10-nm layers of copper and gold.

$$f_{th} = fe^{-(r^2/\sigma^2)} \tag{1}$$

or

$$r^2 = \sigma^2[\ln(f) - \ln(f_{th})] . \tag{2}$$

The solid line in Fig. 8 is a fit to this function for the sharp ring feature, one of which is shown in Fig. 7(c). The fluence threshold for this feature corresponds to the beginning of region III in Fig. 2, the permanent damage region. The dotted line in Fig. 8 corresponds to the radius of the faint region seen in Figs. 7(a) and 7(c). This fluence threshold corresponds to the beginning of region II in Fig. 2, the melting regime.

III. EXPERIMENTAL RESULTS

Figure 2 displays the change in reflectivity of a copper/gold multilayer for a particular pump-probe delay at a variety of fluences. After collecting the reflectivity versus fluence data for a particular time delay, the delay line was changed and the measurements were repeated. The reflectivity versus fluence data were then collected into fluence bins, averaged, and plotted as reflectivity versus time for a fluence bin in the melting fluence regime II. Such a plot is shown in Fig. 9 for a 30-nm-thick gold/copper multilayer with 10-nm repeat length on a glass substrate. The film thickness is of the order of the optical absorption depth. Thus, the drop in reflectivity can be associated with the melting of the entire film, and the recovery of the reflectivity back to its original value with the movement of the crystal/melt interface from the substrate to the free surface. The interface velocity u is given by

$$u = \frac{d}{t} = \frac{300\times10^{-10}}{4000\times10^{-12}} = 7.5\ \text{m/s} , \tag{3}$$

where d is the film thickness and t the recovery time. This is still a relatively low velocity, due to the poor thermal con-

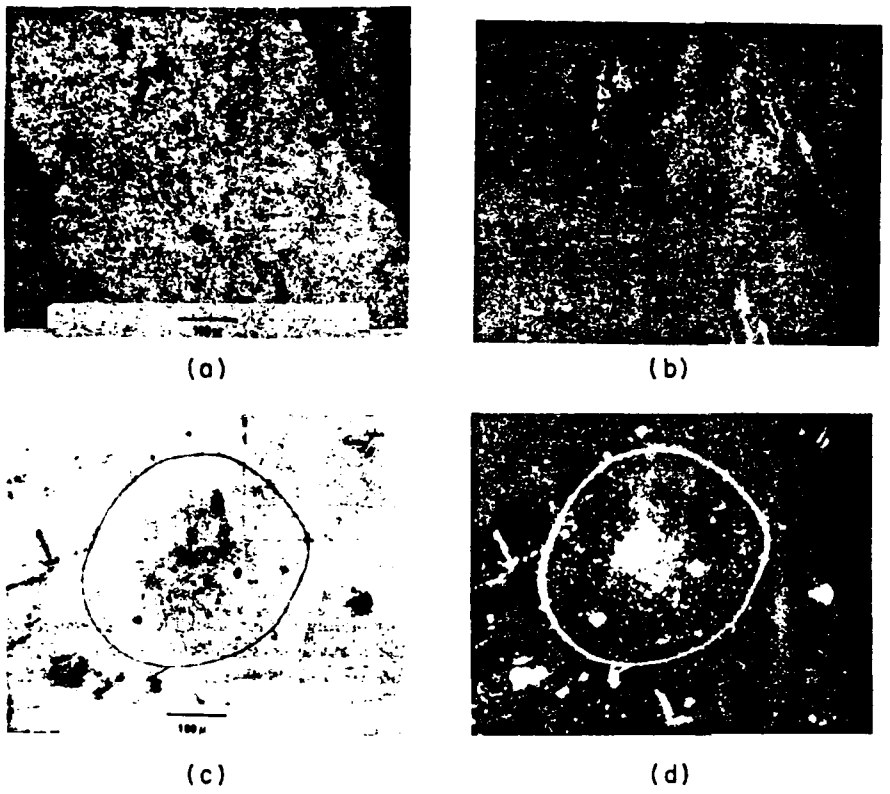

FIG. 7. Optical micrographs of laser-irradiated areas for the sample of Fig. 4. (a) Same fluence as in Fig. 4; bright field. (b) Dark field of (a). (c) Higher fluence; bright field. (d) Dark field of (c).

ductivity of the glass. Note that the maximum change in reflectivity in Fig. 9 is less than 3%. The fluence threshold for melting is lower than for the sample in Fig. 2 because of the smaller film thickness. Measurements in the nanosecond regime, such as those by Tsao *et al.* on aluminum, have shown that velocities deduced from changes in reflectivity are in agreement with those obtained from changes in the conductivity in a partially molten sample.[16] The transient conductivity technique, however, cannot readily be extended to the picosecond regime.

The change in reflectivity as a function of time for a 20-nm gold film on a sapphire substrate is shown in Fig. 10. The reflectivity recovery began at 400 ps and was completed by 600 ps. Equation (3) yields a velocity of 100 m/s in this case. This is the highest velocity for growth of a crystal from its melt ever measured by any technique. This value is probably still only a lower limit. The value of the regrowth time used here is the difference between the last time at which the reflectivity is low and the first at which it has returned to its initial value; the actual recovery time may be smaller. Furthermore, if the interface is not fully planar, the recovery of the reflectivity would be smeared out in time so that the actual velocity would, again, be larger than the value determined above. On the other hand, if the melt front did not reach the back surface, the above value would be too large. If this were the case, however, the reflectivity trace of Fig. 10 should have a V shape; instead, it has a flat portion (between 200 and 400 ps) that corresponds to the time that the entire film was fully melted.

The time-resolved reflectivity technique was also applied to a bulk sample. The resulting data showed more scatter, however, due to spot-to-spot variation of its surface characteristics. A plot of reflectivity versus time is shown in Fig. 11 for a bulk copper sample. In this case it is necessary to

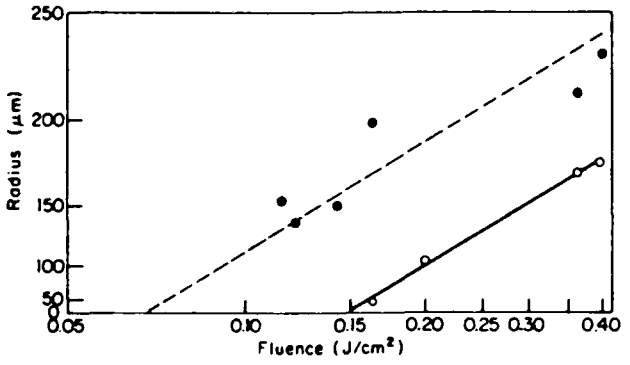

FIG. 8. Square of the radius of the damage features of Fig. 7(c) as a function of the logarithm of the incident laser fluence. The solid line is a a least-squares fit for the sharp ring. The dotted line is a fit with the same slope for the radius of the faint white region.

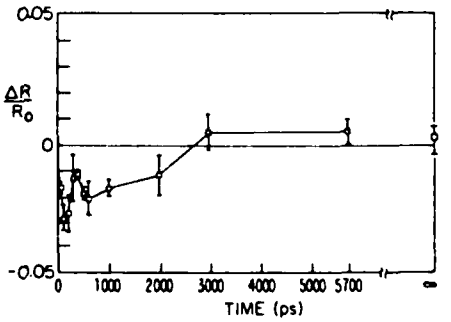

FIG. 9. Relative reflectivity change as a function of time for a 30-nm-thick gold/copper multilayer with 10-nm repeat length on a glass substrate, irradiated with a 4-mJ/cm² laser fluence

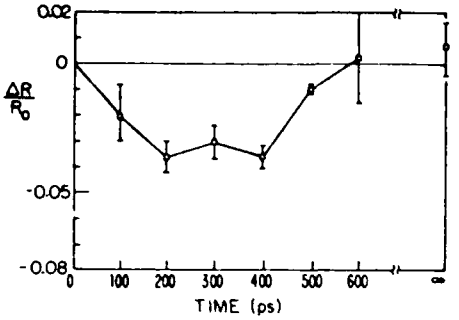

FIG. 10. Relative reflectivity change as a function of time for a 20-nm-thick gold film on a sapphire substrate, irradiated with a 24-mJ/cm^2 laser fluence.

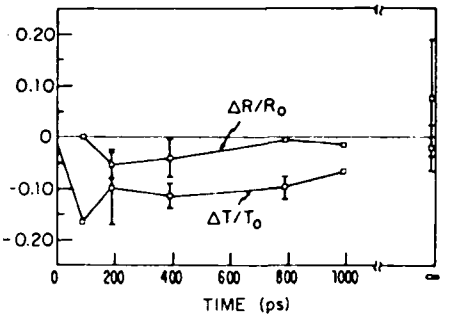

FIG. 12. Relative changes in reflectivity and transmittivity as a function of time for an aluminum film on a sapphire substrate ($R_0 = 0.6$, $T_0 = 0.2$), irradiated with a 23-mJ/cm^2 laser fluence.

associate the reflectivity recovery time with the movement of the interface over the optical absorption depth, 25 nm in this material. This gives a velocity of 60 m/s for the crystal regrowth. It might be expected that the regrowth velocity for a bulk metal would be higher than that for a metal film on sapphire because of the higher thermal conductivity of the metal substrate. However, the melt in the bulk experiment was probably somewhat deeper, and the crystallization front may have slowed due to latent heat rejection by the time it reached the 25-nm surface region where crystallization could be detected.

In all cases, the decrease in reflectivity associated with melting was completed in less than 100–200 ps. This is also shown for the particular case of an aluminum film on a sapphire substrate in Fig. 12. These melting times are in apparent disagreement with the picosecond electron diffraction experiments of Williamson, Mourou, and Li[17] on free-standing 20-nm-thick aluminum films, in which, at low fluence (8 mJ/cm^2 absorbed), no melting was observed until 1 ns after irradiation. Rapid melting, similar to that observed here, was also seen in their experiments, but at higher fluences (13 mJ/cm^2 absorbed). It can be argued[18] that if melting requires 1 ns to be observed at the lower fluences, it would not occur at all in the experiment described in this paper, since by that time all the deposited heat would have drained away through the substrate and cooled the surface to below the melting temperature. Thus, the difference in sample geometry may have led to an apparent higher threshold fluence for melting in the present experiments. The actual absorbed fluence for the sample of Fig. 10 is about 5 mJ/cm^2, at the low end of the values used in the experiments of Williamson and co-workers. The film thickness for our sample, however, is probably smaller than 20 nm, and no doubt has somewhat different optical properties, all of which makes a direct comparison of the fluences in the two experiments difficult.

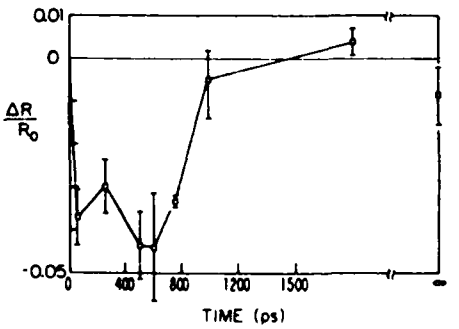

FIG. 11. Relative reflectivity change as a function of time for a bulk copper sample, irradiated with a 23-mJ/cm^2 laser fluence.

IV. DISCUSSION AND COMPUTER MODELING

An analytic calculation of the temperature at each point in the sample under the conditions of pulsed laser quenching is very complex, especially if the temperature dependence of the material properties, the kinetics of the various phase transitions, and the mechanical effects must be taken into account. In order to make the problem tractable, it is necessary to make a series of rather restrictive approximations. The main assumption is that the Laplace equation is a valid description of the heat flow process, even in the presence of large thermal gradients,

$$\frac{\partial T}{\partial t} = \frac{1}{C} I(r,t) + \frac{1}{C} \nabla(\kappa \nabla T) + \frac{1}{C} Q(r,t) , \qquad (4)$$

where T is the temperature, C the heat capacity per unit volume, I the laser heat source, r the position in the film, t the time, κ the thermal conductivity, and Q the heat loss to various sinks as well as the latent heat released. One of the assumptions implicit in the use of the Laplace equation is that convection either does not occur or is negligible. Calculations indicate that this is reasonable because of the small thickness of the melt and its short duration.[19] It has been demonstrated[20] that a one-dimensional equation adequately describes the case of a circularly symmetric Gaussian beam on a laterally homogeneous material if the beam radius is greater than twice the thermal diffusion length, a condition that is well satisfied in the present experiments. Possible heat losses include conduction to the sample holder or the surrounding air, blackbody radiation, and evaporation of the material from the surface. These two types of conduction are negligible for the time of the experiment. Blackbody radiation has been shown to be negligible as well.[21] Evaporation losses were included in the computer model but were also found to be very small, in agreement with earlier simple estimates.[22,23]

Most of the existing computer simulations of pulsed laser-induced transformations are based on the model by Baeri.[24] In this model the differential equation describing the heat flow is replaced with a set of finite element equations.

The sample is divided into slices of width Δz, and time into intervals Δt. The material parameters can be made into functions of both the temperature and the phase of the material. When the temperature of the ith layer reaches the melting point, the temperature change ΔT is held equal to zero until the accumulated heat input is equal to the latent heat of fusion. The intervals Δz and Δt are chosen to fulfill the stability requirements for numerical convergence: $\kappa \Delta t < C(\Delta z)^2/2$. This model has proved to be in good agreement with a variety of experimental results.[25-28]

In this work a similar technique was employed, based on the Crank–Nicholson method for solving the heat flow equation.[29] In this alogrithm a matrix equation is set up that relates the temperature in each layer to the value in the neighboring layers, and this entire matrix equation is solved for each new time interval. Such an implicit algorithm has the advantage that there are no numerical stability restrictions on the size of the time interval for a given distance interval. Approximations must be made for the coefficients, since they are a function of the material parameters at the unknown temperature. A two-step process[30] was employed. Material parameters determined from the previous temperatures were used in the first pass to calculate new estimated temperatures. These estimated temperatures were used to compute new material parameters, which were then used in the second pass to calculate better values for the new temperatures. This procedure, which must include an estimate of the latent heat released by the moving interface, introduces a new restriction on the maximum size of the time step for numerical stability. However, it is linear in Δz and therefore less severe than in the previous model.

For the case of a one-dimensional homogeneous sample of infinite thickness, with temperature-independent material parameters, irradiated at constant power for finite duration, the equation can be solved analytically.[31] The computer model solution for this case agrees well with the exact solution.

The most important difference between the present model and its predecessors is the incorporation of the actual kinetics of melting and crystallization. Unlike in the nanosecond or longer pulse experiments, for which most of the earlier models were developed, in picosecond experiments the interface temperature during regrowth can be several hundred degrees below the melting temperature, and the velocity of the interface can therefore be significantly slower than that of the melting temperature isotherm.

It is clear that the kinetics of crystal growth depend on the nature of the solid-liquid interface and the details of the atomic movements, as well as on the macroscopic heat flow. The crystallization rate can be described as the difference between a freezing and a melting flux. In equilibrium, the two fluxes are equal. The fluxes can be evaluated using transition state rate theory.[32,33] It is assumed that there exists an activated state with a free energy ΔG^* above that of the liquid. If ν is the atomic vibration, or attempt frequency, the number of activated configurations per interfacial atom formed per unit time from the liquid or the solid is, respectively, $\nu e^{-\Delta G^*/RT}$ or $\nu e^{-(\Delta G^* + \Delta G)/RT}$, where ΔG is the free energy of crystallization. The growth velocity u is then obtained from the difference between these two rates

$$u = f\nu\lambda(e^{-\Delta G^*/RT} - e^{-(\Delta G^* + \Delta G)/RT}), \quad (5)$$

where λ is the average jump distance (on the order of an interatomic distance) and f the fraction of interfacial sites at which attachment can occur. This fraction is near unity for "rough" crystal-melt interfaces, such as those in metals, but is small for "smooth" interfaces, such as the low-index ones in silicon at small undercooling.[3]

It is useful to consider the atomic mechanisms associated with particular values of the free energy of activation ΔG^*. If ΔG^* is nonzero, the growth velocity initially increases with undercooling due to the increase in driving free energy ΔG, but eventually it falls off due to the decrease in atomic mobility. A particular example is *diffusion-limited growth*, in which the motion of an atom from the liquid to the crystal requires a rearrangement similar to that for a diffusive jump in the liquid, so that ΔG^* then corresponds to the free energy of activation for the liquid diffusivity. This type of growth occurs, for example, in concentrated metallic alloys or in systems with a large crystalline unit cell. If the interfacial temperature falls below the diffusional freezing temperature T_g, crystal growth stops and the remaining liquid becomes a glass. It should be kept in mind, however, that some very dilute amorphous metallic alloys produced by vapor deposition on a cold substrate can crystallize at temperatures as low as 30 K.[34] This is well below T_g, indicating that crystallization in such systems proceeds by some faster, nondiffusional, process, such as the collision-limited one discussed below. The maximum growth velocity in the diffusion-limited regime u_D can be estimated from the liquid diffusivity, which in metals is $D_L \sim 10^{-5}$ cm^2/s,

$$u_D \sim \lambda/(\lambda^2/D_L) = (D_L/\lambda) \sim 3 \text{ m/s}, \quad (6)$$

since (λ^2/D_L) is the time required to diffuse an interatomic distance λ.

If ΔG^* is zero, the frequency with which atoms cross the interface is the thermal vibration frequency. This corresponds to *collision-limited* growth, in which the maximum velocity is the speed of sound. It has been proposed that this mechanism governs the crystallization of pure metals.[35,36] Perhaps the best evidence for this hypothesis is Walker's measurements[37] of the velocity of nickel dendrites growing into an undercooled melt at apparent velocities up to 50 m/s. An analysis by Coriell and Turnbull[38] indicates that the data is best fit by a model that incorporates collision-limited growth. There is also indirect evidence from a laser quenching experiment. Lin and Spaepen[39] observed that a sputter-deposited iron sample with an initial grain size of 50 nm contained grains with a diameter as large as 1 μm after irradiation with a 30-ps pulse. Using a simple heat flow estimate for melt duration of ~ 2 ns yields an apparent lateral growth velocity of several hundred meters per second, which is much faster than the maximum diffusion-limited growth velocity.

Since the velocities measured in the present experiments are also much greater than the maximum velocity in diffusion-limited growth, the model calculation is done with collision-limited growth kinetics. Furthermore, since it is ap-

plied to metallic systems, the site factor f is set equal to unity. With the approximation $\Delta G = \Delta S(T_M - T)$, where ΔS is the entropy of fusion and T_M is the melting point, Eq. (5) becomes

$$u = u_s(1 - e^{-(\Delta S/R)[(T_M - T)/T]}), \tag{7}$$

where u_s is the speed of sound. For the case of small deviations from equilibrium this becomes

$$u = u_s(\Delta S/RT)(T_M - T), \tag{8}$$

yielding the familiar result that the growth velocity is proportional to the undercooling near equilibrium.

It should be kept in mind that the transition state rate theory is a phenomenological one, which cannot be expected to apply rigorously under all conditions. In particular, the extension of the theory to the condition $\Delta G^* \to 0$ (i.e., the removal of the activation barrier) is open to question. Further, it can be seen that the absolute value of the melting velocity in Eq. (7) is larger than the speed of sound as the temperature goes to positive infinity. This seems physically implausible. Tsao *et al.*[40] resolve this problem by considering separately the entropic and enthalpic contributions to the free energy barrier. By taking the entropy as the barrier to crystallization and the enthalpy as the barrier to melting, they obtain

$$u = u_s(e^{-(\Delta S/R)} - e^{-(\Delta H/RT)}), \tag{9}$$

where ΔH is the enthalpy of fusion. Since $\Delta H = T_M \Delta S$, this can be written as

$$u = u_s e^{-(\Delta S/R)}(1 - e^{-(\Delta S/R)[(T_M - T)/T]}), \tag{10}$$

in which the speed of sound is now the limit for the melting velocity, and the speed of sound reduced by the factor $\exp(-\Delta S/R)$ for the crystallization velocity. Linearizing this equation yields

$$u = u_s \frac{\Delta S}{R} \frac{(T - T_M)}{T_M} e^{-\Delta S/R}. \tag{11}$$

This is the equation used in the computer model.

The model was tested by applying it to nanosecond pulses on silicon, and comparing the results to those obtained with Thompson's computer code,[27] which was based on Baeri's model described above, with good agreement. This version of Thompson's code, which requires a smaller time step and does not include an interface response function, is not expected to be accurate in the picosecond regime, but has been found to agree well with nanosecond results on silicon.[27]

To model the present experimental results, a computation was made for a 20-nm gold film on a sapphire substrate irradiated with a 20-ps pulse, using the materials parameters[41] listed in Table I. The melt depth and the corresponding interface velocity were calculated as a function of time, and are shown in Fig. 13. The model predicts velocities on the order of 100–200 m/s, for a fluence very near the melting threshold. A larger fluence gives a longer melt duration and a lower velocity. Figure 13 is in general agreement with the experimental results in Fig. 10. An exact comparison is difficult because of the uncertainty in many of the materials parameters at high temperatures, particularly in the absorbtivity and reflectivity at the pump pulse wavelength. Calculations for a bulk copper specimen gave similar results.

V. CONCLUSIONS

The experiments described in this paper demonstrated that pump-probe reflectivity measurements can be used to make time-resolved studies of melting and crystallization induced by picosecond pulsed laser irradiation of simple met-

TABLE I. Parameters used in the simulations.

	Comparison with analytic solution	Silicon	Copper	Gold	Sapphire
κ, solid (J/cm s K)	4.0	1.68	4.0	3.18	0.3
C, solid (J/cm^3 K) $= A + BT + D/T$					
A	3.04	1.17	3.19	2.52	4.25
B	...	0.209	− 0.885	0.072	0.714
D	...	− 0.217	...	...	...
α, solid (cm^{-1})	10^6	$1340 \times \exp(T/427)$	4.84×10^5	4.84×10^5	0.01
R, solid	0.6	0.337	0.6	0.6	...
F (J/cm^2)	0.5	1.0	0.07	0.06	...
L_{vap} (J/mol)	4.3×10^4	14.5159	4.3×10^5	3.2×10^5	...
T_B (K)	2867	2673	2867	3080	...
ρ (g/cm^3)	8.96	2.33	8.96	19.32	3.97
M (g/mol)	63.5	63.5	28.1	197	102
T_M (K)	...	1687	1356	1336	2300
L (J/cm^3)	...	2270	1836	1243	4230
$\Delta S/R$	...	3.6	1.12	1.11	5.33
C, liquid (J/cm^3 K)	...	2.56	4.43	2.87	...
κ, liquid (J/cm s K)	...	1.4	4.0	3.18	...
R, liquid	...	0.72	0.5	0.5	...
α, liquid (cm^{-1})	...	69 325	4.8×10^5	4.8×10^5	...

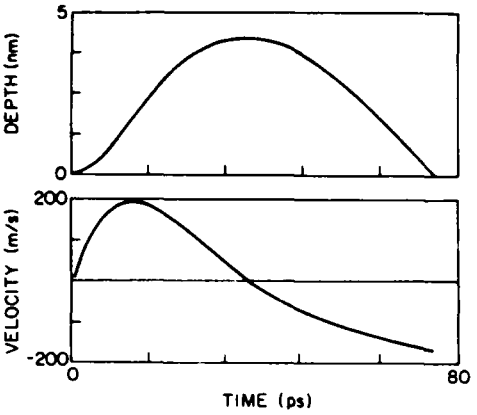

FIG. 13. Model calculations of the melt depth and interface velocity as a function of time for a 20-nm gold film on a sapphire substrate. The simulation parameters are listed in Table I.

als, such as gold, copper, or aluminum, even though the difference between their reflectivities in the liquid and crystalline is small.

That the observed reflectivity changes corresponded to melting was demonstrated by performing the experiments on artificial multilayers of fully miscible metals, such as copper and gold, and confirming that melting occurred by observing the leveling of the composition profile as a result of liquid phase diffusion by Auger spectroscopy.

Crystallization velocities up to 100 m/s were measured. These are the largest directly measured values for any material. It is clear that the atomic scale mechanism governing crystallization in these simple metals cannot be purely diffusional in nature, since the measured velocities are substantially greater than the maximum growth velocity in the diffusion-limited growth regime. On the other hand, these experiments lend strong support to the idea that crystallization in these systems is collision limited, since they could be accounted for satisfactorily by a computer model that incorporated both the heat flow processes and collision-limited kinetics.

ACKNOWLEDGMENTS

We thank David Turnbull and Michael Aziz for helpful discussions, Michael Thompson for making his computer code available, and Libby Shaw for assistance with the scanning Auger measurements. This work has been supported by the Office of Naval Research under Contract No. N00014-85-K-0684.

[1]N. Bloembergen, in *Laser-Solid Interactions and Laser Processing*, edited by S. D. Ferris, H. J. Leamy, and J. M. Poate (American Institute of Physics, New York, 1979), p. 1.
[2]R. W. Shoenlein, W. Z. Lin, J. G. Fujimoto, and G. L. Eesley, Phys. Rev. Lett. **58**, 1680 (1987).
[3]F. Spaepen and D. Turnbull, in *Laser Annealing of Semiconductors*, edited by J. M. Poate and J. W. Mayer (Academic, New York, 1982), p. 15.
[4]J. Y. Tsao, M. J. Aziz, P. S. Peercy, and M. O. Thompson, Mater. Res. Soc. Symp. Proc. **74**, 117 (1987).
[5]P. H. Bucksbaum and M. O. Thompson, Mater. Res. Soc. Symp. Proc. **74**, 123 (1987).
[6]See, for example, Mater. Res. Soc. Symp. Proc. **35** (1985); **51** (1986); **74** (1987).
[7]C. A. MacDonald and F. Spaepen, in *Laser Surface Treatment of Metals*, edited by C. W. Draper and P. Mazzoldi, NATO ASI Series E, No. 115 (Martinus Nijhoff, 1986), p. 111.
[8]C. A. MacDonald, A. M. Malvezzi, and F. Spaepen, Mater. Res. Soc. Symp. Proc. **51**, 227 (1986).
[9]Additional information about the experiment is available in C. A. MacDonald, Ph.D. thesis, Harvard University (1986).
[10]See Refs. 14 and 15; G. S. Arnold, Appl. Opt. **23**, 1434 (1984); H. G. Dreehsen, C. Hartwich, J. H. Schaefer, and J. Uhlenbusch, J. Appl. Phys. **56**, 238 (1984).
[11]F. Spaepen, A. L. Greer, K. F. Kelton, and J. L. Bell, Rev. Sci. Instrum. **56**, 1340 (1985).
[12]A. L. Greer and F. Spaepen, in *Synthetic Modulated Structures*, edited by L. L. Chang and B. C. Giessen (Academic, New York, 1985), p. 419.
[13]M. Born and E. Wolf, *Principles of Optics* (Pergamon, New York, 1980), 6th ed.
[14]K. H. Hellwege and A. M. Hellwege, Eds., *Landolt-Bornstein Zahlenwerte und Funktionen*, 6th ed. (Springer, Berlin, 1962), Series II, Vol. 8.
[15]J. C. Miller, Philos. Mag. **20**, 1115 (1969).
[16]J. Y. Tsao, S. T. Picraux, P. S. Peercy, and M. O. Thompson, Appl. Phys. Lett. **48**, 278 (1986).
[17]S. Williamson, G. Mourou, and J. C. M. Li, Phys. Rev. Lett. **52**, 2364 (1984).
[18]S. Williamson (personal communication).
[19]M. J. Aziz, J. Appl. Phys. **53**, 1158 (1982).
[20]R. Mehrabian, in *Laser-Solid Interactions and Laser Processing*, edited by S. D. Ferris, H. J. Leamy, and J. M. Poate (AIP, New York, 1979), p. 129.
[21]C. J. Lin, Ph.D. thesis, Harvard University (1983).
[22]F. Spaepen, in *Ultrafast Phenomena V*, Springer Series in Chemical Physics, edited by G. R. Fleming and A. E. Siegman (Springer, New York, 1986), p. 174.
[23]C. J. Lin, Ph.D. thesis, Harvard University (1983), p. 40.
[24]B. Baeri, J. Appl. Phys. **50**, 788 (1979).
[25]C. M. Surko, A. L. Simons, D. H. Auston, J. A. Golovchenko, R. E. Slusher, and T. N. C. Venkatesan, in *Laser-Solid Interactions and Laser Processing*, edited by D. Ferris, H. J. Leamy and J. M. Poate (AIP, New York, 1979), p. 155.
[26]D. H. Lowndes, G. E. Jellison, and A. G. Cullis, Mater. Res. Soc. Symp. Proc. **4**, 73 (1982).
[27]G. J. Galvin, M. O. Thompson, and P. S. Peercy, Phys. Rev. Lett. **48**, 33 (1982).
[28]M. J. Aziz, C. W. White, J. Narayan, and B. Stritzker, in *Energy Beam-Solid Interactions and Transient Thermal Processing*, edited by V. T. Nguyen and A. G. Cullis (Les Editions de Physique, Les Ulis, France, 1986), p. 231.
[29]D. K. U. von Rosenberg, *Methods for the Numerical Solution of Partial Differential Equations* (Elsevier, New York, 1969).
[30]J. Fröhlingsdorf (personal communication).
[31]C. J. Lin, Ph.D. thesis, Harvard University (1983), p. 57.
[32]K. A. Jackson, Acta Metall. **1**, 428 (1953).
[33]A review is given in Ref. 3.
[34]W. Buckel, Z. Phys. **138**, 136 (1954).
[35]D. Turnbull, in *Physical Processes in Laser-Materials Interactions*, NATO ASI Series B (Plenum, New York, 1983), Vol. 84, p. 117.
[36]D. Turnbull and B. G. Bagley, in *Treatise on Solid State Chemistry*, edited by N. B. Hannay (Plenum, New York, 1975), Vol. 5, p. 513.
[37]Described in B. Chalmers, *Principles of Solidification* (Krieger, New York, 1977), p. 114.
[38]S. R. Coriell and D. Turnbull, Acta Metall. **30**, 2135 (1982).
[39]C. J. Lin and F. Spaepen, in *Chemistry and Physics of Rapidly Solidified Materials*, edited by B. J. Berkowitz and R. O. Scattergood (TMS-AIME, New York, 1983), p. 273.
[40]J. Y. Tsao, M. J. Aziz, M. O. Thompson, and P. S. Peercy, Phys. Rev. Lett. **56**, 2712 (1986).
[41]R. C. Weast, Ed., *Handbook of Chemistry and Physics*, 60th ed. (CRC, Boca Raton, FL, 1980).

Rapid Solidification Processing: Principles and Technologies IV, eds. R. Mehrabian and P.A. Parrish, Conference held Dec. 15-18, 1986 at U. of CA, Santa Barbara (Claitor's Publishing Division, Baton Rouge, LA 1988) pp. 1-12.

CRYSTAL NUCLEATION AND GROWTH IN RAPID SOLIDIFICATION

Frans Spaepen and David Turnbull

Division of Applied Sciences
Harvard University
Cambridge, MA 02138

1. Introduction

The rapid extraction of heat from a metallic melt can lead to a substantial undercooling below the thermodynamic crystallization temperature. In this paper some of the fundamental kinetic processes of crystallization at large undercooling are reviewed: homogeneous crystal nucleation, high-velocity crystal growth induced by pulsed laser irradiation, and the formation of metastable crystalline phases. An extended version of this paper can be found in two recent publications by the authors [1,2].

2. Homogeneous Nucleation

a. Experimental observations.

Using dispersion and fluxing techniques Turnbull and his associates demonstrated in the early 1950's that $\Delta T_{o,r} = \Delta T_o/T_\ell$ (ΔT_o: undercooling at measurable homogeneous nucleation; T_ℓ: liquidus temperature) was at least ~0.18 for most of the close-packed and b.c.c. metals [3] and ~0.32 for Hg [4]. At the time the large magnitudes of these undercoolings were quite unexpected because of the then prevalent view that the atomic short range order (SRO) in liquid metals was essentially similar to that in close-packed crystals. Less surprising were the results of Vonnegut [5], Turnbull, and others that the $\Delta T_{o,r}$ in liquids that crystallize to structures with a coordination number less than eight, also were 0.15-0.20, at least.

Later investigators using similar techniques found onset undercoolings greater than 0.3 for some of these liquids and between 0.2 and 0.3 for several close packed metals. More particularly, Bosio et al. [6] reported $\Delta T_{o,r}$ approaching 0.5 for certain emulsions of Ga droplets. Perepezko and coworkers [7] obtained $\Delta T_{o,r}$ in the range of 0.3 to 0.4 for droplet emulsions of In, Sn and Bi. Recently Devaud and Turnbull [8] observed that some 0.3-0.5 mm diameter Ge droplets, fluxed in molten dehydrated B_2O_3, exhibited $\Delta T_{o,r} \approx 0.35$. Ovsienko [9], Gomersall et al. [10] reported $\Delta T_{o,r}$ ranging between 0.23 and 0.27 for droplets of Ge, Co, Ni. Table I summarizes some of the more recent data on onset undercooling.

It is generally presumed that the undercoolings at the onset of measurable homogeneous nucleation must equal or exceed the maximum reported experimental values, *properly*

adjusted for cooling rate and specimen size. However, there are conditions, as explained by Turnbull [12], under which this presumption may not be correct. First, it is evident that, when comparing results of different investigators, proper allowance must be made for experimental uncertainties in the calibration of T_o, the temperature at nucleation onset, relative to the liquidus, T_ℓ. However, apart from calibrational disparities there are other reasons why there might be some apparent or actual specimen-to-specimen dispersion of $\Delta T_{o,r}$ values at homogeneous nucleation.

Table I. Reported scaled undercoolings, $\Delta T_{o,r}$ (except for Hg uncorrected for differences in cooling rate) at measured nucleation onset for several pure metals.

Metals	$\Delta T_{o,r}$	Specimen Diameter	Ref.
Fe	0.23 ± 0.01	~ 0.7 cm	10
Co	0.27 ± 0.01	60-200 μm	9
Ni	0.27 ± 0.01	80-200 μm	9
In	0.26	2-5 μm	7
Hg	0.33 - 0.35	2-5 μm	4,11
Ga	0.50 ± 0.02	2-5 μm	6
Ge	0.35 ± 0.02	0.05 cm	8
Sn	0.37	2-5 μm	7
Bi	0.42	2-5 μm	7

An apparent dispersion may arise between various emulsions of droplets coated by solid films, because substantial hydrostatic stresses can develop in the smaller droplets (diamater <2-3 microns) as they are undercooled, due to the differential volume response of the liquid relative to its coating film. Consequently, the apparent $\Delta T_{o,r}$ could be displaced considerably from that which would be exhibited by the unstressed liquid. An analysis by the authors [13] indicated that this displacement could be as large as +10% for small Aℓ droplets coated by thin films of their oxide. In view of the high mechanical strength of solids in thin film form and the great resistance of liquid metals to cavitation, the possible importance of such stress effects in experiments on small droplets cannot be lightly dismissed.

An actual dispersion of $\Delta T_{o,r}$ for homogeneous nucleation can result from specimen-to-specimen variation in the concentrations of those *homophase* impurities which have a lower standard free energy of solution in the crystalline than in the liquid phase of the metals [12]. Such impurities, even in amounts of order of a few at ppm, can, without measurably displacing T_ℓ, reduce $\Delta T_{o,r}$ considerably from its pure metal value. This "chemical" effect on nucleation is distinct from that of the *heterophase* impurities which lead to heterogeneous nucleation.

At steady state, isothermal homogeneous nucleation should be stochastic in volume and time. This condition requires that in droplet emulsions the nucleation probability, k_d, in a droplet of diameter, d, be proportional to Id^3, where I is the nucleation frequency/volume-time. If the undercooling is chosen so that the time for crystal growth is negligible compared with that for nucleation k_d becomes, virtually, the crystallization frequency. Then the isothermal kinetics of crystallization of droplet emulsions can be analyzed to ascertain the dependence of k_d on d. In one method (a) developed by Turnbull [4] and described in detail by Pound [14], the size dispersion of the droplet population is exploited to discriminate between the possibilities.

However, a more conclusive discrimination is achieved by method (b) in which $k_{\bar{d}}$, where $\bar{d}$ is the diameter of the droplet of average volume, are compared for separate emulsions with substantially differing $\bar{d}$; then $k_{\bar{d}_1}/k_{\bar{d}_2} = (\bar{d}_1/\bar{d}_2)^3$ if nucleation is homogeneous.

Turnbull's measurements of the isothermal rates of solidification of Hg-Laurate (Hg-L) coated Hg droplet dispersions [4], as well as those with Cormia [15] on n-hepta- and n-octadecane dispersions, fulfilled both tests (a) and (b) for volume nucleation. Thus at a given undercooling the rates were satisfactorily described by a single nucleation frequency/volume. The onset undercooling of Hg in these experiments was ~78° ($\Delta T_{o,r} \approx 0.33$). Somewhat higher onset undercoolings in differently prepared Hg dispersions were reported by Monge [16] and by Perepezko and Rasmussen [11]. When adjusted to the cooling rate of Turnbull's experiments the Monge result is about 3° and that of Perepezko and Rasmussen about 4-5° greater than obtained by Turnbull. These differences are not large and could reflect only the temperature calibration uncertainties in the separate studies. Alternatively, they could be due to small "chemical" effects [12] as discussed in the foregoing. Thus the evidence that homogeneous nucleation was exhibited in Turnbull's experiments on HgL coated Hg droplets seems quite conclusive.

The temperature dependence of I in Turnbull's experiments on Hg was satisfactorily described by the equation derived from classical nucleation theory but with a prefactor about 10^7 times too large [4], when σ and the entropy of crystallization/volume, ΔS_v, were assumed constant. It was shown elsewhere [12] that this disparity could result from the chemical effect noted above. Alternatively, it might, as Turnbull suggested earlier [4], arise from temperature variations of ΔS_v and σ. The temperature variation of $\Delta S_v(T)$ in the undercooled regime can be estimated roughly from heat capacity, $C_p(T)$, measurements [1]. Putting $\Delta S_v(T)$ into the classical expression for I, with the theoretical prefactor, the Hg data can then be fit within experimental error, with an interfacial tension increasing by 0.10 ergs/cm^2-deg with temperature. Over the temperature regime of the I measurements the fitting σ could be described by:

$$\sigma = 11.9 + 0.10T \text{ ergs/cm}^2 \qquad (1)$$

where T is the absolute temperature. This result is in rough agreement with that of a calculation of Mijazawa and Pound [17] assuming $\Delta C_p \sim 0$.

Mijazawa and Pound [17] measured the isothermal rates of solidification of two dispersions of Ga droplets which exhibited onset undercoolings ~100°, well below the maximum ~150° claimed by Bosio et al. [6]. Their data on the separate dispersions seemed to meet test (a) for volume nucleation. However, they appear to fail to meet test (b). Thus, at $\Delta T = 100°$ the solidification time constant $(1/k_{\bar{d}})$ for their first dispersion, in which $\bar{d} = 5$ μm, was only 3.5 times greater than that for their second dispersion in which $\bar{d}$ (= 21 μm) was about four times larger. Thus their $k_{\bar{d}}$ appeared to be proportional to $\bar{d}$, rather than to $\bar{d}^3$, which would have been required by test (b) for volume nucleation. The origin of such an unusual dependence of $k_{\bar{d}}$ on $\bar{d}$ is not clear.

b. Theoretical developments

The crystal-melt interfacial tension. Macroscopically the nucleation resistance indicates, in terms of simple nucleation theory, a scaled crystal-melt interfacial tension at the *temperature of measurable nucleation onset* of about 0.55 for the close-packed metals and 0.60 for Hg. This scaled tension is defined as:

$$\alpha = v^{2/3}\sigma/\Delta h_f \qquad (2)$$

where v is the volume/atom and Δh_f is the heat of fusion/atom.
In metals the volume changes on solidification are small and at constant density the energy is quite insensitive to the prexie atomic siting. From this it appears that a crystal-melt interface, *without a density deficit* should be formable at little energy cost. However, depending on liquid structure, formation of such an interface may require localization, with consequent entropy loss, of atomic positions in the liquid adjacent to the interface [18].

Spaepen and Meyer [19,20] calculated that the contribution to the scaled tension, α, associated with this localization at the (111) face of an f.c.c. crystal is ~0.86 at T_m. This value of α should be an upper limit and it is, indeed, well above those indicated by the crystal nucleation kinetics. *Either the negentropy or the excess energy of the interface could be made to vanish by particular choices of the interfacial configuration but they cannot be made to vanish simultaneously* [18]. The nature of the interfacial tension (negentropic or energetic) *does* make a difference for the temperature dependence. Specifically, if the interfacial tension is negentropic in nature, it is expected to have a positive temperature coefficient. This is what is observed in the Hg experiments, as shown by equation (1), and the results can be accounted for quantitiatively by a *fully* negentropic model [21].

Microscopically the high onucleation resistance of liquid metals implies that their crystallization must be attended by some essential reconstruction of the atomic short range order. Frank [22] suggested that this reconstruction might be from a predominantly icosahedral short range order in the liquid to that in the close packed crystal. In support of this suggestion he showed that if the interatomic interaction potential is of the Lennard-Jones type, the energy of a 13 atom cluster is actually lower in the icosahedral than in either of the close-packed crystalline configurations. The icosahedral configuration is a polytetrahedral one and includes no half-octahedra, which are essential components of close-packed crystalline structures. It has also been established that the energetic preference for polytetrahedral over close-packed crystalline configurations extends well beyond 13 to several tens of atoms clusters and that the density in these polytetrahedral clusters is higher than in the crystalline ones [23]. In the dense random packed structure of uniform hard spheres it is found that tetrahedral configurations predominate while there is a conspicuous paucity, relative to the crystals, of half-octahedral ones [24]. The appearance of a polytetrahedral type structure in random packing suggests that it is entropically favored and that it may be the most likely prototypical model structure for monatomic liquids. The entropy of a condensed system should increase with the range of local density fluctuations permissible at a given energy. Because of the high density of polytetrahedral clusters this range should be substantially greater in random packed structures than in those where the crystalline type of short range order predominates. Thus this microscopic theory for the nucleation resistance requires that atoms in the liquid be positioned randomly within the repulsive constraints. These atoms would then have to be localized sharply to form a crystal-melt interface with no density deficit.

Effect of alloying on crystal nucleation. There have been several studies of the dependence of the temperature $T_o(x)$, at measurable nucleation onset, on melt composition, x. They generally indicate [25] that in the labile regime $T_o(x)$ roughly parallels the liquidus $T_\ell(x)$. Thompson and Spaepen [26] showed that this behavior can be explained with simple solution models by supposing that: (i) The scaled crystal-melt tension, α, as in Spaepen's model, is mainly topological in origin and only weakly dependent on x. (ii) The crystal nucleus is always in contact with melt of average composition; this supposition is the analog of the "mean field approximation".

3. Laser Quenching

a. Quenching mechanism.

Irradiating a metallic surface with a short laser pulse results in the melting and subsequent quenching of a thin overlay. It is useful to analyze this process as a succession of three stages: energy deposition, melt-in, and regrowth. They are illustrated in Figure 1.

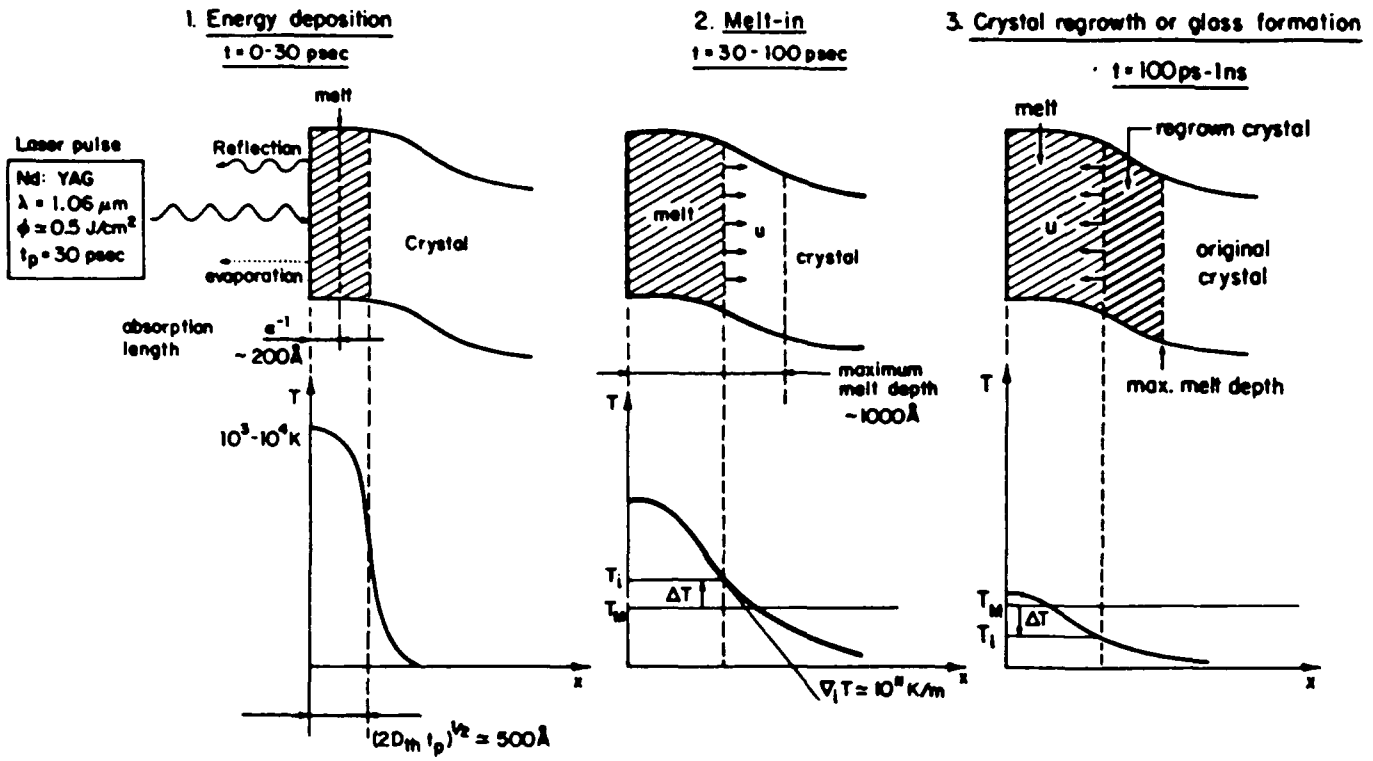

Fig. 1. Schematic illustration of the mechanism of pulsed laser quenching.

During the first stage, the laser energy is deposited in a layer of thickness α^{-1}, where α is the absorption coefficient. For optical light on metals, or for UV light on semiconductors, this layer is a few hunderd Å thick. Since the transfer of the energy from the electrons, which interact with the light, to the lattice occurs within less than 1 ps [27], the energy deposition process, which lasts for the duration of the pulse, t_p, can be considered a purely thermal one. The thermal diffusion length during that time is $\ell_T = (2D_{th}t_p)^{1/2}$, which, for metals is between 250 and 700 Å, depending on the thermal diffusivity (D_{th}= 10^{-4} to 10^{-5} m^2/s). For fluences, ϕ, in the indicated range, a layer of thickness l_T is melted and heated to several thousand degrees.

Note that for a pulse duration of less than 1 ps, ℓ_T is less than α^{-1}. The thickness of the initial molten layer, and hence also the thermal gradients, are then independent of the pulse duration. Femtosecond pulses, therefore, although very useful for time-resolved spectroscopy of the various phenomena associated with the irradiation process, do not produce a higher quench rate. A general discussion of the regimes associated with the relative values of l_T and α^{-1} can be found in Bloembergen's paper [28].

Following the termination of the irradiation pulse, the heat from the very hot liquid continues to diffuse into the substrate, which results in further melting, until the temperature of the crystal-liquid interface drops to the equilibrium melting temperature. For the conditions of Figure 1, the maximum melt depth, d, is about 1000Å. The overheating of the crystal during the melt-in process is considerable. The thermal gradients are very high (10^{11} K/m), as is the melt-in velocity ($u \sim 10^3$ m/s). The duration of the melt-in stage of the process is therefore on the order of $d/u \sim 100$ ps.

The third stage is that of resolidification, either by regrowth of the underlying crystal, by growth of a new crystal, or by glass formation if the melt cools to its

configurational freezing point before the crystallization front passes. A number of sophisticated numerical analyses have been made of the thermal quantities of this process, but their order of magnitude can easily be estimated from dimensional arguments. The temperature scale is set by the melting temperature, T_m, which is on the order of 10^3K. The length scale is set by the melt depth d~10^{-7}m. The corresponding temperature gradient is then $\nabla T = T_m/d \sim 10^{10}$K/m, and the cooling rate $\dot{T} = D_{th} \nabla T/d \sim 10^{12}$ K/s. The lifetime of the melt can be estimated as $\tau = T_m/\dot{T} = 10^{-9}$ s, which is in agreement with the experimental values obtained from transient reflectivity measurements [29-32]. The velocity with which the isotherms move toward the surface during cooling is an important quantity to be compared to the crystal growth velocity, and can be estimated as $u_T = \dot{T}/\nabla T \sim 100$ m/s. These parameters, together with those for a "conventional" melt quenching process such as melt spinning, are summarized in Table II, using the thermal data for iron.

Table II. Thermal parameters in melt quenching.

		Laser Quenching	Melt Spinning
Melt temperature	T_m(K)	10^3	10^3
Melt thickness	d(m)	10^{-7}	5×10^{-5}
Temperature gradient	∇T(K/m)	10^{10}	2×10^7
Cooling rate	$\dot{T}$(K/s)	10^{12}	4×10^6
Melt lifetime	t(s)	10^{-9}	not applicable
Isotherm velocity	u_T(m/s)	100	0.2
Heat-flow limited crystal growth velocity	u_h(m/s)	230	0.5

b. Thermodynamics and kinetics of phase formation.

The short timescale of the picosecond melt quenching process puts restrictions on the transformations that can occur. For the entire liquid layer, of thickness d = 1000 Å, to crystallize during the cooling time, τ, of 1 ns, the velocity must be at least $u = d/\tau \sim 100$ m/s. The time, t_1, to crystallize a monolayer at this speed is about 3 ps, and the distance an atom can diffuse in that time, $(D_\ell t_1)^{1/2}$, is less than an interatomic distance (D_ℓ is the diffusivity in the liquid phase). This means that under these short pulsed laser quenching conditions no long-range diffusion can occur, and that the only possible transformations are *partitionless* ones, either growth of a crystal of the same composition of the liquid, or glass formation.

The thermodynamic restrictions imposed by the partitionless conditions are illustrated by the phase diagram of Figure 2, which contains two primary solid solutions (α,δ) and two intermetallic compounds (β,γ). The free energy diagram on Figure 2 shows how the T_o-lines for the transformations of these four phases from the liquid are constructed. At a sufficiently low temperature, T_g, the atomic transport rate in the liquid state becomes negligibly small, so that no more transformations can occur on a reasonable timescale. The liquid is then configurationally frozen and becomes a glass. For a composition in the range x'-x" in Figure 2, no crystallization is possible under picosecond laser quenching conditions, and therefore only glass formation is thermodynamically possible. This criterion for glass formation is only a *sufficient* one, and not a necessary one, as

has been claimed [33]. In fact, more often than not, picosecond quenching experiments yield glasses over a wide range of compositions below the T_o-lines for both intermetallic compounds and primary solutions. To explain this, it is necessary to consider the kinetics of partitionless crystallization in some detail.

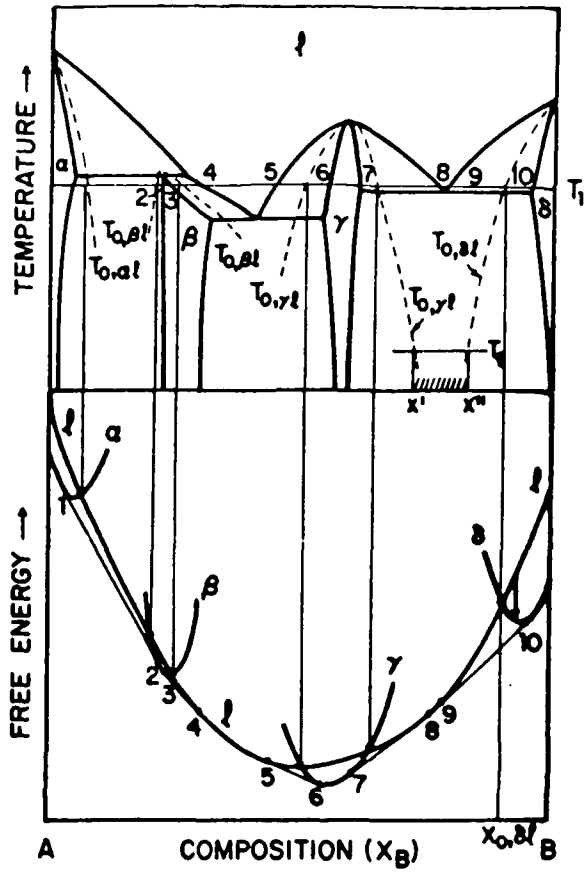

Fig. 2. Schematic phase diagram (top), and corresponding free energy diagram at temperature T_1 (bottom), illustrating the construction of the T_o-lines for the primary solid solutions and the intermetallic compounds. In the composition range x'-x" (dashed), only glass formation is possible under conditions of partitionless solidification. The numbers correspond to the same compositions in the top and bottom diagrams.

The basic theory for crystal growth far from equilibrium has been formulated by Turnbull, and can be found in a number of publications [34,35], including the first paper in the present volume. The crystal growth velocity can be written as:

$$u = fk\lambda \left[1 - \exp\left(-\frac{\Delta G_c}{RT_i}\right)\right] \qquad (15)$$

where k is the atom jump frequency across the crystal-melt interface, f is the fraction of interface sites that can incorporate a new atom, λ is the interatomic distance, ΔG_c is the difference in molar free energy between crystal and melt, and T_i is the interface temperature.

If the undercooling of the interface, $\Delta T_i = T_m - T_i$, is small, the driving free energy can be approximated by:

$$\Delta G_c = \Delta S_c \, \Delta T_i \qquad (16)$$

where ΔS_c is the molar entropy of crystallization. The exponential in equation (15) can be linearized to:

$$u = fk\lambda \frac{\Delta S_c}{R} \frac{\Delta T_i}{T_i} \tag{17}$$

where, for metals, $f \sim 1$ and $\Delta S_c \sim R$.

The crystal growth rate also depends on the rate at which the heat of crystallization, $\Delta h_{c,v}$ per unit volume, can be removed. Since this must occur by heat flow down the temperature gradient at the interface, $\nabla_i T$, the heat flux, J, must obey the relations:

$$J = u\, \Delta h_{c,v} = \kappa\, \nabla_i T \tag{18}$$

where κ is the thermal conductivity. Conversely, equation (18) can be turned around to define a heat flow-limited velocity:

$$u_h = \frac{\kappa \nabla_i T}{\Delta h_{c,v}} \tag{19}$$

Table I gives values for u_h for the laser quenching conditions as well as for melt spinning.

Combining equations (17) and (19) then gives for metals:

$$\frac{u_h}{k\lambda} = \frac{T_m - T_i}{T_i} \tag{20}$$

In conventional solidification, the interface kinetics are much faster than the rate of heat removal, so that $u_h \ll k\lambda$, and ΔT_i is small. This type of growth is called *heat flow-limited*. In laser quenching, depending on the nature of the interface rearrangements (see below), the rate of heat removal can be much faster than the interface kinetics, so that $u_h \gg k\lambda$, and the undercooling ΔT_i is large, so that metastable phases can be formed. This corresponds to *interface-limited* growth.

The maximum growth velocity of a crystal, $u_{max} = k\lambda$, is determined by the nature of the atomic rearrangements that control the growth process. In pure metals, dilute alloys or compounds with simple crystal structures, k can be taken as the frequency of thermal vibration (~ Debye frequency), so that $u_{max} \sim u_s$, the speed of sound in the liquid, which is on the order of several thousand m/s. This is called the *collision-controlled* regime, because the growth occurs by simple impingement of the liquid atoms onto the crystal.

In more concentrated alloys or in compounds with a more complicated crystal structure, where a change of the nearest neighbor configuration, i.e. diffusion, is necessary, the jump frequency can be taken as D_ℓ/λ^2, and $u_{max,D} = D_\ell/\lambda$, which is on the order of 10 m/s. This is the *diffusion-controlled* regime. Table I shows that for picosecond laser quenching $u_{max,D} \ll u_T, u_h$, so that this type of growth can easily be suppressed. Equation (20) shows that under these conditions T_i falls far below T_m, and glass formation becomes possible.

Although in partitionless growth of crystals there is no *long-range* diffusional transport, the growth can still be diffusion-controlled if a drastic change of the nearest neighbor environment is necessary to transform the liquid structure into the crystalline one. This is the case, for example in metal-metalloid alloys such as Fe-B, where the chemical interaction leads to a very pronounced short range order in the liquid (9 Fe atoms around each B in a capped trigonal prism arrangement [36]), which is very different from that in the crystal (B interstitial in bcc Fe [37]). As a result, it is possible to produce Fe-B glasses containing as little as 5 at.% B [38], which is far below the T_o-line. Similarly, if the unit cell of an intermetallic compound is large, or if long-range chemical order must be established, crystal growth is diffusion-limited, and the growth of these compounds is easily suppressed in picosecond pulsed laser quenching. Numerous experiments on a variety of binary metallic systems (Ni-Nb, Ni-Mo, Co-Mo, Nb-Co [30,39-43]) have demonstrated that glasses can be formed at the intermetallic compositions. On the other hand, in pure metals with simple crystal structures, and, by extension, disordered alloys with the same simple structures (e.g. disordered fcc in Cu-Co or Ag-Cu), growth is collision-limited and cannot be suppressed even by picosecond pulsed laser quenching. This is confirmed by direct measurements of the growth velocity of pure metals and disordered alloys (Au, Cu, Cu-Au) by transient reflectivity [30,31] which yield large values (>100 m/s) that can only be accounted for by a collision-controlled mechanism.

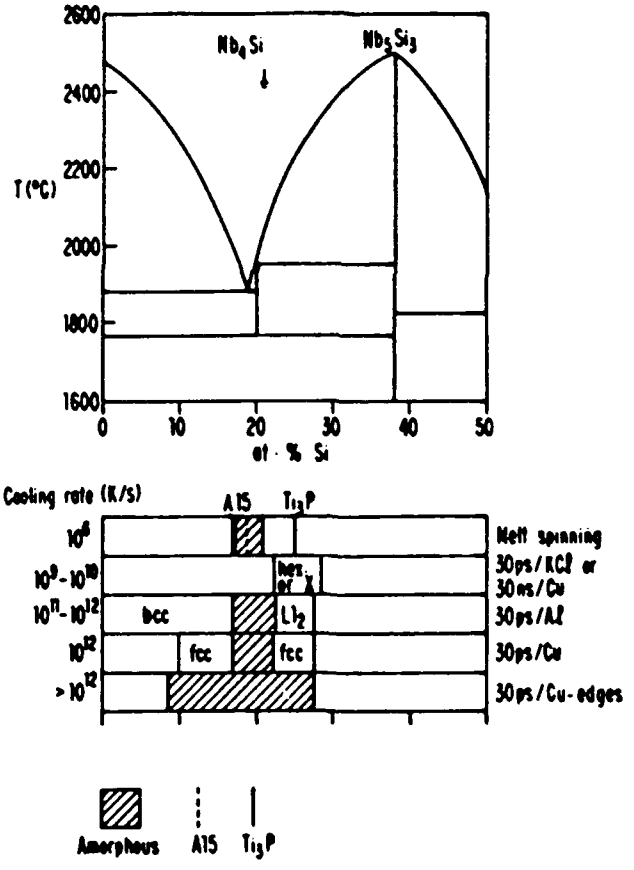

Fig. 3. Phase diagram of the Nb-Si system (top), and schematic illustration of the phases obtained by different methods of liquid quenching. The melt spinning results are from refs. [48-51]; the laser quenching results are from refs. [45-47]. The pulse length and the substrate for the laser experiments are indicated.

c. Phase selection

An undercooled liquid can often crystallize into any of a number of thermodynamically allowed stable or metasable phases. The selection of the phase

that actually forms depends on the details of the transformation kinetics. Some general empirical rules to predict this have been formulated. The best known one of these is Ostwald's rule, which states that the phase nearest to the liquid in free energy is kinetically favored. There are, however, numerous counterexamples to this rule. Turnbull has proposed that phases closest in entropy to the parent phase are kinetically favored [44]. He pointed out that that transformation processes requiring the smallest changes in the positional and maitonal correlations of the atoms are likely to be the easiest ones. For tranformations from the liquid this implies that a small unit cell and a high degree of isotropy are favorable kinetic factors for crystallization.

A recent pulsed laser quenching study of the Nb-Si system illustrates these factors very clearly [45-47]. The results are summarized in Figure 3.

At the highest quench rates ($>10^{12}$ K/s), obtained in the thinnest sections of the spots irradiated with a 30 ps pulse on a copper substrate the amorphous phase was formed over a wide composition range. Such broadening of the range of amorphous phase formation is consistent with our earlier observations on other metal-metalloid and metal-metal systems.

At slightly lower quench rates (10^{12} K/s), obtained in the remaining area of those spots, a new phase was found: a disordered f.c.c. solid solution [46]. Although the formation of disordered f.c.c. solid solutions in metal-metal alloys cannot be suppressed by picosecond laser quenching, the growth rate of the f.c.c. phase in this system, although still the highest one observed, is probably slightly lower due to the short range order around the Si.

By lowering the quench rate to 10^{11}-10^{12} K/s by supporting the films on an aluminum substrate, a supersaturated b.c.c solid solution was found at low Si contents, and an ordered f.c.c. phase ($L1_2$, Cu_3Au-type) around 25 at.% Si.

A cooling rate of 10^9-10^{10} K/s was obtained, either by supporting the ps-irradiated films on a salt substrate, or by irradiating the films on a copper substrate with a 30 ns pulse. Under these conditions two entirely new phases were found around 25 at.% Si: a hexagonal phase with a 250 $Å^3$ unit cell and an as yet unidentified phase [47].

Conventional melt spinning, during which the cooling rate is 10^6 K/s, produces the Ti_3P-type structure [48].

Important to note here is that the degree of isotropy and the unit cell size of the phases formed at 25 at% Si decrease with decreasing quench rate: amorphous (isotropic, no unit cell), disordered fcc (1 atom unit cell, cubic point group), ordered f.c.c (4 atom unit cell, cubic point group), hexagonal (~ 16 atom unit cell, uniaxial point group), Ti_3P-type (32 atom unit cell, uniaxial point group). Qualitatively similar observations have been made in laser quenching of Ga [52] and Mn [53].

Acknowledgements

The authors' work in this area has been supported by the Office of Naval Research under contract number N00014-85-K-0684 and by the National Science Foundation through the Harvard Materials Research Laboratory under contract number DMR-83-16979.

References

1. D. Turnbull, *Undercooled Alloy Phases*, ed. by E.W. Collings and C.C. Koch, The Metallurgical Society, Warrendale, PA (1987), p.3
2. F. Spaepen, ibid, p. 187.
3. D. Turnbull and R.E. Cech, J. Appl. Phys. 21, 804 (1950).

4. D. Turnbull, J. Chem. Phys. 20, 411 (1952).
5. B. Vonnegut, J. Colloid Sci. 3, 563 (1948).
6. L. Bosio, A. Defrain, M. Erney and E. Epelboin, Mem. Sci. Revue Metall. 58, 43 (1961); L. Bosio and A. Defrain, J. Chem. Phys. 61, 859 (1964); L. Bosio, A. Defrain and M. Dupont, ibid. 68, 542 (1971).
7. J.H. Perepezko and J.S. Paik, *Rapidly Solidified Amorphous and Crystalline Alloys*, ed. by B.H. Kear, B.C. Giessen and M. Cohen, 49, North-Holland, Amsterdam (1982).
8. G. Devaud and D. Turnbull, Mats. Res. Soc. Symp. Proc., ed. by G.S. Cargill III, F. Spaepen and K.N. Tu, in press (1987).
9. D.E. Ovsienko, V.P. Maslov and V.P. Kostyuchenko, Kristallografiya 16, 405 (1971); see also A.A. Chernov, Ann. Revs. Mats. Sci. 3, 397 (1973).
10. D.W. Gomersall, S.Y. Shiraishi and R.G. Ward, J. Austral. Inst. Metals 10, 220 (1965).
11. J.H. Perepezko and D.H. Rasmussen, Met. Trans. 9A, 1490 (1978).
12. D. Turnbull, Progress in Materials Science, ed. by J.W. Christian, P. Haasen and T.B. Massalski, Chalmers Anniversay Volume, 269, Pergamon (1981).
13. F. Spaepen and D. Turnbull, Scripta Met. 13, 149 (1979).
14. G.M. Pound, *Liquid Metals and Solidification*, pp. 87-105, Am. Soc. Metals, Metals Park, Ohio (1958).
15. D. Turnbull and R.L. Cormia, J. Chem. Phys. 34, 820 (1961).
16. P. Monge, Colloque International sur les proprietes des Etats Metastable, Pau-France, Resumes, Univ. of Bordeaux, 41 (1968).
17. Y. Miyazawa and G.M. Pound, J. Cryst. Growth 23, 45 (1974).
18. D. Turnbull, *Physics of Non-Crystalline Solids*, ed. by J.W. Prins), 41, North-Holland, Amsterdam (1964).
19. F. Spaepen, Acta Met. 23, 729 (1975).
20. F. Spaepen and R.B. Meyer, Scripta Met. 10, 257 (1976).
21. F. Spaepen, to be published.
22. F.C. Frank, Proc. Roy. Soc. 215A, 43 (1952).
23. M.P. Hoare and P. Pal, Adv. Phys. 24, 643 (1975).
24. J.L. Finney, Proc. Roy. Soc. 319A, 497 (1970); C.H. Bennett, J. Appl. Phys. 43, 2727 (1972); J.D. Bernal, Nature 185, 68 (1960).
25. J.H. Perepezko, Proc. 2nd Int. Conf. Rapid Solidification Processing, ed. by R. Mehrabian, B.H. Kear and M. Cohen, 56 Claitore, Baton Rouge, La. (1980).
26. C.V. Thompson and F. Spaepen, Mats. Res. Soc. Proc. 9, 603 (1982); Acta Met. 31, 2021 (1983).
27. For a review of these relaxation processes, see W.L. Brown, Mat. Res. Soc. Symp. Proc., 23, 9 (1984).
28. N. Bloembergen, in *Laser-Solid Interactions and Laser Processing*, ed. by S.D. Ferris, H.J. Leamy and J.M. Poate, AIP, New York (1979), p. 1.
29. J.M. Liu, R. Yen, H. Kurz, and N. Bloembergen, Appl. Phys. Lett., 39, 755 (1981).
30. C.A. MacDonald, Ph.D. Thesis, Harvard University (1986).
31. C.A. MacDonald and F. Spaepen, in *Laser Surface Treatments of Metals*, ed. by C.W. Draper and P. Mazzoldi, NATO ASI Series, Martinus Nijhoff, Dordrecht, The Netherlands (1986) p. 111.
32. C.A. MacDonald, A.M. Malvezzi and F. Spaepen, Mat. Res. Soc. Symp. Proc. 51, 277 (1986).
33. T.B. Massalski, Proc. 4th Int. Conf. on Rapidly Quenched Metals, ed. by T. Masumoto and K. Suzuki, Jap. Inst. Metals, Sendai (1982) p. 203.
34. D. Turnbull, in *Physical Processes in Laser-Materials Interactions*, NATO-ASI Proc., ed. by M. Bertollotti, Plenum, NY (1983), p. 117.
35. F. Spaepen and D. Turnbull, in *Laser Processing of Semiconductors*, ed. by J.M. Poate and J.W. Mayer, Academic, NY (1982), p. 15.
36. For a review of the short-range order in metal-metalloid glasses, see J.M. Dubois and G. Le Caer, Acta Metall., 32, 2101 (1984).
37. R. Ray and R. Hasegawa, Sol. St. Comm., 27, 471 (1978).
38. C.J. Lin and F. Spaepen, Appl. Phys. Lett., 41, 721 (1982).
39. C.J. Lin, F. Spaepen and D. Turnbull, J. Non-Cryst. Solids, 61/62, 767 (1984).
40. C.J. Lin and F. Spaepen, Mat. Res. Soc. Symp. Proc., 28, 75 (1984).
41. C.J. Lin and F. Spaepen, in *Chemistry and Physics of Rapidly Solidified Materials*, ed. by B.J. Berkowitz and R.O. Scattergood, AIME-AIME, NY (1983), p. 273.

42. C.J. Lin and F. Spaepen, Acta Metall. 34, 1367 (1986).
43. F. Spaepen, in *Advances in Cryogenic Engineering*, ed. by R.P. Reed and A.F. Clark, Plenum, NY (1986) p. 1019.
44. D. Turnbull, Met. Trans. 12A, 695 (1981).
45. W.K. Wang, C.J. Lobb and F. Spaepen, in preparation.
46. W.K. Wang and F. Spaepen, J. Appl. Phys. 58, 4477 (1985).
47. W.K. Wang and F. Spaepen, Appl. Phys. Lett. 49, 295 (1986).
48. W. Rossteutscher and K. Schubert, Z. Metallk. 56, 813 (1965).
49. A. Inoue and T. Masumoto, Sci. Rep. Res. Inst. Tohoku University, A28, 165 (1980)
50. R.M. Waterstrat, F. Haenssler and J. Müller, J. Appl. Phys, 50, 4763 (1979).
51. K. Togano, H. Kamakura and K. Tachikawa, Phys. Lett. 76A, 83 (1980).
52. J. Fröhlingsdorf and B. Stritzker, Mat. Res. Soc. Symp. Proc. 51, 271 (1986).
53. D.M. Follstaedt, P.S.Peercy and J.H. Perepezko, Appl. Pjys. Lett. 48, 338 (1986).

Materials Science and Engineering, 98 (1988) 325–328

Formation of Metastable Nb–Si Phases by Picosecond and Nanosecond Pulsed Laser Quenching*

W.-K. WANG†, C. J. LOBB and F. SPAEPEN

Division of Applied Sciences, Harvard University, Cambridge, MA 02138 (U.S.A.)

Abstract

Laser quenching was used to investigate the formation of metastable phases in the Nb–Si alloy system in the range 8–27 at.% Si. By varying the duration of the laser pulse between 30 ps and 30 ns, and by changing the conductivity of the substrate, melt quench rates between 10^8 K s^{-1} and 10^{13} K s^{-1} were obtained. At the highest cooling rates, amorphous alloys were formed over the entire composition range. At progressively lower quench rates the following metastable phases are formed: face-centered cubic solutions, supersaturated body-centered cubic solutions, the $L1_2$ ordered phase, and a new hexagonal compound. This progression illustrates how phase formation from the melt is kinetically favored by higher isotropy and a smaller unit cell size. All the phases exhibited superconductivity, with a T_c between 2 K and 6 K.

1. Introduction

Pulsed laser quenching is the fastest melt quenching technique available: picosecond pulses can give quench rates of the order of 10^{12} K s^{-1}. The technique has been used to investigate the compositional limits of glass formation and to expose new metastable phases [1–4]. Until very recently, the stoichiometric A-15 phase of Nb–Si was the prime theoretical candidate for the highest critical temperature. Since this phase is metastable, it must be prepared by non-equilibrium methods. Conventional melt spinning can produce the A-15 structure, but only if it is niobium rich. At 25 at.% Si, it produces the tetragonal Ti_3P structure [5–8].

Although the laser quenching experiments described here did not produce the A-15 phase, they led to the discovery of some new metastable phases and provided insight into the fundamentals of metastable phase selection. This paper explains the basics of laser quenching and phase selection, and reports the results of its application to Nb–Si.

2. Laser quenching

Irradiating a metallic surface with a short laser pulse results in the melting and subsequent quenching of a thin overlay. This process can be analyzed as a succession of three stages: energy deposition, melt-in and regrowth [1, 9]. They are illustrated in Fig. 1 for a pulse of 30 ps.

During the first stage, the laser energy is deposited as heat in a layer of thickness α^{-1}, where α is the absorption coefficient, which for metals is a few hundred ångstroms. The thermal diffusion length during that time is $l_T = (2D_{th}t_p)^{1/2}$, which is between 250 Å and 700 Å for metals, depending on the thermal diffusivity. For fluences ϕ in the indicated range, a layer of thickness l_T is melted and heated to several thousand degrees.

After the pulse, the heat from the very hot liquid continues to diffuse into the substrate, resulting in further melting, until the temperature of the crystal–liquid interface drops to the equilibrium melting temperature. For the conditions of Fig. 1, the maximum melt depth d is about 1000 Å.

The third stage is that of resolidification, either by regrowth of the underlying crystal, by growth of a new crystal, or by glass formation if the melt cools to its configurational freezing point before the crystallization front passes. The quench parameters can be estimated by the following dimensional argument. The characteristic temperature is the melting temperature T_m which is of the order of 10^3 K. The characteristic length is the melt depth $d \simeq 10^{-7}$ m. The corresponding temperature gradient is then $\nabla T = T_m/d \simeq 10^{10}$ K m^{-1}, and the cooling rate $\dot{T} = D_{th}\nabla T/d \simeq 10^{12}$ K s^{-1}. The lifetime of the melt is $t = T_m/\dot{T} = 10^{-9}$ s, which is also the value found in transient reflectivity measurements [10, 11].

*Paper presented at the Sixth International Conference on Rapidly Quenched Metals, Montreal, August 3–7, 1987.

†Permanent address: Institute of Physics, Academia Sinica, Peking, PRC.

0025-5416/88/$3.50

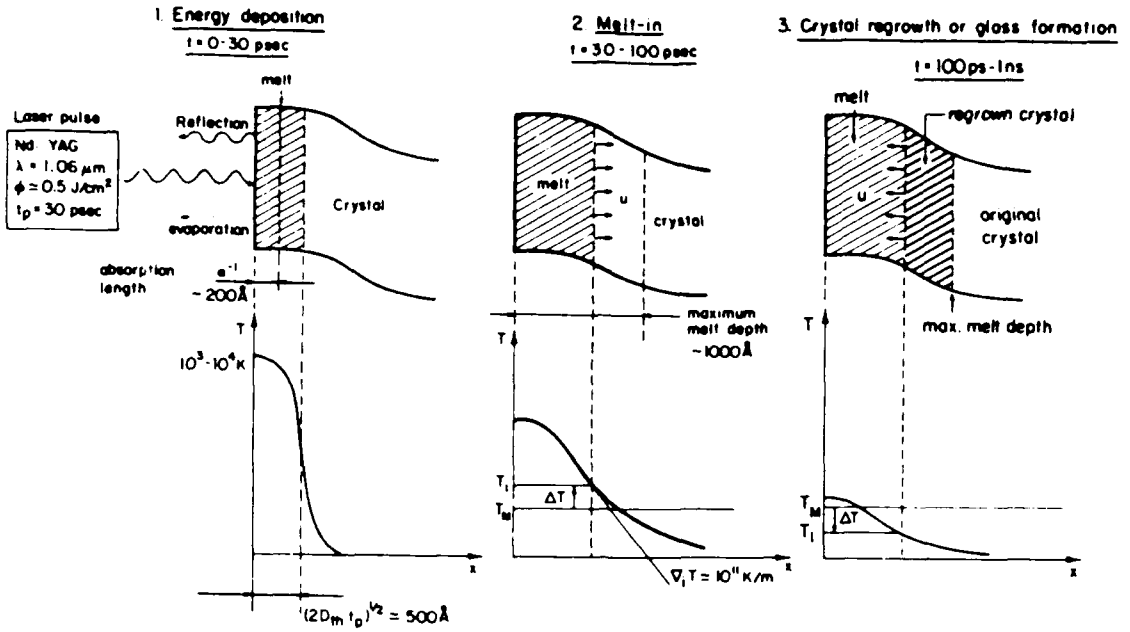

Fig. 1. Schematic illustration of the mechanism of pulsed laser quenching.

3. Phase selection

The short timescale of the picosecond melt quenching process puts restrictions on the transformations that can occur. For the entire liquid layer, of thickness $d = 1000$ Å, to crystallize during the cooling time t of 1 ns, the velocity must be at least $u = d/t \simeq 100$ m s^{-1}. The time t_1 to crystallize a monolayer at this speed is about 3 ps, and the distance an atom can diffuse in that time, $(D_l t_1)^{1/2}$, is less than an interatomic distance (D_l is the diffusivity in the liquid phase). This means that under these short pulsed laser quenching conditions, no long-range diffusion can occur and the only possible transformations are *partitionless* ones, either growth of a crystal of the same composition of the liquid, or glass formation. For nanosecond pulses or for high fluences, which result in a larger melt depth, the regrowth velocity is lower, and some degree of phase separation, usually on a very fine scale, becomes possible.

In conventional solidification, the interface kinetics are much faster than the rate of heat removal, so that the undercooling at the interface, ΔT_i, is small. This type of growth is called *heat flow-limited*. In laser quenching, depending on the nature of the interface rearrangements, the rate of the heat removal can be much faster than the interface kinetics, so that ΔT_i is large, and metastable phases can be formed. This corresponds to *interface-limited* growth [1, 12, 13].

The number of metastable phases with a free energy lower than that of the liquid can be considerable at large undercooling, even under the constraint of partitionless growth. The principle that governs the selection among them has been the subject of continuing debate. The best known of these is the Ostwald step rule, which states that the transformation to the phase closest in free energy is most likely to occur. Turnbull has recently suggested that it is the phase that is closest in *entropy* that is kinetically favored [14]. He pointed out that transformation processes that require the smallest changes in the positional and motional correlations are likely to be the easiest ones. For a crystallization process, this means that phases with a small unit cell and a high degree of isotropy are favored to nucleate or grow.

4. Experiments

The starting samples for laser irradiation were prepared as artificial multilayers by sputtering alternating targets [4, 15]. The substrates were either copper, aluminum or KCl. The geometry is shown schematically in Fig. 2. The periodicity of the layers was kept smaller than 3 nm, which is the diffusional mixing length in the liquid for the 1 ns lifetime of the melt. The individual layers were elemental niobium (polycrystalline body-centered cubic (b.c.c.)) and elemental silicon (amorphous); for the low silicon concentrations, the silicon target was replaced by a composite Nb-Si target. The average composition of the samples could be adjusted by changing the relative thicknesses

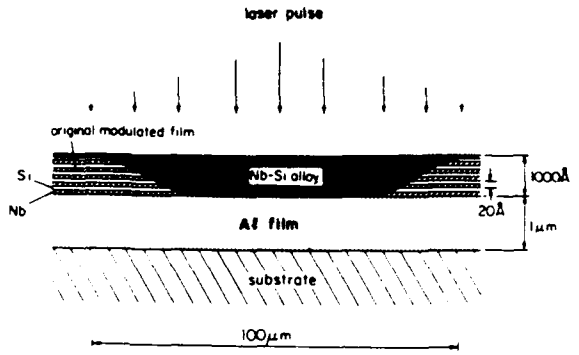

Fig. 2. Schematic diagram (on a variable scale) of a multilayer film after irradiation with a laser pulse with a gaussian intensity profile.

of the layers, and covered the range 8–27 at.% Si. After irradiation with a 30 ps Nd:YAG laser or with a 30 ns ruby laser, the films were chemically removed from the substrate. They could then be examined in the transmission electron microscope without further thinning.

The superconducting transition temperature T_c was determined on samples that had a line of irradiation spots between the electrodes. The transition could be identified by a drop in the resistance.

5. Results

The results of the quenching experiments are summarized in Fig. 3. At the highest quench rates (above 10^{12} K s^{-1}), obtained in the thinnest sections of the spots irradiated with a 30 ps pulse on a copper substrate, the amorphous phase was formed over the entire composition range investigated. This is a much wider range of amorphous phase formation than is possible by other melt-quenching methods. This observation is consistent with our earlier observations on other metal–metalloid [2] and metal–metal [4] systems.

At slightly lower quench rates (10^{12} K s^{-1}), obtained in the remaining area of those spots, a new phase was found: a disordered f.c.c. solid solution [16]. Although the formation of disordered f.c.c. solid solutions in metal–metal alloys cannot be suppressed by picosecond laser quenching [1, 3], the growth rate of the f.c.c. phase in this system, although still the highest observed, is probably slightly reduced because of the short-range order around the silicon [2].

By lowering the quench rate to (10^{11}–10^{12}) K s^{-1} by supporting the films on an aluminum substrate, a supersaturated b.c.c. solid solution was found at low silicon contents, and an ordered f.c.c. phase ($L1_2$, Cu_3Au type) at around 25 at.% Si.

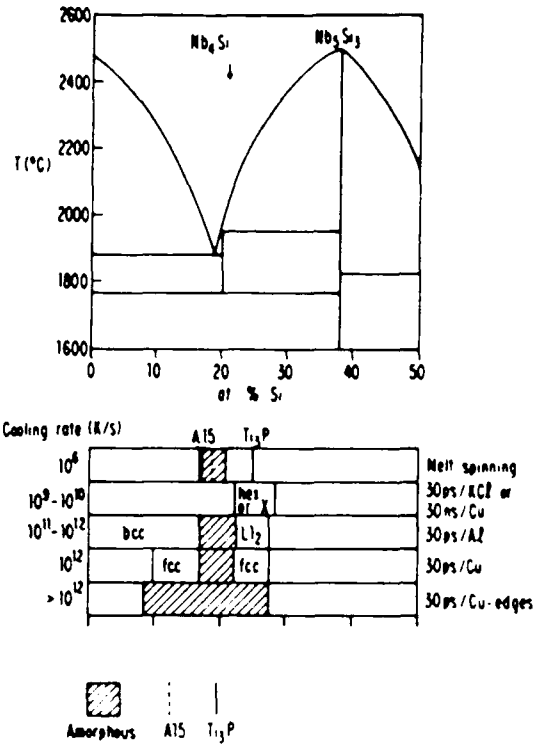

Fig. 3. Phase diagram of the Nb–Si system (top), and schematic illustration of the phases obtained by different methods of liquid quenching. The melt-spinning results are from refs. 5–8.

A cooling rate of (10^9–10^{10}) K s^{-1} was obtained, either by supporting the picosecond-irradiated films on a salt substrate, or by irradiating the films on a copper substrate with a 30 ns pulse. Under these conditions, two entirely new phases were found around 25 at.% Si: a hexagonal phase with a 250 Å^3 unit cell and an as-yet unidentified phase [17].

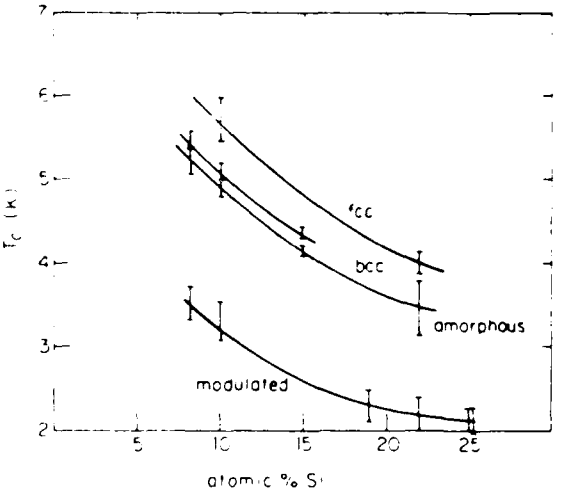

Fig. 4. Superconducting transition temperature as a function of silicon content for the as-prepared modulated Nb–Si films, and for the amorphous, b.c.c. and f.c.c. phases.

The results of the superconductivity measurements are summarized in Fig. 4. A general decrease of T_c with silicon content is observed. T_c values for the new hexagonal phase and the as-yet unidentified phases were 2.7 K and 2.3 K respectively.

6. Discussion

As an illustration of the phase selection rules discussed above, it is interesting to note the degree of isotropy and the unit cell size of the phases formed at 25 at.% Si in order of decreasing quench rate: amorphous (isotropic, no unit cell), disordered f.c.c. (one-atom unit cell, cubic point group), ordered f.c.c. (four-atom unit cell, cubic point group), hexagonal (unit cell of about 16 atoms, uniaxial point group), Ti_3P type (32-atom unit cell, uniaxial point group). Increasing the quench rate increases the undercooling and exposes phases that are increasingly more metastable. It is clear from the experiments that the more isotropic phases with a smaller unit cell are kinetically favored.

The decrease of T_c with silicon content in the modulated films was also observed by Denhoff and Gygax [18]. A similar decrease in the amorphous phase may be the result of the increase in the number of electrons per atom, as proposed by Collver and Hammond for metallic glasses [19]. The same explanation may hold for the f.c.c. and b.c.c. solid solutions. The value of T_c for the f.c.c. solution found here is almost the same as that found for the same phase produced by shock compression [20]. It is interesting to note that T_c for the metastable f.c.c. solutions is higher than that for the b.c.c. solutions by roughly the same amount over their entire composition ranges. One might speculate that T_c for metastable pure f.c.c. niobium should be higher than the 9.25 K value for the stable b.c.c. phase. The T_c values for the hexagonal and unidentified phases are relatively high, since the non-cubic Nb–Si compounds usually have T_c values below 1 K.

Acknowledgments

We thank J. L. Bell for assistance with the sample preparation, and A. M. Malvezzi and C. A. MacDonald for help with the laser irradiation. This work has been supported by the Office of Naval Research under contract N00014-K-85-0684. W.K.W. has been a participant in the Chinese–American Cooperative Basic Research Program in Atomic, Molecular and Condensed Matter Physics of the American Physical Society.

References

1 F. Spaepen, in E. W. Collings and C. C. Koch (eds.), *Undercooled Alloy Phases*, TMS-AIME, New York, 1987, p. 187.
2 C. J. Lin and F. Spaepen, *Appl. Phys. Lett.*, *41* (1982) 721.
3 C. J. Lin, F. Spaepen and D. Turnbull, *J. Non-Cryst. Solids*, *61/62* (1984) 767.
4 C. J. Lin and F. Spaepen, *Acta Metall.*, *34* (1986) 1367.
5 A. Inoue and T. Masumoto, *Sci. Rep. Res. Inst. Tohoku University, A*, *28* (1980) 165.
6 R. M. Waterstrat, F. Haenssler and J. Müller, *J. Appl. Phys.*, *50* (1979) 4763.
7 K. Togano, H. Kamakura and K. Tachikawa, *Phys. Lett. A*, *76* (1980) 83.
8 W. Rossteutscher and K. Schubert, *Z. Metallkd.*, *56* (1965) 813.
9 N. Bloembergen, in S. D. Ferris, H. J. Leamy and J. M. Poate (eds.), *Laser-Solid Interactions and Laser Processing*, AIP, New York, 1979, p.1.
10 J. M. Liu, R. Yen, H. Kurz, and N. Bloembergen, *Appl. Phys. Lett.*, *39* (1981) 755.
11 C. A. MacDonald, A. M. Malvezzi and F. Spaepen, *Mater. Res. Soc. Symp. Proc.*, *51* (1986) 277.
12 D. Turnbull, in M. Bertollotti (ed.), *Physical Processes in Laser-Materials Interactions*, NATO-ASI Proc., Plenum, New York, 1983, p. 117.
13 F. Spaepen and D. Turnbull, in J. M. Poate and J. W. Mayer (eds.), *Laser Processing of Semiconductors*, Academic Press, New York, 1982, p. 15.
14 D. Turnbull, *Metall. Trans. A*, *12* (1981) 695.
15 F. Spaepen, A. L. Greer, K. F. Kelton and J. L. Bell, *Rev. Sci. Instrum.*, *56* (1985) 1343.
16 W. K. Wang and F. Spaepen, *J. Appl. Phys.*, *58* (1985) 4477.
17 W. K. Wang and F. Spaepen, *Appl. Phys. Lett.*, *49* (1986) 295.
18 M. Denhoff and G. Gygax, in U. Eckern, A. Schmidt, W. Weber and H. Wuhl (eds.), *Proc. Conf. on Low Temperatures, LT17*, Elsevier, Amsterdam, 1984, p. 1317.
19 M. M. Collver and R. H. Hammond, *Phys. Rev. Lett.*, *30* (1973) 92.
20 W. K. Wang, Y. Syono, G. Goto, H. Iwasaki, A. Inoue and T. Masumoto, *Scr. Metall.*, *15* (1981) 1313.